



Utrecht University

GROUNDWATER RESEARCH IN NEPAL FOR TIGER CONSERVATION

A reconnaissance study to groundwater dynamics in an alluvial mega-fan in Bardiya National Park (Terai), focusing on the interaction between groundwater and the Karnali river.



Author: Hanne. Berghuis. MSc. Thesis. Program: Earth, Surface and Water at Utrecht University.
1st Supervisor: Prof. Dr. Jasper Griffioen. 2nd Supervisor: Dr. Derek Karssenbergh.
Date: 28-06-2019. Student No.: 6190987. Contact: h.s.berghuis@students.uu.nl.
Photo credits: Esther Leystra (2019). Nepal: Bardiya National Park.

Acknowledgement

I'd like to thank my supervisor Jasper Griffioen for the opportunity to hydrologically explore Bardiya. His enthusiasm for the project was inspiring and his close involvement was very motivating. My friend Ewa van Kooten introduced me to this project. Together we travelled to Nepal for three months. Thanks to her I enjoyed every single day of our time in Bardiya. She often came up with new ideas for field measurements, creative ways to fabricate field equipment or interpretations for unexpected observations.

I am grateful for the Himalayan Tiger Foundation (HTF), who took the initial initiative for hydrological research in Bardiya. I very much appreciate their efforts for the conservation of the wild tiger. During the meetings in the Netherlands and around the campfire in Bardiya with the members and co of HTF, I have learned and laughed a lot. Moreover, I like to thank them for getting us in touch with the National Trust for Nature Conservation (NTNC). The staff of NTNC heartily welcomed us in Bardiya and at their office. They made us feel like a part of the NTNC-family by letting us join their festivals, dinners and campfires. At the same time, they facilitated our research in every possible way. Besides the NTNC staff, we have also met a lot of other nice and interesting people who made us feel at home in Bardiya. Among them Sonia, Buddhi and the family.

I want to express my thankfulness for our friend and guide Telak BK. He always tried to teach us about the Nepalese language, culture whilst protecting us from elephants. He always surprised me with his optimism and inventive solutions. Much of our work in Bardiya would have been impossible without him. Finally, I would like to thank geohydrologist Piet Veel, who joined our field work for two weeks. He left us with new insights regarding both hydrology and life.

Abstract

Bardiya National Park (BNP) is located in the lowlands of Nepal, the Terai. It is one of the five national parks of the Terai where the endangered wild tiger *Panthera Tigris* occurs. The government of Nepal commits to the global agreement of 2009 to double the tiger population by 2022. The survival of the tiger species in Nepal largely depends on the availability of its prey, the deer. The habitat of the deer consists of tall grasses and riverine forests. This type of vegetation thrives by a shallow groundwater table. The groundwater table is therefore regarded as a critical factor in the distribution of the wild tiger. The subsurface of Bardiya National Park is associated with a high permeability as it consists of coalescing alluvial fans, including the alluvial mega-fan of the Karnali river. Therefore, the groundwater head may be dependent on the water level in the Karnali river. The relation between the groundwater and the Karnali river is especially important as the water level in the Karnali river is prone to changes – both natural and human induced. To predict and potentially adapt the groundwater management to these changes, an understanding of the groundwater dynamics is required. Yet, no geohydrological studies have been conducted in BNP.

The objective of this reconnaissance study is to understand the groundwater dynamics in BNP, focusing on the interaction between the Karnali river and groundwater. The research consisted of a three months during field study from the end of September to the beginning of December in 2018, followed by a laboratory- and desk study at Utrecht University. The characteristics of the subsurface were examined by observations in the field, an analysis of existing well log data, grain size analyses of soil samples and by pumping tests. Thereafter, the groundwater dynamics were examined by observations in the field, the monitoring of the groundwater head at various locations and the analysis of the isotopic composition of the groundwater samples, river water samples and rain water samples.

The subsurface consists of alluvial and limnological deposits, forming at least 2 aquifers in the first 100 m from the surface. The subsurface is well permeable, especially near the Karnali river. There, the transmissivity of the shallow aquifer is between $1.9 \cdot 10^3$ and $2.8 \cdot 10^3$ m²/day. In the lower Terai, the shallow aquifer is generally confined by a loamy top layer. Approximately 23% of the annual rain fall may infiltrate through this layer. Thus, the bulk of groundwater recharge by rain water infiltration occurs in the upper Terai, or where the top layer has eroded in the lower Terai.

In the post-monsoon of 2018, the Karnali river drained the groundwater. The effect was the largest for the groundwater head in the south of BNP near the Karnali river, where the groundwater head dropped on average 18.2 mm/day in the shallow aquifers during the post-monsoon. At the most northern monitoring location, further from the Karnali river, the groundwater head dropped with only 7.3 mm/day. The isotopic composition of water samples showed that recharge of the groundwater from the Karnali river is also negligible in other periods of the year, but also that the groundwater was substantially recharged by irrigation with Karnali river outside the park boundaries.

In conclusion, the Karnali river is controlling the groundwater head near the river. Thus, changes in the Karnali river may have problematic consequences for the depth of the groundwater head and thereby potentially also for the habitat of the wild tiger. At the same, the groundwater head may be managed with relatively simple interventions in the Karnali river. However, this research is not sufficient for making quantitative predictions about the effect of potential changes or interventions. Therefore, I recommend to develop a geohydrological computer model of Bardiya National Park and surroundings, based on the results of this study.

Table of Contents

1	Introduction	6
1.1	Relevance.....	6
1.2	Research questions.....	7
1.3	Study area	8
2	Methods	10
2.1	Introduction.....	10
2.2	Field observations of the subsurface	11
2.3	Well log analysis	12
	Data source.....	12
	Background information (Collier, 1993).....	12
	Data processing	14
2.4	Grain size analysis	16
	Field methods	16
	Laboratory analysis.....	16
	Data processing	17
2.5	Pumping test.....	18
	Field methods	18
	Data processing	18
2.6	Field observations of water dynamics.....	22
2.7	Groundwater head monitoring.....	22
	Field methods	22
	Data processing	22
2.8	Isotopic composition.....	24
	Field methods	24
	Laboratory analysis.....	24
	Data processing	25
3	Results & Discussion.....	27
3.1	Field obserbations of the subsurface	27
	Results and discussion	27
3.2	Well log analysis	30
	Results	30
	Discussion	34
3.3	Grain size analysis	37
	Results	37
	Discussion	38

3.4	Pumping test.....	40
	Results.....	40
	Discussion.....	43
3.5	Field observations water dynamics.....	45
	Results and discussion.....	45
3.6	Groundwater heads.....	47
	Results.....	47
	Discussion.....	54
3.7	Isotopic composition.....	59
	Results.....	59
	Discussion.....	62
4	Synthesis.....	67
5	Conclusion.....	69
6	References.....	72
7	Appendices.....	76

1 Introduction

1.1 Relevance

The lowlands at the foot of the Himalayas constitute the lush *Terai region*. It comprises both south Nepal and a part of north India. The region is formed by coalescing alluvial fans from the Siwalik Hill and fluvial deposits (Dhital, 2015). There are several protected areas in the Terai, which are characterized by abundant wild life. In five of these national parks, the imposing wild tiger occurs (DNPWC & DFSC, 2018). The world tiger population is threatened by extinction, which was the incentive for the global agreement (2009) to double the tiger population by 2022. The government of Nepal also commits to this goal (DNPWC & DFSC, 2018). The survival of the tiger species in Nepal largely depends on the availability of its prey: the chital, hog deer and wild boar (Støen & Wegge, 1996; Wegge et al., 2009). The habitat of these deer species consists of tall grasses and riverine forests (Wegge & Storaas, 2009). This type of vegetation thrives by a shallow groundwater table (Wegge & Storaas, 2009; Seidensticker et al., 2015). The groundwater table is therefore regarded as a critical factor in the distribution of the wild tiger (Seidensticker et al., 2015). Additionally, the tall grasslands are maintained by disturbance from cutting, fires, grazing and flooding (Peet et al., 1999). The tall grasses and riverine forests of the Terai are mainly found in the floodplains of dynamic rivers (Peet et al., 1999). Presumably because of flooding. Besides, the riparian vegetation is supposedly also supported by a shallow groundwater table - which may be largely governed by the water level of the river as alluvial fan deposits are associated with a high permeability (Dhital, 2015). The only study that has thus far examined the interaction between the river and groundwater in the Terai, supports the link between these two water bodies (Siegel and Jenkins, 1987). However, the research was not conducted in an area where the wild tiger occurs.

The second largest tiger population of Nepal is found in Bardiya National Park (81.20'E, 28.35'N). The park is located in the Bardiya region in the southwest of Nepal. Bardiya National Park (BNP) covers 986 km² and is surrounded by a buffer zone (Figure 2). The Karnali river is the main river of BNP and flows on top of an alluvial mega-fan (DeCelles & Cavazza, 1999). The branches of the Karnali river are constantly shifting due to sediment transport during floods (Hugh et al., 2017) and to gravel mining in the river beds (USAID, 2018). Moreover, Karnali river water extraction will be intensified in the near future as an irrigation inlet is being constructed in the Karnali river in the north of BNP (Rana, 2018) and in the Bheri river, a tributary of the Karnali river (Adhikari et al., 2009). Since these changes possibly also affect the groundwater table along the Karnali river, an understanding of the current groundwater dynamics is required to predict and potentially adapt to the geohydrological consequences of these changes. Therefore, the objective of the research is to gain insight into the groundwater system in Bardiya National Park, focusing on the role of the Karnali river.

1.2 Research questions

The objective is achieved by a reconnaissance study. There are two research questions formulated regarding the subsurface and the current groundwater dynamics. The research questions are specified by four sub-questions:

1. **What are the main characteristics of the subsurface?**

- a. How does the subsurface of BNP relate to the general geological setting of the Terai?
- b. What is the transmissivity of the shallow aquifer?
- c. What is the hydraulic conductivity of the top layer?
- d. What aquifer type is the shallow aquifer?

2. **What are the current groundwater dynamics?**

- a. What is the depth of the groundwater head along the Karnali river and in the rest of the study area during the post-monsoon?
- b. What are the main zones of groundwater recharge and discharge?
- c. How does the groundwater head change during the post-monsoon?
- d. What is the role of the Karnali river in the changes of groundwater head in the post-monsoon?

1.3 Study area

Bardiya National Park (81.20'E, 28.35'N) is located in the region of Bardiya, a part of the outer Terai (Figure 1). The Terai region is represented by Pleistocene to Holocene sediments and is divided into three geological zones from north to south: the upper-, the middle- and the low Terai. The upper Terai or *Bhabar Zone* was formed by coalescing alluvial fans at the foot of the Siwalik Hills. Among them, the Karnali megafan in Bardiya National Park. The alluvial fans are made of poorly sorted boulders, cobbles, pebbles, and sand. The upper Terai is 10-15 km wide, characterized by gentle slopes of a few degrees. The lower boundary of the upper Terai is often marked by springs. In central Nepal this spring line was found at the transition between steep and gentle slopes. The middle Terai or *Marshy land* comprises the end of the alluvial fans and consists of silt, clay and alternating layers of gravel or sand. The slopes are less than 1°. The lower Terai is formed by *Gangetic alluvium*, which consists of sand, silt and clay with some pebbles. The lower Terai is well-nigh flat: the slopes are less than 0.1 % (Dhital, 2015). The Terai Plain consists of both unconfined to semi-confined shallow aquifers and confined deep aquifers. Perched aquifers are also common in this region. The shallow aquifers are 50 to 60 m deep (Shrestha et al., 2018). The range of transmissivity of shallow aquifers in Terai plains is large. It is found to be between 5 m²/day and 1.6·10⁴ m²/day. In Bardiya, the lowest measured transmissivity is 2.6·10² m²/day and the highest 6.1 ·10² m²/day (Onta, 2004).

Rain water infiltration is the major source of groundwater recharge in the Terai, with an annual recharge of 1100 mm. One-third of the total rainwater recharge infiltrates in the Upper Terai (Shresta et al., 2018). The Terai has a tropical Savannah climate (Karki et al., 2016) with four seasons: the hot monsoon (June – September), the warm and humid post-monsoon (October-November), the cool winter (December - February) and the hot pre-monsoon (March-May) (DHM, 2017). The groundwater is mainly recharged during the monsoon, with an average rain fall between 1000-1500 mm. This is approximately 80% of the annual rainfall. (DHM, 2017). The average rainfall is 50-100 mm in the post-monsoon, 30-50 mm in the winter and 100-200 mm in the pre-monsoon (DHM, 2017).

The groundwater is also recharged by streams and rivers (Shrestha et al., 2018). The rivers of the Terai can roughly be divided into three groups: 1. Snow-fed rivers from the Himalayas. The discharge of these rivers is largely governed by the melting of snow and glaciers. Therefore, snow-fed rivers contain water year-round. 2. Rain-fed rivers from the middle mountains. These rivers are recharged during the monsoon season. However, they do usually not fall dry during the dry seasons as the base-flow is maintained by groundwater exfiltration. 3. Monsoon-rivers from the Siwalik zone. The monsoon-rivers are relatively small and often only active during the monsoon season. Between 60–85% of the annual run-off in the Terai is transported through these rivers (Shrestha et al., 2018).

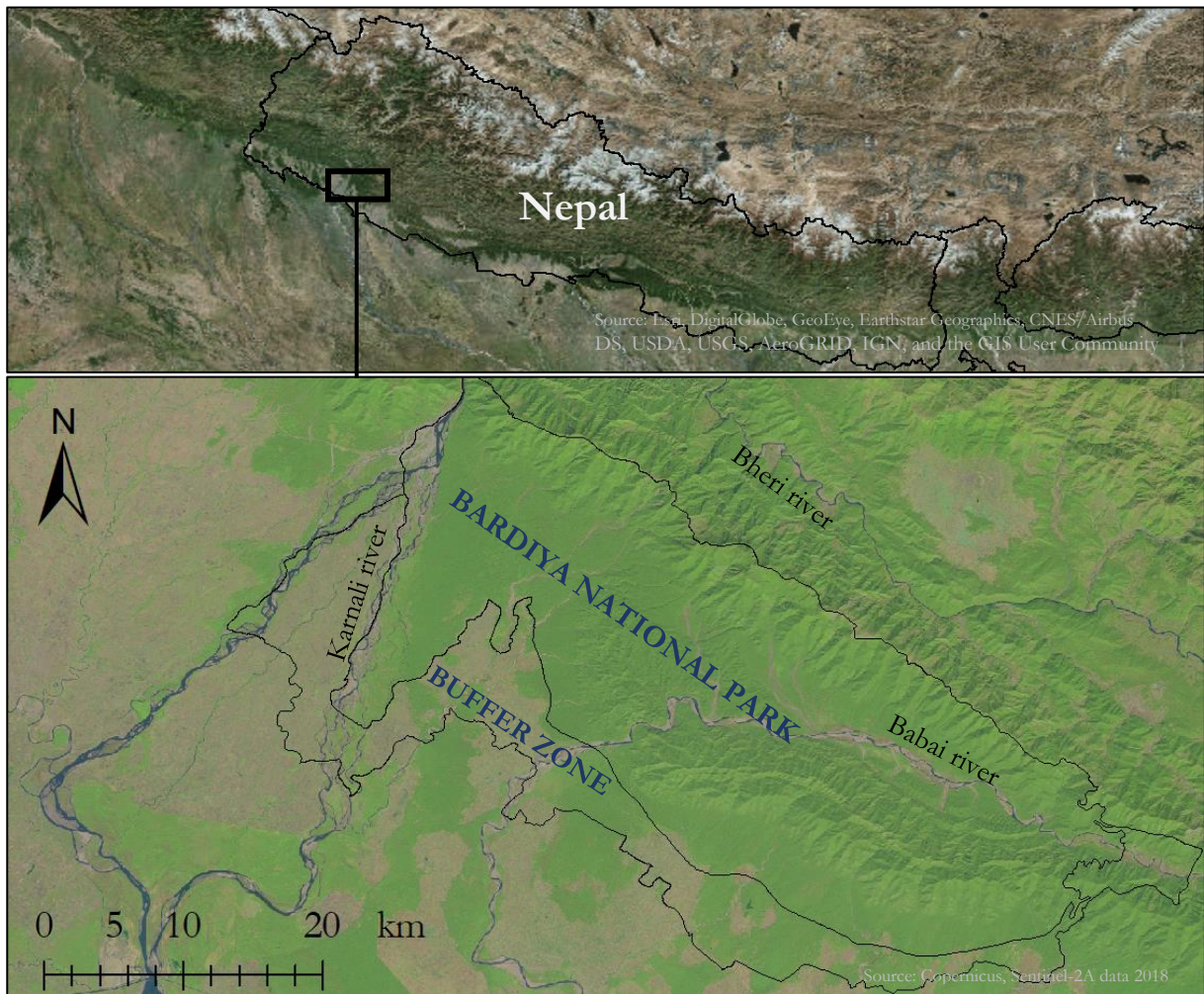


Figure 1. Overview Bardiya National Park

The Karnali river is the only snow-fed river of BNP (Shrestha et al., 2018). Its mean annual discharge is 1369 m³/s (Khatiwada et al., 2016). The Karnali river splits up in the north of BNP (Figure 1). The Geruwa river is the eastern branch of the Karnali river and flows along the western border of BNP. The Geruwa used to be the main stream, but from 2009 the bulk of the river water in the dry season is flowing through the western branch. The Babai river is rain-fed. The mean annual discharge of the Babai is 72 m³/s (Adhikari et al., 2009). The flow in the Babai is controlled by a dam at the southern border of BNP. There are multiple rivers originating from the Siwalik hills. The monsoon-rivers often end in the Aurahi river, which initially flows between the Karnali river and the Babai river and eventually joins with the Karnali river.

The Terai is the most densely populated region of Nepal, with 330 inhabitants per square kilometre (HMGN, 2003). Moreover, it is the most important agricultural region of Nepal – especially for rice production (Chakraborty, 2001). The groundwater is extracted for domestic use (24%), irrigation (68%) and industry (8%). The domestic wells are usually shallow. The municipal and community wells usually extract water from the deeper aquifers (Shrestha et al., 2018).

2 Methods

2.1 Introduction

The research includes a field study from the end of September 2018 to the beginning of December 2018. The study area is defined in Figure 2. The northern boundary of the study area is at the water divide, marked by the rim of the nearest Siwalik Hills. This is also the northern border of BNP. The eastern branch of the Karnali river and the Babai river are respectively the west- and east boundary of the study area. The southern boundary follows approximately the border with India instead of the border of BNP as there were additional field research opportunities south of the park.

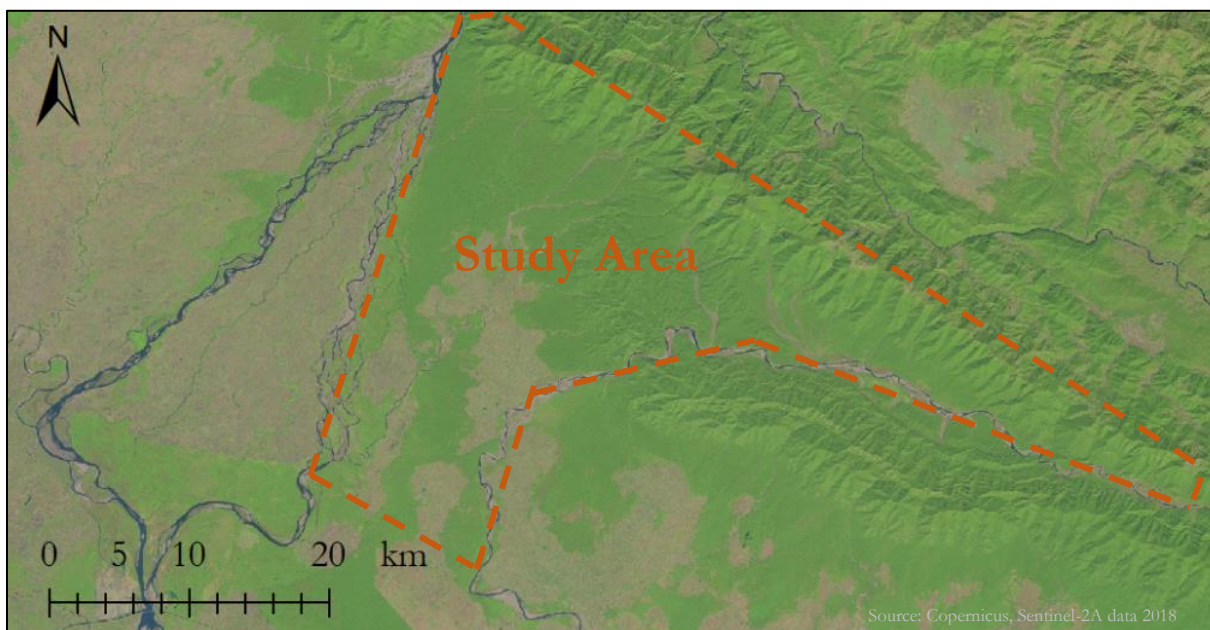


Figure 2. Boundaries of the study area

The field research was conducted on the basis of the sub-questions (chapter 1.2). The methods applied to answer the sub-questions are described in the next chapters as follows: the subsurface of BNP was compared to the general geological setting of the Terai (question 1a) based on field observation and drillings with an hand auger (chapter 2.2). The transmissivity of the aquifers (question 1b) was assessed by analysing existing geophysical well logs of 16 deep wells (chapter 2.3) and by conducting two pumping tests (chapter 2.5). The hydraulic conductivity of the top layer (question 1c) was derived from the analysis of grain size distributions of soil samples (chapter 2.4). The aquifer type (question 1d) was evaluated by comparing the depth of the top layer, as measured by the hand auger drillings (chapter 2.2), with the depth of the groundwater head. Additionally, the pumping test also provided information regarding the confinement of the shallow aquifer (chapter 2.5).

The depth of the groundwater head (question 2a) was monitored in various wells during the study period (chapter 2.7). For the examination of the main zones of groundwater recharge and discharge (question 2b), I only took the infiltration of rain water and in- and exfiltration of rivers into account. The extent of rain water infiltration was estimated by combining the acquired hydraulic conductivity of the top layer with existing rain fall and rain intensity data (chapter 2.4). The zones of increased infiltration were discussed based on field observations (chapter 2.6). Infiltration- and exfiltration of the main rivers were examined based on the groundwater flow direction as indicated by the piezometric surface obtained from the groundwater monitoring network (chapter 2.7). Furthermore, field observations provided additional information regarding the exfiltration of rivers (chapter 2.6).

The change of the groundwater head during the post-monsoon (question 2c) was monitored by the automatic pressure transducers in the monitoring wells (chapter 2.7). The role of the Karnali in these changes (question 2d) was interpreted by the comparison of the monitored groundwater head fluctuations with existing water level data of the Karnali river (chapter 2.7). Additionally, I examined the role of the Karnali by analysing rain water samples, river water samples and groundwater samples on their isotopic composition (chapter 2.8). The composition of the samples contains information about the origin of the groundwater. Besides, the water samples were tested for electrical conductivity (EC), pH, oxygen, alkalinity and the content of the major cations and anions – including arsenic. The results were not used in the research, but the data is provided (Appendix J, Appendix L, Appendix M and Appendix N). The chemical analysis was performed after the field research in the laboratory of Utrecht University.

2.2 Field observations of the subsurface

The subsurface of the study area was first described based on field observations. The observations were supplemented with borehole profiles made with a hand auger. The maximum drilling depth of the hand auger was initially 2.7 m, later it was extended to 5.1 m. Thereafter, the description of the study area was compared with the characteristics of the subsurface in other parts of the Terai.

2.3 Well log analysis

Data source

The government of Nepal installed deep groundwater wells (85 – 160 m) at various locations in the region of Bardiya. In the boreholes of these tube wells, resistivity logs were made to determine the depth and length of the filters. For three of the sixteen tube wells, there was also a borehole description available. These three logs will further be referred to as *logs with borehole description*. The drilling and resistivity logging were performed by *Sushil Constructions* (Nepalgunj) and commissioned by *Water Supply and Sanitation division office*, (Gulariya).

Background information (Collier, 1993)

The logs were made with a *normal tool*, as I recognized by the *short normal* and *long normal* resistivity outputs. Figure 3 shows a schematic overview of the field setup. A constant survey current flows from electrode A to electrode B. The normal device measures the voltage between electrode M and electrode N. The resistivity between A and B is derived based on the equal ratio method, using the voltage ratio between the two circuits and the resistivity between electrode A and B. The distinction between short normal and long normal is made based on the distance between electrode A and electrode M. The most popular spacing between A

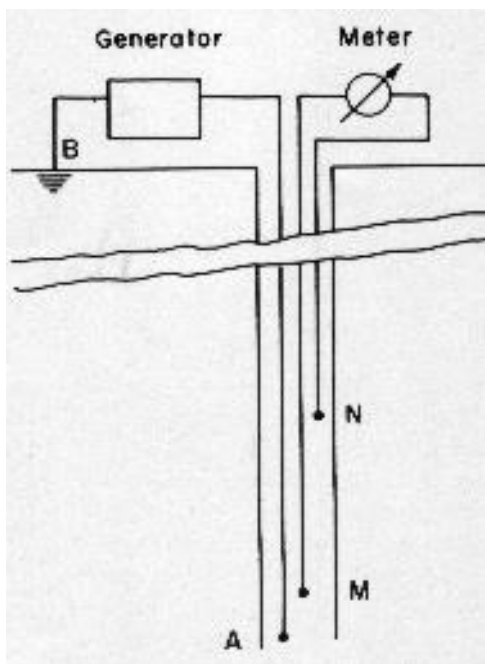


Figure 3. Schematic overview of well logging normal tool. Adapted from: Crain (1999).

and M for short normal and long normal is respectively 16'' and 64''. As the spacing between the electrodes increases, the depth of investigation – i.e. the horizontal distance up to where the resistivity is measured - increases as well. Therefore, the short normal is relatively sensitive for disturbances caused by the process of drilling in comparison to the long normal.

For high formation resistivities, the resistivity is generally underestimated. Whereas the resistivity is generally overestimated when the formation resistivity is low. The thicker the formation bed, the smaller the error. A thin bed of high resistivity can even be missed by this tool, instead a distortion above and below the bed is shown. Also, the severity of the error is stronger close to the bottom of the hole. For more detailed information refer to Appendix A.

The resistivity and the hydraulic conductivity of a formation are governed by the interaction of various processes (Figure 4; information box). Therefore, the nature of the relation between the resistivity and the hydraulic conductivity is complex. The relation between resistivity and hydraulic conductivity is generally positive (Mazáč et al., 1985; : dashed line), because both the resistivity and the hydraulic conductivity are positively related to the grain size (Figure 4). At the same time, changes in resistivity within a certain sediment type are negatively related to the hydraulic conductivity (Mazáč et al., 1985; : solid line). This is caused by the process of packing, which negatively impacts the hydraulic conductivity while it positively impacts the resistivity (Figure 4).

Information box: explanation processes of Figure 4

The resistivity mainly depends on the amount (L1) and characteristics of the groundwater, as the sediment grains are generally not conductive (Collier, 1993). The higher the total amount of dissolved solids in the groundwater, the higher the electrical conductivity (EC) and the lower the resistivity (Collier, 1993; L2). The water content is a function of the porosity (Collier, 1993; L3). The porosity decreases due to packing (Kim, 2013; L4) and for a larger grain size (Kim, 2013; L5). Finally, the clay content influences the resistivity (L6), as clay minerals are conductive. This is ascribed to its cation exchange capacity (CEC): the loosely attached ions conduct an electrical current (Collier, 1993). The hydraulic conductivity is determined by the pore size (Mazáč et al., 1985; Kim, 2013; L7). The pore size on its turn is positively related to the grain size (Mazáč et al., 1985; Kim, 2013; L8) and negatively to the extent of packing (Mazáč et al., 1985; Kim, 2013; L9).

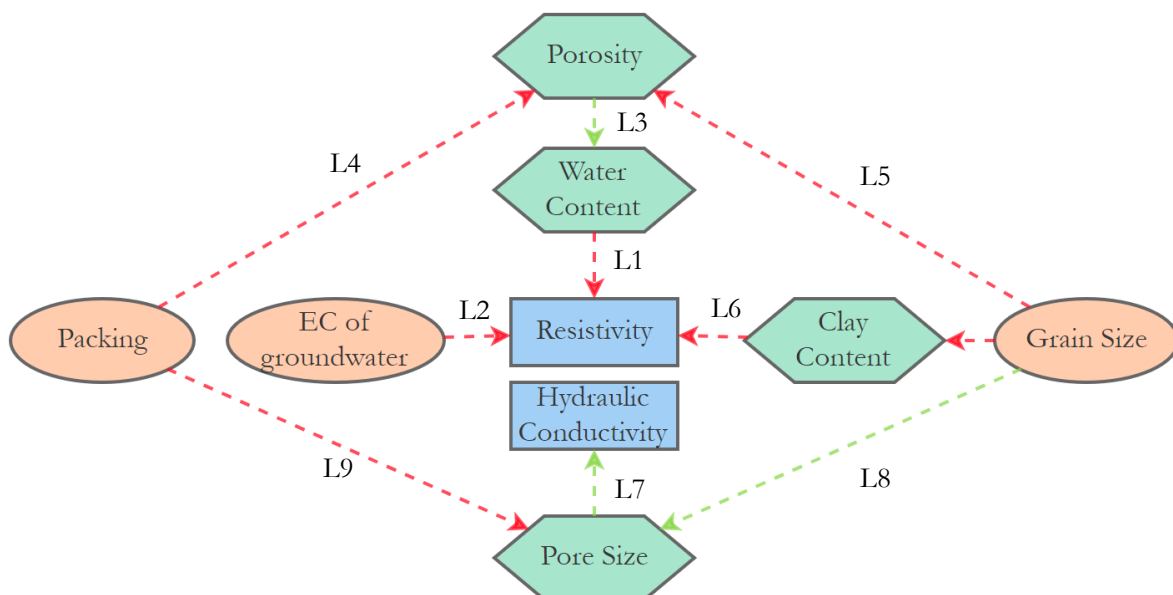


Figure 4. Schematic overview of processes governing the resistivity and hydraulic conductivity of the subsurface. The positive relations are indicated by the green arrows, the negative relations by the red arrows. See also information box above. Made at: www.insightmaker.com.

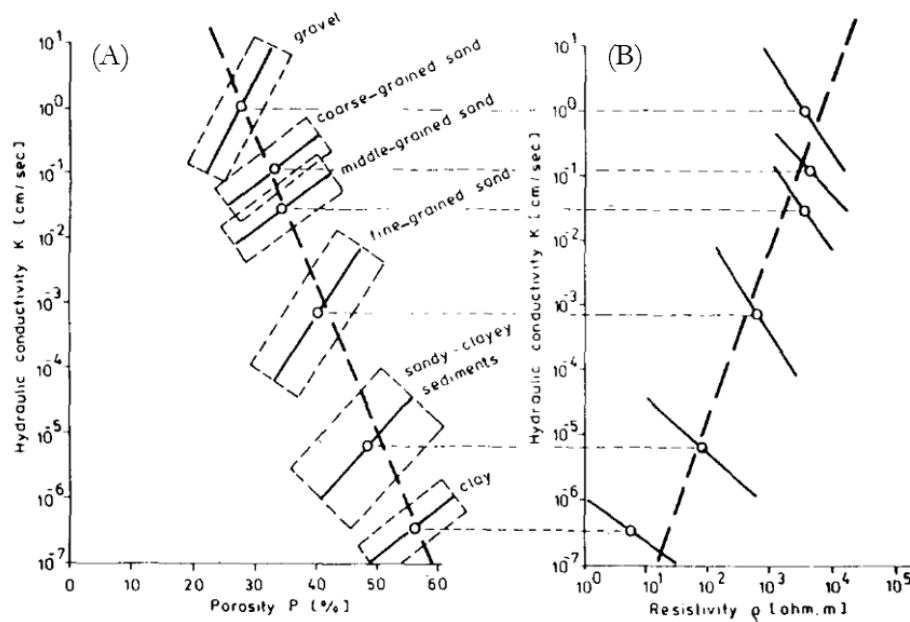


Figure 5. Relations between hydraulic conductivity, porosity and resistivity. From: Mazáč et al., (1985).

Data processing

Locations

The locations of the well logs were usually only indicated by the name of the village and the region. I obtained the coordinates of the locations either by visiting the locations, interviewing NTNC staff or internet research (Appendix B). The absolute altitude of the location was then derived from the digital elevation model (Lehner et al., 2008). The well log data of all locations is available Appendix B. Three well logs were not analysed as their location was either unknown or too far from the study area (Appendix C).

The effect of the groundwater composition

The resistivity of the formation is highly influenced by the resistivity of the water. Therefore, I examined the range and spatial distribution of the electrical conductivity (EC) of the groundwater. I measured the EC in the same wells as where I sampled the groundwater (chapter 2.8). Note that these wells did not correspond to the wells from the well log analysis. I used a HQ14D Portable meter from HACH® to measure the EC, which I calibrated daily. Additionally, there was EC data available from the *Water Supply and Sanitation division office*.

From resistivity to lithology

From the resistivity I calculated the apparent formation factor (FF). This is the formation resistivity corrected for the groundwater resistivity (Huntley, 1986):

$$FF = \frac{R_0}{R_w} \quad (1)$$

where FF = apparent formation factor [-], R_0 = total resistivity [Ω -m] and R_w = resistivity of the water [Ω -m]. The latter is the inverse of the EC. For the resistivities, I only took the tops of the peaks and the valleys into account. Subsequently, I linked the FFs to the lithology based on the three logs with borehole description.

Spatial distribution

I categorized all the resistivity logs based on the range of resistivity. There were three categories: the resistivity of the log is 1. completely within the range of the three logs with borehole description, 2. completely outside the range of the three logs with borehole description and 3. both within and outside the range of the logs with borehole description.

Transects

The data within the study area formed two transects – both fairly parallel to the Babai river and the Karnali river. One transect consisted of 5 well logs, including one log with borehole description. The other transect consisted of 2 well logs. The previously found relation between the FF and lithological group was used to categorize the resistivity data of the transects. However, the FF is dependent on the resistivity of the water (R_w), which was unknown. Therefore, the transects were drawn for two realistic R_w -values. The two different interpretation methods were based on the spatial trend of the EC of the groundwater. The profiles were visualized using *Strater 5* software. The conclusions about the lithology of the subsurface were drawn upon these two possible interpretation methods of the transects.

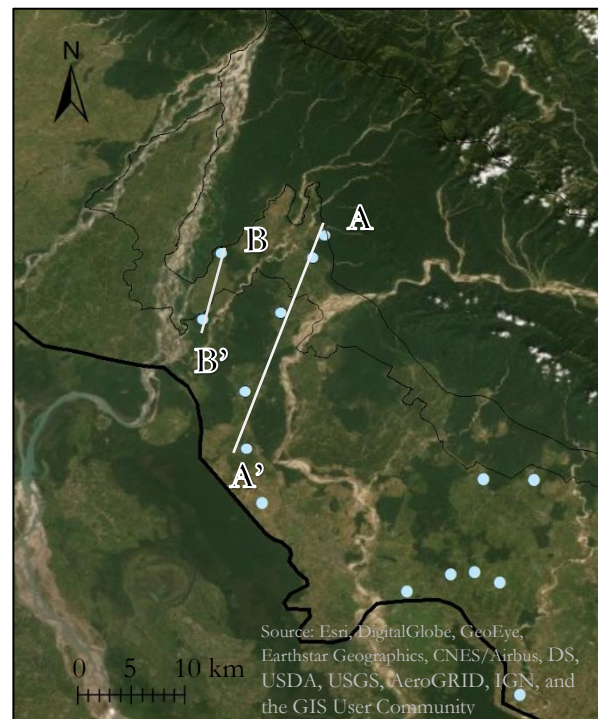


Figure 6. Location well logs and transects.

2.4 Grain size analysis

Field methods

To roughly estimate the soil hydraulic conductivity for the Terai Plain, I used a simplified model of the subsurface. In this model, the subsurface was divided into two layers: 1. a permeable layer of gravel filled up with finer material, overlain by 2. a less permeable top layer. The samples from the less permeable top layer were collected using a hand auger. When there were soil profiles uncovered by erosion, the finer material between the gravel of the permeable layer was collected. Furthermore, when the groundwater is extracted with a hand pump, it may contain sandy material. When this occurred, the material was collected and assumed to originate from the permeable layer.

Laboratory analysis

At the end of the field research, I subdivided the collected soil samples into 5 groups based on soil texture and colour. From each group, one representable sample was analysed on grain size in the laboratory of Utrecht University. The grain size distributions were measured with the *Malvern Mastersizer 2000*. The samples were introduced to the measuring device with the *Hydro2000G*. Each sample was measured twice: In the first measurement the samples were mixed with water and stirred manually. In the second measurement the grains were further separated by adding *PEP*, a solution of pyrophosphate and sodium carbonate.

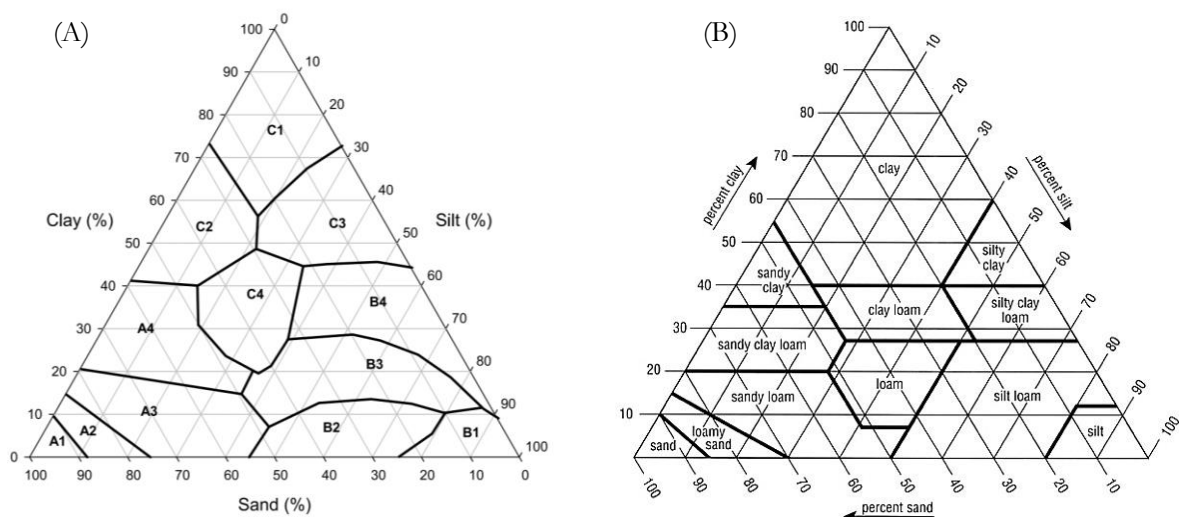


Figure 7. Soil classification triangles of (a) the hydraulic group and (b) the soil type in accordance with USDA. From: Twarakavi et al., (2010).

Data processing

The grain size distributions were expressed in volume percentages of clay ($< 2 \mu\text{m}$), silt ($2 - 50 \mu\text{m}$) or sand ($50 - 2000 \mu\text{m}$). Thereafter, I classified the soil samples into hydraulic groups according to the method of Twarakavi, Šimůnek, & Schaap (2010) (Figure 7A). Every hydraulic group is associated with a certain hydraulic conductivity. Furthermore, I also classified the soil type in accordance with the USDA soil texture triangle (Figure 7B; Twarakavi et al., 2010)

2.5 Pumping test

Field methods

Location 1: Dalla

I installed a diesel pump for irrigation purposes to a shallow communal well at location 1, Dalla (Figure 8). During the pumping, I measured the water head manually in two wells– the distances were obtained from satellite images (Google, n.d.). I also measured the pumping discharge with an electromagnetic flow meter (Appendix D). When there was no measurable change in water head in both monitoring wells for at least 10 minutes, I assumed that semi-steady state was reached. Consequently, turned off the pump, removed the vacuum and measured the groundwater head of the pumping well manually with an accuracy of 0.5 cm. The depth of the pumping well was also measured.

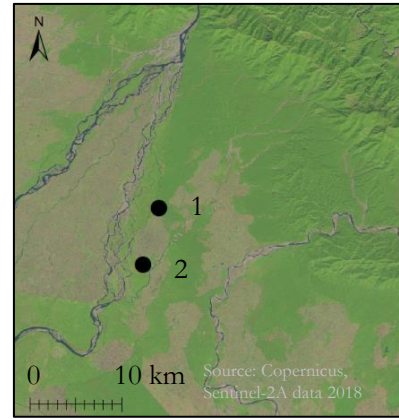


Figure 8. Location numbers of pumping tests

Location 2: Betahanni

In Betahanni at location 2, (Figure 8) a recently installed deep well was pumped through for the first time using a truck-sized pumping installation. After the pump was turned off, I manually monitored the water head of the pumping well with an accuracy of 0.5 cm. The pumping time and discharge were retrieved by interviewing the pumping operators. The depth of the well was obtained from the drilling report of *Sushil Constructions* (chapter 2.3).

Data processing

I calculated the transmissivity at both locations from the results of the recovery tests. At location 1, I also calculated the transmissivity based on the groundwater heads for steady-state conditions during the test.

Recovery test

According to the Theis method, the residual drawdown is described as (Kruseman et al., 1970):

$$s' = \frac{2.30Q}{4\pi KD} \log \frac{t}{t'} \quad (2)$$

where s' = residual drawdown [m], Q = pumping rate [m^3/d], K = hydraulic conductivity [m/d], D = thickness of the aquifer [m], t = time since the start of the pumping [d] and t' = time since cessation of pumping [d]. The transmissivity is defined as KD [m^2/d]. Refer to Appendix E for additional information about eq. 2. Plotting s' versus t/t' on semi-log paper gives slope $\Delta s'$ [-], from which I calculated the transmissivity:

$$\Delta s' = \frac{2.30Q}{4\pi KD} \quad (3)$$

However, plotting s' versus t/t' on semi-log paper does generally not directly result in a straight line. There are a few processes which may cause the deviation from a straight line (Kruseman et al., 1970). I only list the processes which were potentially applicable to these recovery tests, namely: 1. a delayed water head response - which occurs in unconfined aquifers (Figure 9A), 2. a steeper recovery slope just after the pumping has stopped due to either a not fully penetrating well (Figure 9B) or to inflow of water stored in the well (Figure 9C) and 3. a deflecting slope towards the end of the recovery test, caused by leakage from semi-permeable layers (Figure 9D). When these deviations occur, only a certain part of the slope is a reliable input for equation 2 – marked by the arrows (Figure 9; Kruseman et al., 1970). Therefore, I aimed to identify the above described processes by comparing the actual drawdown curve with theoretical drawdown curves. Then, the relevant part of the slope was selected and used for further transmissivity calculations. Note that these figures (Figure 9) show the drawdown patterns during the pumping instead of during the recovery period. The drawdown patterns of the recovery test are equal to the drawdown pattern of the pumping but mirrored in the y-axis, as the principle of superposition applies (Kruseman et al., 1970). Thus, for comparison of the actual- and the theoretical drawdown curve, the actual drawdown was expressed as a negative value.

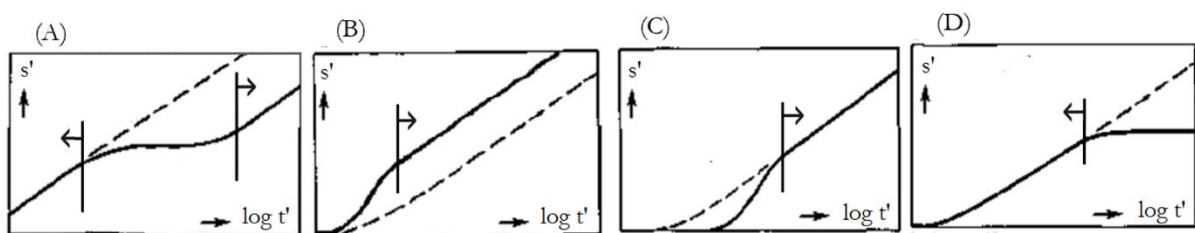


Figure 9. Theoretical drawdown curves during pumping. The effect of (A) an unconfined aquifer, (B) partial penetration, (C) well-bore storage and (D) leakage on the drawdown (solid line) in comparison with the drawdown in a confined, fully penetrating well without well-bore storage (dashed line). Adapted from: Kruseman et al., 1970.

The Theis recovery is only valid under specific conditions (Kruseman et al., 1970): 1. The aquifer is confined, 2. The aquifer has a seemingly infinite areal extend, 3. The aquifer is homogeneous, isotropic, and of uniform thickness over the area influences by the test, 4. Prior to pumping, the piezometric surface is horizontal (or nearly so) over the area that will be influenced by the test, 5. The aquifer is pumped at a constant discharge rate and 6. The well penetrates the entire thickness of the aquifer and thus receives water by horizontal flow. We tested conditions 1 and 6 by comparing the actual drawdown curves with the theoretical drawdown curve of an unconfined aquifer (Figure 9A) and of a partial penetrating well (Figure 9B). Condition 4 was checked based on the groundwater below the surface of the pumping well and the monitoring wells of location 1. For location 2, the condition was assumed to be met. Condition 2 and condition 3 are not relevant for this research as I am interested in the general transmissivity of the aquifer rather than in the local variations of the transmissivity. Finally, condition 5 was secured during the test.

The condition regarding partial penetration (condition 2) may be bypassed. When a test is performed in a partly penetrating well, the same results are achieved when the pumping time is sufficiently long (Hantush 1961):

$$t > \frac{D^2 S}{2KD} \quad (4)$$

where t = pumping time [days], D = thickness of the aquifer [m] and S = storativity [-] and K = hydraulic conductivity [m/d]. Thus, the validity of the Theis method in a partially penetrating well depends on pumping time, transmissivity, storativity and aquifer depth. The pumping time and transmissivity were known, the storativity was estimated (Appendix F) and the maximum depth of the aquifer was calculated to validate the assumption for a partial penetrating well.

Additionally, I tested whether the pumping discharge was sufficient to accurately determine slope $\Delta s'$ (Uffink, 1982):

$$\frac{2.30Q}{4\pi KD} > 0.1 \text{ m} \quad (5)$$

Steady state test

The transmissivity was also derived from a steady state test at location 1, according to Thiem's method (Kruseman et al., 1970):

$$Q = \frac{2\pi KD(S_{m,i} - S_{m,j})}{2.30 \log \frac{r_j}{r_i}} \quad (6)$$

where S_m = drawdown in steady state [m] and r = is the distance from the pumping well [m]. The wells are indicated by the subscripts i and j .

Since the water head was monitored at three locations, the transmissivity was determined for three different combinations of the wells. In theory, the results of all well combinations should be equal. For the pumping well, r is equal to the radius of the well.

The water head in the pumping well was not immediately measured after the vacuum was released. Thus, the first measurement does not represent the water head at steady state correctly. The water head at steady state was estimated by extrapolating the first three measurements (Appendix G). The water head in the second monitoring well remained constant during the entire pumping test, meaning that the water head may not have changed either closer to the pumping well. Therefore, the distance between the pumping well and the second well r_2 was decreased until the results of all three combinations corresponded best.

The conditions of 'Theis' method for the recovery test also apply for Thiem's method for the steady-state test, except for the additional requirement of 'Theis' method (eq. 5). Since the steady-state was conducted in the same well as the recovery test and the conditions were already validated for the recovery test, Thiem's method did not require additional validation of conditions.

Sensitivity analyses

The results of both the recovery test and the steady state test are dependent on the pumping discharge, which is prone to measurement errors. Therefore, a sensitivity analysis was performed for a realistic deviation of the pumping discharge for both locations. At location 1, maximum deviation of the pumping discharge was determined by the maximum error of the electromagnetic flow meter – which is dependent on the flow (Hartong & Termes, 2009). For location 2, the pumping operators indicated the possible range of the pumping discharge.

There may be an error in the water head at steady state since it was obtained from extrapolation. The impact of an extrapolation error on the transmissivity was evaluated by a sensitivity analysis for the drawdown in steady state (S_m), ranging from 1. the drawdown of the first measurement up to 2. the extrapolated drawdown plus the difference in drawdown between the first and the extrapolated measurement.

The results of the recovery test also depend on the pumping time. At location 1, the pumping time was measured. At location 2, however, the pumping time was derived from an interview with the pumping operators. They may only have given an indication of the pumping time. Therefore, a sensitivity analysis was performed for the pumping time up to a deviation of an hour.

2.6 Field observations of water dynamics

The field observations of the water dynamics included the system of rivers, exfiltration of groundwater, irrigation techniques and rain fall.

2.7 Groundwater head monitoring

Field methods

The water heads were measured by automatic pressure transducers. In Bardiya National Park, the pressure transducers were installed in the handpumps at military posts and in an inactive handpump, formerly used to fill a drinking water pond for wild life. Additionally, a new monitoring well was installed. In the buffer zone, the pressure transducers were installed in active handpumps, inactive handpumps and deep tube wells. The water head was monitored every 15 minutes during 1.5 – 2.5 months in the period between October 2nd and December 13th 2018. Additionally, I manually measured the water head in each well at the end and at the beginning of monitoring. The depth of the well was also measured. When the well was too deep to measure (> 30 m), the depth was obtained from interviewing the well owners. I used two types of pressure transducers: the *Keller (DCX-22 AA)* and the *Diver (DI5xx)*. The Keller measures both the barometric pressure and the pressure in the water column. The Diver only measures the pressure in the water column. Therefore, I also installed a Diver barometer at one of the monitoring locations.

Data processing

The water head was calculated from the pressure data as follows (Van Essen Instruments, 2016; Steiner, G., & Gautschi, M., 2014):

$$WC = \frac{P_w - P_a}{\rho_w \cdot g} \quad (7)$$

where WC = height of water column above pressure sensor [m], P_w = water pressure as measured by the pressure transducer [pascal], P_a = air pressure as measured by the Barometer [pascal], g = acceleration due to gravity [kg/m^3] and ρ_w = water density [kg/m^3]. The water density was derived based on the experimental link between water temperature and the density of fresh water (ITTC, 2011).

From the WC and the distance between the pressure sensor and the surface, I calculated the depth of the water head below the surface. Since the air pressure was not monitored locally for the Divers, small error

may have occurred. Therefore, when the Diver measurements systematically deviated from the manual data, the Diver data was adapted. Thereafter, the water heads below the surface were converted to water head relative to mean sea level, where the absolute altitude of the surface was obtained from the AW3D30 DEM (JAXA, 2015). I chose for this DEM since it is the most accurate open source DEM, with a horizontal resolution of 30 m and a maximum vertical RMSE of 6.75 m (Santillan & Makinano-Santillan, 2016). When a monitoring point was located in the forest, the elevation of the nearest low vegetated area – with a maximum distance from the monitoring point of 30 m - was used.

The groundwater fluctuations are also dependent on whether the aquifer is confined or unconfined (Goulburn-Murray Water, 2015). If this layer is less permeable than the aquifer itself, the aquifer is considered to be confined (Fitts, 2002). However, if the groundwater head is deeper than the top layer, the aquifer is considered to be unconfined (Fitts, 2002). Therefore, I compared the depth of the top layer with the groundwater head below the surface to identify the aquifer type. The depth of the top layer was determined based on drillings with a hand auger (chapter 2.2). For the groundwater heads below the surface, the data from the first day that all pressure transducers were active was used. Furthermore, I examined whether the deep and the shallow wells were extracting groundwater from the same aquifer based on the differences between the shallow and deep wells.

The groundwater dynamics were interpreted based on both the spatial differences and the fluctuations with time of the groundwater head relative to mean sea level. For the spatial dynamics, I used the data of the shallow wells of the first and the last day that all the pressure transducers were active. The spatial analysis included 1. the groundwater flow direction and 2. the hydraulic gradient of the groundwater in a 2D transect parallel to the slope of the surface elevation. The groundwater flow direction was estimated based on the spatial difference in groundwater head relative to mean sea level and was further analysed by comparing the height and gradient of the Karnali river with the hydraulic head and gradient of the groundwater on a transect along the Karnali river. Since the Karnali is meandering and braided, I made 10 parallel transects in the floodplain and assumed that the local minima reflected the height of the river beds.

The fluctuations in groundwater head with time at different monitoring locations were compared based on the slope and on the shape of the curve. Similarly, I compared the fluctuations in groundwater head with the fluctuations of the heads in the Karnali river and the Babai river. The data of these rivers was acquired by the Department of Hydrology and Meteorology (DHM), Nepal. For the Babai river, the data of 2018 was not yet available. Therefore, the most recent data was used. Additionally, the data from the past 10 years was examined. The year that the Babai river demonstrated similar fluctuations in water head as the groundwater near the Babai river in 2018 was also visualized. For the Karnali river, only a few data points of 2018 were available. Therefore, the groundwater was not only compared with 2018 data but also the previous most recent year.

2.8 Isotopic composition

Field methods

I collected 30 samples from shallow wells, 3 from deep wells, 4 from spring water, 4 samples from the Karnali river, 2 samples from the Aurahi river, 3 samples from the Babai and 4 samples from rain water (Figure 10). The active shallow wells were pumped through with a handpump for a while before sampling. The inactive or abandoned wells were pumped through for at least 5 minutes before sampling. Since it was not possible to attach a pump to the deep wells, the deep wells were not pumped through before sampling. The samples from the deep wells were collected with a sampling hose. The spring water was collected from running springs. The river water samples were collected from at least a few meters from the river bank, a few centimetres underneath the water surface. In the Karnali, I sampled a transect from upstream to downstream. The Aurahi river water was sampled in the beginning and in the end of the field research at the same location. The Babai river was sampled twice in the south of Bardiya National Park and once in the north. I collected the first rain water sample with a sampling hose from the accumulated water in the steel pipes from a watch tower construction. The other three rain samples all originated from the single rain event during the field study. It was a nocturnal rain in November 2018. One sample was collected during the rain event (2 AM), one sample was collected in the morning after (8 AM) and one sample was collected in the afternoon after the rain (5 AM). The samples were filtered with 0.2 μm filter and stored in a plastic 15 ml tube. All the equipment was rinsed three times with the sampling water before using. The samples were stored in the refrigerator. During the transport from Nepal to the Netherlands by airplane, the samples were not cooled.

Laboratory analysis

The samples were analysed on stable isotopes $\delta^2\text{H}$ and $\delta^{18}\text{O}$ with continuous flow measurements. The results were calibrated for the Vienna Standard Mean Ocean Water (VSMOW) and the Standard Light Antarctic Precipitation (SLAP) according to the VSMOW/SLAP normalization method (Nelson, 2000). The $\delta^2\text{H}$ and $\delta^{18}\text{O}$ abundance were expressed as deviation from VSMOW in per mille. Since 50 samples can be analysed per run, some samples were measured twice. These samples were chosen randomly.

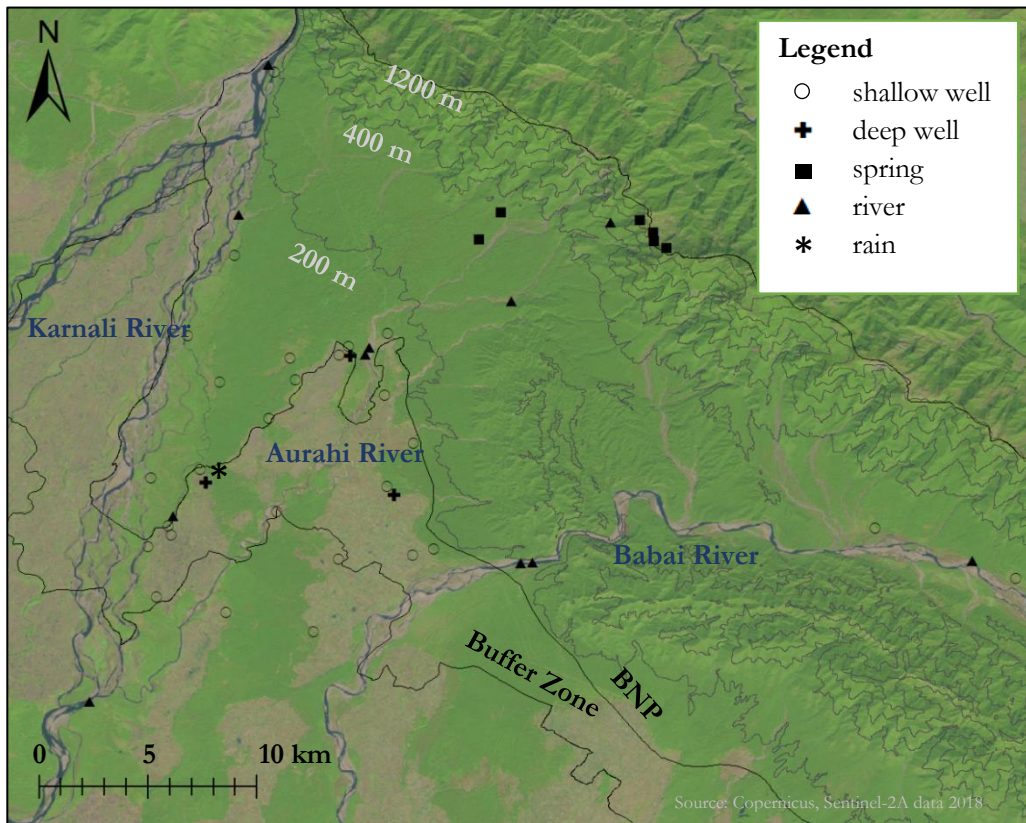


Figure 10. Water sample locations.

Data processing

For the replicated samples, the average isotopic composition was calculated. The $\delta^2\text{H}$ value were plotted versus the $\delta^{18}\text{O}$ value . Then, I compared this ratio with the Global Meteoric Water Line (GMWL) (Hoefs, 2009):

$$\delta^2\text{H} = \delta^{18}\text{O} \cdot 8 + 10 \quad (8)$$

With $\delta^2\text{H}$ and $\delta^{18}\text{O}$ in ‰ VSMOW. Deviation from the GMWL can often be attributed to fractionation. The type and degree of fractionation provides information about which evaporation or condensation processes have occurred before sampling (Dansgaard, 1964; Gat & Tzur, 1967).

The isotopic composition of precipitation is highly dependent on the season, rain intensity and altitude (Dansgaard, 1964; Gat & Tzur, 1967). This implies that the rain samples do not necessarily represent the average isotopic composition of rain fall at the sampling location. Therefore, I also examined the fluctuation in isotopic composition of precipitation at 5 nearest monitoring points in the period between 1960 and 2012 (Figure 11). The data was acquired from IAEA/WMO (2019).

I aimed to examine the interaction between the Karnali river and the groundwater. To do so, I first compared the differences in isotopic composition in terms of fractionation and $\delta^{18}\text{O}$ abundance between the main sample categories: groundwater, spring water, rain water and snow-fed river water and rain-fed river water. Secondly, I explored the general spatial distribution of the isotopic composition of the groundwater. Hereby, I related the composition of the groundwater to the isotopic composition of the rain water and the spring water. After these steps, I identified which groundwater samples were affected by the Karnali river. Lastly, the effect of the groundwater on the Karnali was analysed by comparing the isotopic composition of the Karnali river upstream and downstream.

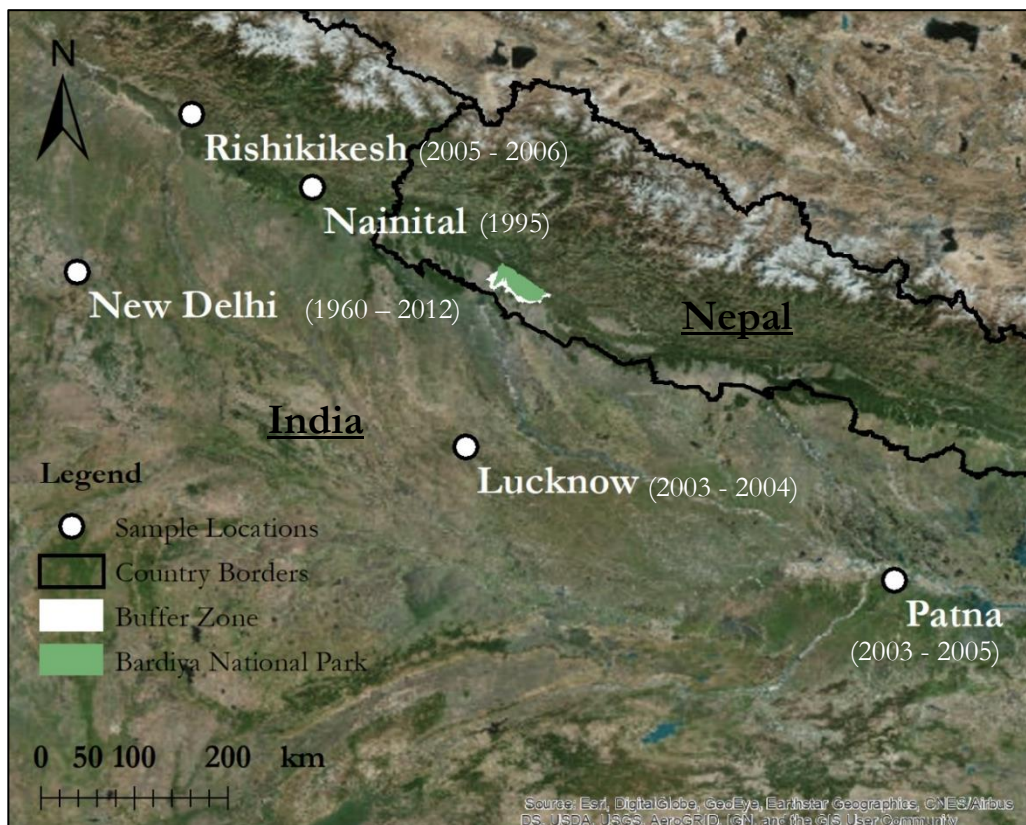


Figure 11. Sample locations from nearby monitoring point in India: Nainital (Kumar et al. 2010a), Lucknow, Rishikikesh, Patna (Kumar et al. 2010b) and New Delhi (India Meteorological Dept., Safdarjung Airport, Delhi). Collected from: IAEA/WMO (2019).

3 Results & Discussion

3.1 Field observations of the subsurface

Results and discussion

In the flat part of the study area (elevation < 200 m relative to the mean sea level), the toplayer consisted of fine silty material. The soil texture was uniform over the whole depth of the hand auger drillings (Figure 12). The depth of the hand auger drilling was usually limited by the maximum drilling depth of the hand auger. Except for one drilling location near the Karnali river, where drilling could not be continued after ~40 cm due to rocks. According to NTNC staff, this location used to be a river bed of the Karnali river. There were a few uncovered profiles, usually found at active and dry beds of brooks or small rivers, generally



Figure 12. Representative soil profile of the lower Terai.

consisting of a gravel in a sandy matrix overlain by a relatively thin layer of fine material (Figure 13C). This could be a representation of the subsurface, however it could also be recent deposits of these rivers. The bottoms of the river beds were often sandy or gravelly.

The fine and uniform soil texture of the top layer indicates a lacustrine deposit (Nichols, 2009). This is an interesting finding as it suggests that the top layer of Bardiya National Park was formed by lake deposits. To the best of my knowledge, no lake deposits are reported in the geological descriptions of the geology of the Terai region (Dhital, 2015; Shrestha et al., 2018). Furthermore, I expect that little rainwater will recharge the groundwater through the thick layer (>1.6 m) of silty material. The bulk of infiltrated rainwater of this area has most likely travelled through (former) river beds.

Walking up towards the north, the top layer seemed to exist of similar material as in the flat area but then with cobbles and boulders at the surface. The locations where the first cobbles at the surface were found going from south to north, were marked (Figure 13A). The further towards the north, the larger the size and quantity of the boulders – at least up to a diameter of ~1 m. In this area, the drilling depth was restricted by rocks in the soil at depths between 0.2 and 1.6 m (Figure 13A). Rock fragments at the surface generally increase the infiltration capacity of the soil (Poesen & Lavee, 1994). Nevertheless, the infiltration capacity

seemed to be low: There was an artificial pond in this area (Figure 13A) with a water depth of approximately 50 cm, which had at most dropped a few centimeters from the end of the rainy season in September to observation moment in November – judging by the water level and height of the pond banks. There was a ~15 m soil profile uncovered by erosion (Figure 13B). The profile consisted of alternating layers of gravel, sand and finer material. There were various springs close to the ridge (Figure 13A).

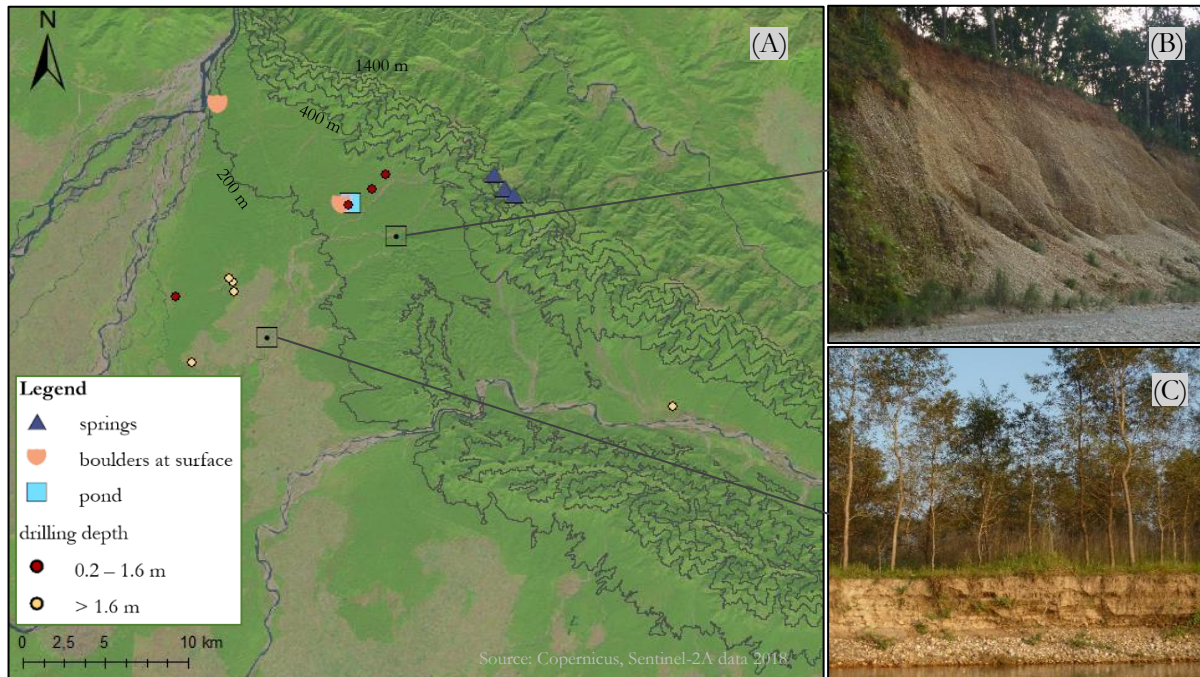


Figure 13. Overview of the area. (A) map study area, (B) uncovered soil profile and (C) profile river bank.

Table 1. Overview of width and slope of the upper Terai for two possibilities.

	boundary	width [km]	slope [°]
Terai (Dhital, 2015)	Spring line & slope transition	10 - 15	>1
Bardiya - option 1	Spring line (Figure 13A)	0.5	20
Bardiya - option 2	Slope transition between 200 - 400 m (Figure 13A)	6.5	8

There are two plausible options for the boundary between the upper and middle Terai, judging by the comparison between the general geological description of the Terai and the field observations in Bardiya. In the first option, the upper Terai comprises the area from the ridge to the springs as springs often mark the boundary between the middle and the upper Terai (chapter 1.3; Table 1). However, this would imply that the width and the slope of the upper Terai of Bardiya strongly deviates from the general situation in the Terai (chapter 1.3; Table 1). For the second option, the boundary between the upper and the middle

Terai is located at the boundary between steep and gentle slopes – which is between an elevation of 200-400 m (Figure 13A). This option is suggested as the springline is also often located at the boundary between steep and gentle slopes (chapter 1.3; Table 1). In Bardiya, there were no springs encountered at this elevation but this area has also not been explored very well. This option corresponds better to the general situation in the Terai regarding the width and the slope (chapter 1.3; Table 1). Both options are not contradicted by the location of the pond and the soil profile: the low infiltration of the pond and the geology of the profile are rather associated with the middle- or the lower Terai than with the upper Terai (chapter 1.3). In conclusion, the possible boundaries between the upper- and the middle Terai suggest that the upper Terai of Bardiya is relatively small. This implies that there would be less groundwater recharge through the upper Terai than in other parts of the Terai. The location of the boundary between the middle and the lower Terai was not evaluated due to a lack of information. However, this boundary is also less important since the lower- and middle Terai differ less in terms of groundwater recharge potential (chapter 1.3).

3.2 Well log analysis

Results

Conductance of the groundwater

During the field study, the electrical conductivity (EC) of the shallow groundwater ranged between 239 and 616 $\mu\text{S}/\text{cm}$. The EC of the deep tube wells were within the same range, except for the deep tube well between the Aurahi river and the Babai river, for which an relatively low EC of 174 $\mu\text{S}/\text{cm}$ was measured (Figure 14). There was no clear spatial pattern for the EC, but the EC of the groundwater between the Karnali river and the Aurahi river was generally a little higher than in the area between the Aurahi river and the Babai river (Figure 14). The EC data acquired from the Water Supply and Sanitation division office was equal to 413 and 317 $\mu\text{S}/\text{cm}$ and thus within the range of the field data of this study.

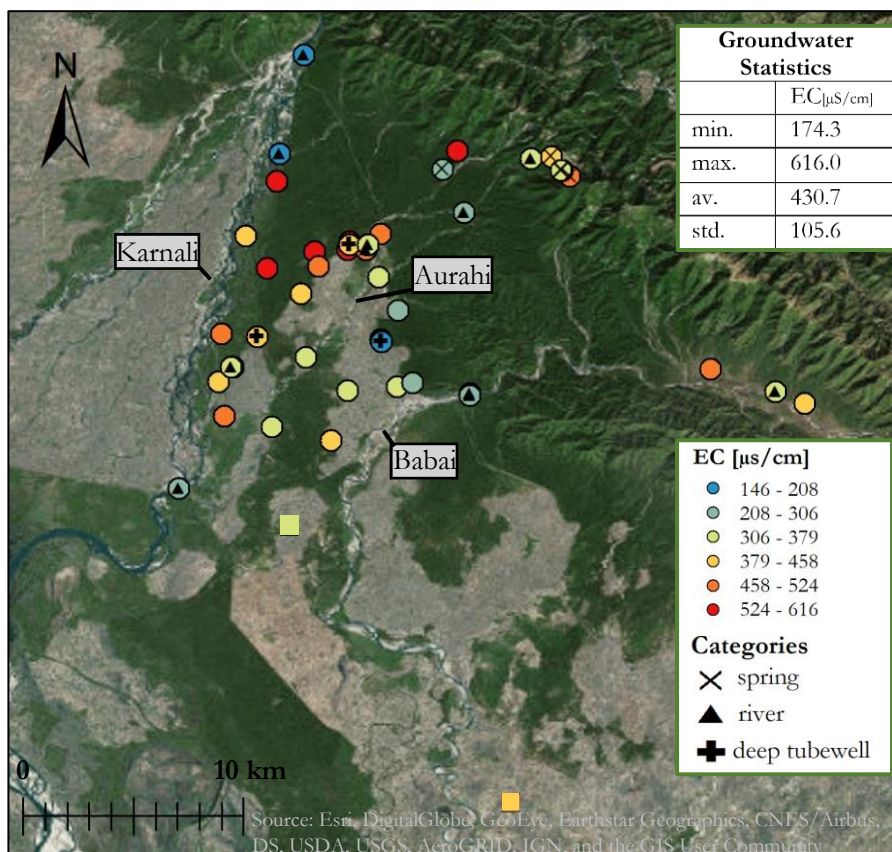


Figure 14. Spatial distribution of the electrical conductivity from field data (circles) and Water Supply and Sanitation division office (squares).

Relating resistivity to lithology

The resistivity of the logs with borehole description ranged from 24 to 93 Ω -m except for coarse sand, for which a resistivity of 175 Ω -m was measured. The FFs of the logs with borehole description were calculated from their formation resistivity assuming an EC of 413 μ S/cm (Figure 15). This is the EC of the nearest measuring point of two of the logs with borehole description: Mainapokhar and Mayurbasti (Figure 14; Figure 16). The relation between apparent formation factor (FF) and grain size is positive (Figure 15). The FF of some lithological groups overlap. Furthermore, the difference between the FF of coarse sand and the other groups is striking.

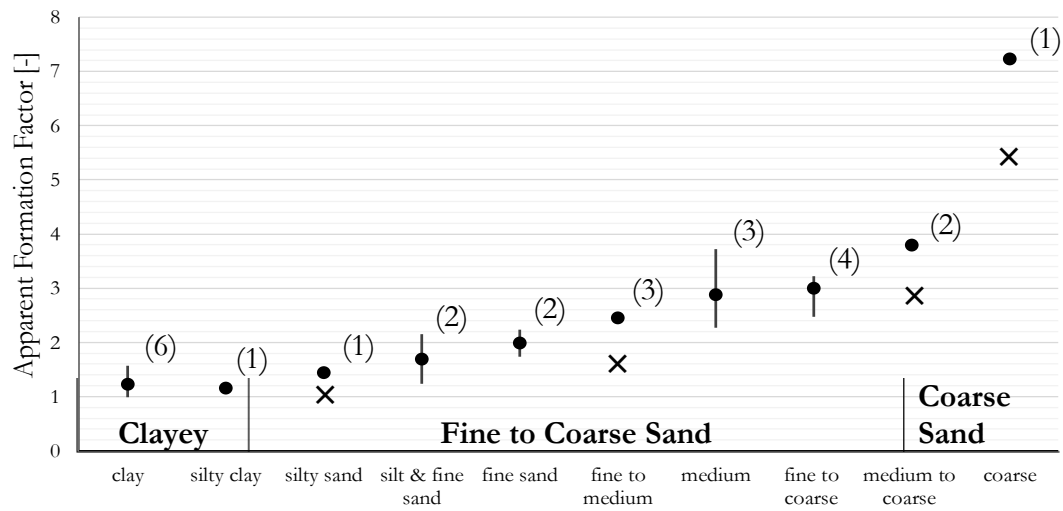


Figure 15. Apparent formation factor (FF) linked to logs with borehole description. The FF was derived from long normal resistivity measurements and assumes a constant EC of 413 μ S/cm. The dots indicate the average formation factor of the lithological category, the lines show the range. The number of data points are given in brackets.

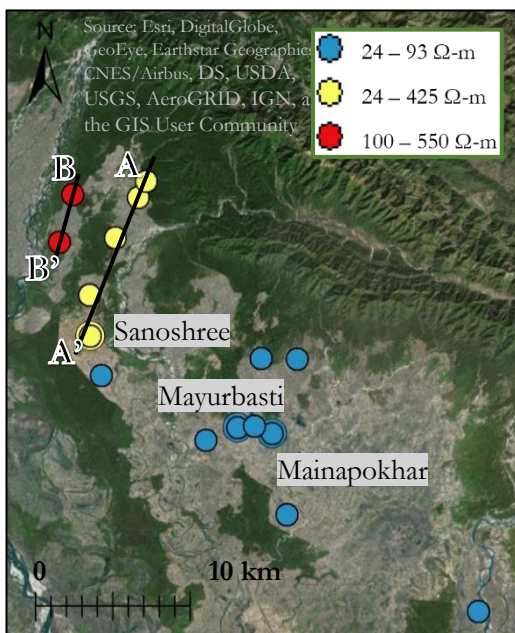


Figure 16. The range of resistivity per tube well. The double circles represent the well logs with borehole description.

Spatial distribution

The spatial difference in resistivity range was shown by categorizing the wells based on the range of resistivity of the three logs with borehole description – excluding the deviating resistivity of coarse sand - as follows:

1. only resistivities within that range (24-93 Ω -m),
2. only resistivities outside that range (100-550 Ω -m) and
3. resistivities both within and outside that range (24-425 Ω -m) (Figure 16).

The observed range of resistivity in the well logs outside the study area were all within the range of the logs with borehole description. Whereas the resistivities of well logs inside the study area were largely outside the range of the logs with borehole description. In transect A-A', the resistivities of the well logs were within the range of the logs with borehole description or higher. In transect B-B', the highest resistivities were found. The resistivities of this transect did not overlap with the resistivities of the logs with borehole description.

Transects.

The resistivities of the well logs were converted to FFs for two different interpretation methods: 1. the EC of the groundwater at the transects is equal to the EC of the logs with borehole description and 2. the EC of the transects are equal to the lowest measured EC of the study area (Figure 14). Note that the lithology groups were simplified into four main categories: *clayey*, *fine to coarse sand*, *coarse sand* and *outside range of the well logs with borehole description* (Figure 15; Figure 17).

Interpretation method 1 (Figure 17A; Figure 17B) represents the situation where the difference between the observed resistivities is entirely due to a difference in lithology. In this interpretation the FFs of the logs along transect A-A' and B-B' exceed the FFs of the logs with borehole description. The FFs of the most northern log of transect A-A' (Figure 17A), starts to exceed the FFs of the logs with borehole description at a depth of ~20 m. The further to the south, the deeper these high FFs are found. For transect B-B' (Figure 17B), the FFs are outside the range for almost the entire depth. For this transect also applies that in the north there was more formations with an FF outside the range of the logs with borehole description than in the south.

The aim of interpretation method 2 was to examine to which extend the differences resistivities can be due to high groundwater resistivity (Figure 17C; Figure 17D). According to this interpretation, the FFs of the transect A-A' were all in range of the logs with borehole description (Figure 17C). However, even for this low EC, a part of the sediment was categorized as coarse sand – the type of sediment which was not found in the well logs with borehole description southeast to the study area. For this interpretation, much sediment was categorized as clayey. However, this is an overestimation since the FF of clay is less prone to changes in groundwater resistivity as the clay particles itself also conduct electrical current. For transect B-B' (Figure 17D), there was still some sediment for which the FF exceeded the range of the logs with borehole description - even for this EC. Furthermore, a substantial portion of the sediment was categorized as coarse sand and there was no clayey material.

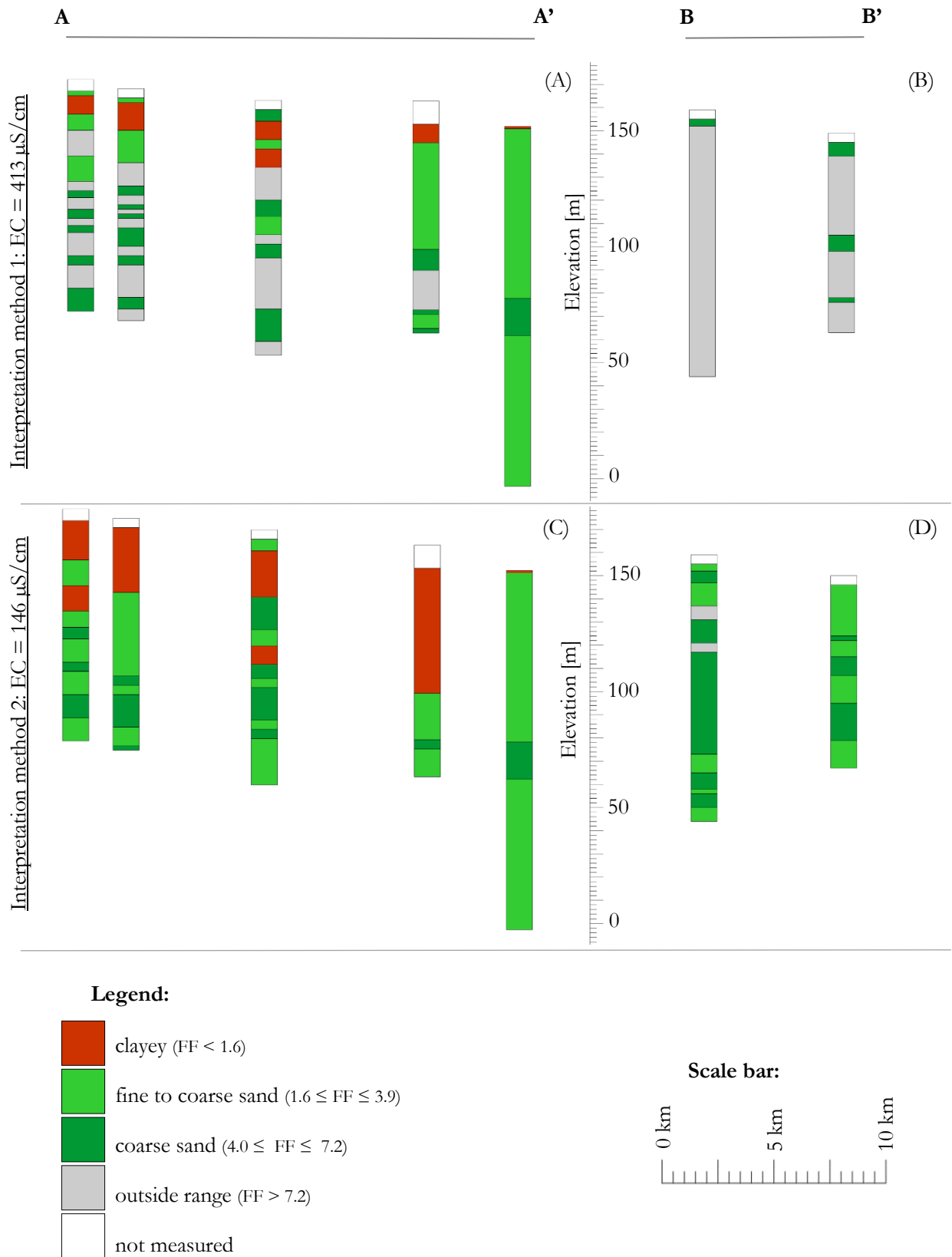


Figure 17. Lithologies of transects based previously found relation between apparent formation factor and lithology (Figure 15). Apparent formation factors were calculated for two interpretations: 1. The EC of transects are equal to EC of logs with borehole description (A+B), 2. The EC of transects are equal to lowest EC of study area (C+D).

Discussion

There were two main obstacles for deriving the sediment types from the well log data. The first obstacle was the uncertainty concerning the EC of the groundwater. Nevertheless, correcting the apparent formation factors (FF) for different EC interpretation methods showed that some conclusions were valid independently of the EC. Note that the actual influence of the EC is probably even less than shown by interpretation method 2: the EC was assumed to be equal to the EC of the Karnali river (interpretation method 2) which was lower than the groundwater at all locations. Moreover, there was no indication that the EC was lower in the study area than at the locations of the logs with borehole description: In transect B-B' the EC was always higher than at the location of the logs with borehole description. Thus, the differences in EC cannot explain the differences in resistivity. On the other hand, I only measured in a certain period of the year, the EC may be different in other seasons – especially in the shallow aquifer. The well logging of transect B-B' was performed in June-July and it was located close to the river, thus if the groundwater was more influenced by the river in June-July, it may have resulted in a lower EC. The second obstacle concerned the division between the *clayey* and the *fine to coarse* material as the resistivities slightly overlap. Furthermore, the conductance of the clay particles was not taken into account for the calculation of the FF since the clay content was unknown – meaning that for interpretation method 2 the amount or thickness of the clay layer was overestimated. However, it does not impact the general conclusions.

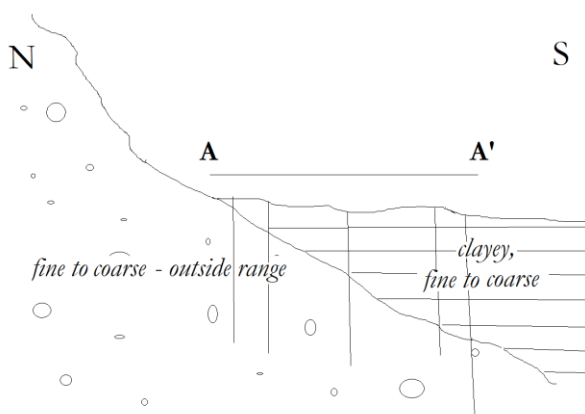


Figure 18. Schematic overview profile A-A'.

There were four main trends independently of assumed EC of the groundwater. Firstly, the FFs of the well logs along the transects were higher than of the well logs southeast of the study area. Secondly, the *clayey* and *fine to coarse* material was generally found on top of the *fine to coarse* and *outside range* material in transect A-A', where the top layer of relatively fine material reached deeper into the subsurface towards the south (Figure 18). Thirdly, the top layer of *clayey* and *fine to coarse* material was not found in the well logs along transect B-B'. Fourthly, the FFs of transect B-B' were higher than the FFs of transect A-A' – including the deeper, coarse sediments of transect A-A'.

The difference between well logs of the study area and the well logs southeast of the study area in terms of FFs may be ascribed to the difference in sediment origin as the Gangetic alluvium is generally finer than the deposits from Siwalik alluvial fans (Dhital, 2015). However, all the well logging was conducted in the lower Terai (chapter 3.1) – which according to previous studies solely consists of alluvium from the Ganges (Dhital, 2018). Interestingly, the shape of the top layer in transect A-A' (Figure 18) suggests that the Gangetic alluvium overlays the Siwalik alluvial fan deposits. This implies either that the lower Terai does not solely exist of Gangetic alluvium or that the boundaries between the upper- and the lower Terai need to be redefined. I concluded previously (chapter 3.1) that the first few meters of the surface consist of lacustrine deposits. It is likely that the entire fine top layer consists of these lake deposits instead of alluvium from the Ganges - especially judging by the large distance between the Ganges and Bardiya National Park.

The absence of the top layer of Gangetic alluvium or lacustrine deposits in transect B-B' is probably because the transect is close to the Karnali river. The fine material at the top may have been eroded and replaced by coarser river sediment. In this case, the FFs of transect B-B' solely represents the deposits of the Karnali mega-fan. This also explains why the FFs of transect B-B' are larger than of transect A-A', though the explanation is dependent on the size of the mega-fan. If both transects are located in the Karnali mega-fan, the sediments in transect B-B' are coarser because coarse material deposits first. If only transect B-B' is located in the Karnali mega-fan and the subsurface at transect A-A' is formed by smaller alluvial fans, the deposits of transect A-A' may be finer because the sediment from mega-fans is usually coarser.

Table 2. Range of hydraulic conductivity of lithological classes. Adapted from Domenico & Schwartz (1990).

material	min. k [cm/sec]	max. k [cm/sec]
gravel	$3 \cdot 10^{-2}$	$3 \cdot 10^0$
coarse sand	$9 \cdot 10^{-5}$	$6 \cdot 10^{-1}$
medium sand	$9 \cdot 10^{-5}$	$5 \cdot 10^{-2}$
fine sand	$2 \cdot 10^{-5}$	$2 \cdot 10^{-2}$
silt	$1 \cdot 10^{-7}$	$2 \cdot 10^{-3}$

Different deposits are associated to different permeabilities. In general, the hydraulic conductivity (K) and the grain size are positively related (Domenico & Schwartz, 1990). Since the logs with borehole description also showed a positive relation between the FF and the grain size, the FF and K are also positively related. However, this is only demonstrated for FFs within the range of the logs with borehole description. To examine whether this relation may be extended to FFs outside this range, the results were compared with the results of previous research in other areas.

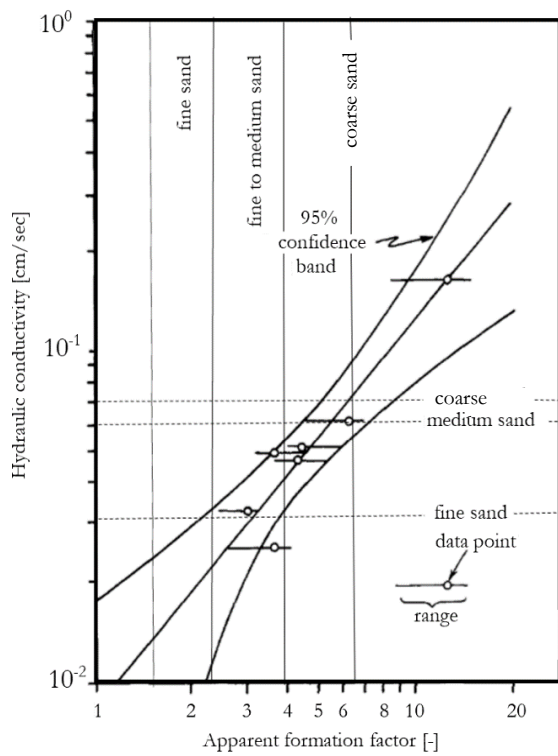


Figure 19. Relation between apparent formation factor and hydraulic conductivity for New England glaciofluvial deposits. Circles represent data points, horizontal lines through data points represent possible range of apparent formation factor for typical groundwater salinity range (100-1000 $\mu\text{S}/\text{cm}$). The apparent formation factor ranges and corresponding lithology of Bardiya (solid line) and the upper conductivity boundaries for three sediment types (dashed line) are drawn in the figure. Adapted from: Kosinski & Kelly (1981).

The relation between FF and K varies per location (Mazáč et al., 1985). Regarding this relation, the sediment of Bardiya is similar to the New England glaciofluvial deposits (Figure 19; Kosinski & Kelly, 1981) – where the grain sizes were derived from the hydraulic conductivity (Table 2; Domenico & Schwartz, 1990). For the New England deposits, the positive relation between FF and K also holds outside the range of the logs with borehole description ($\text{FF} > 7$). This suggests that high FFs ($\text{FF} > 7$) represent high hydraulic conductivities – meaning that the hydraulic conductivity of the transects in the study area is generally higher than towards the southeast and that the conductivity in transect B-B' is even higher than of transect A-A'. Furthermore, the hydraulic conductivities of the FFs outside the range of the logs with borehole description correspond to the hydraulic conductivity of gravel. This supports the hypothesis that the high FFs represent Siwalik alluvial fan deposits.

3.3 Grain size analysis

Results

There were soil samples taken from various locations. The samples were divided into 5 groups based on soil texture and colour. A representative sample from each group was analysed on the grain size distribution. The sample locations are shown in Figure 20A, where the different sample types are represented by colour. The locations of the representative samples which were actually analysed are marked with a sample type label. Sample type I – III were collected from the top layer, sample type IV and V originated from the permeable layer (Figure 20B).

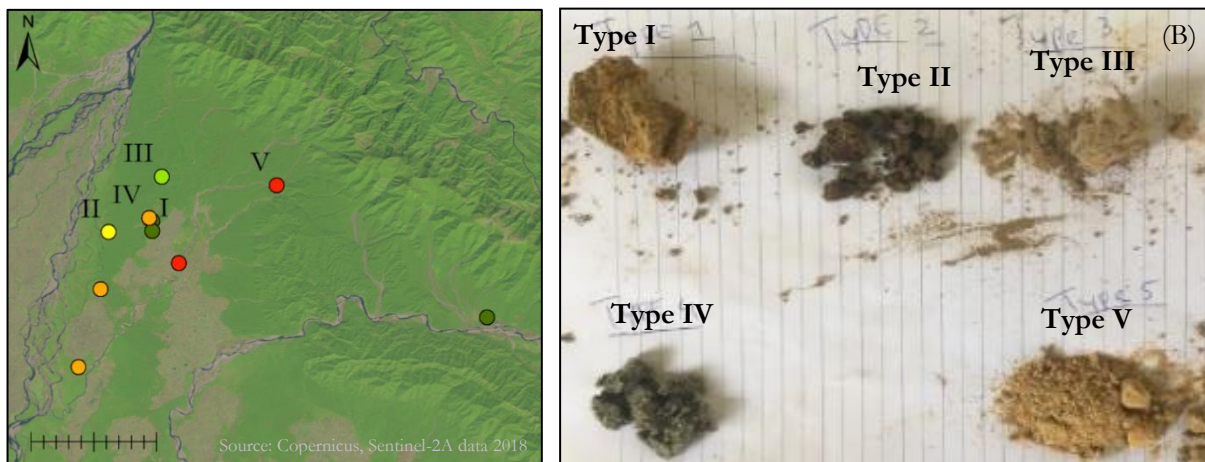


Figure 20. (A) sample locations: the different sample types are represented by colour. The locations of the analysed samples are marked with a sample type label. (B) photo of representative sample types.

Table 3. Results grain size analysis, including soil class, hydraulic class and corresponding hydraulic conductivity with its standard deviation in brackets.

No.	layer	sep. method	clay (vol. %)	silt (vol. %)	sand (vol. %)	hydr. class	$\log_{10}(\mathbf{K}) + \text{std.}$ (\mathbf{K} in cm/day)	soil class
I	top	stirring	2.25	82.93	14.82	B1	1.641 (0.273)	silt
		PEP	1.93	82.62	15.44	B1	1.641 (0.273)	silt
II	top	stirring	1.04	58.79	40.17	B2	1.714 (0.594)	silt loam
		PEP	0.97	61.85	37.18	B2	1.714 (0.594)	silt loam
III	top	stirring	0.83	58.10	41.07	B2	1.714 (0.594)	silt loam
		PEP	0.70	60.84	38.46	B2	1.714 (0.594)	silt loam
IV	second	stirring	0	2.39	97.61	A1	2.853 (0.544)	sand
		PEP	0	2.50	97.50	A1	2.853 (0.544)	sand
V	second	stirring	0.77	26.55	72.68	A3	1.641 (0.659)	sandy loam
		PEP	0.73	27.02	72.25	A3	1.641 (0.659)	sandy loam

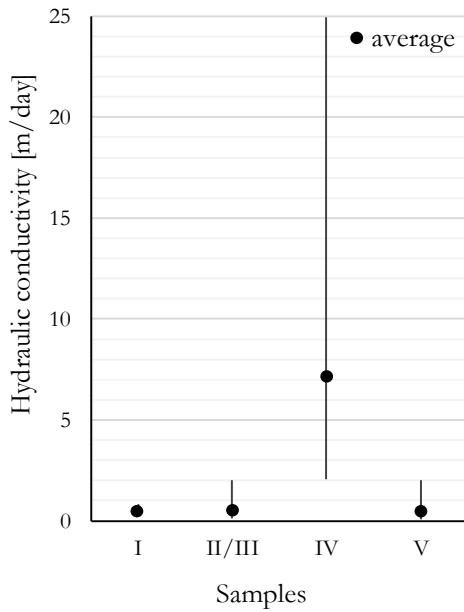


Figure 21. Average hydraulic conductivity and its standard deviation, calculated according to the soil classification triangle of the hydraulic group (Twarakavi et al., 2010).

The soil texture class, the hydraulic group and the corresponding hydraulic conductivity (K) were determined based on the soil classification triangle (Twarakavi et al., 2010) and are given in Table 3. The separation method does not impact the hydraulic and soil type classification (Table 3). For the hydraulic conductivity, the differences between the samples from the second layer (sample IV and V) are larger than the differences between top layer (sample I, II and III) and the second layer. Interestingly, sample type V is more similar to sample IV than to the other samples in terms of volume fraction of sand and silt but is more similar to the other samples in terms of hydraulic conductivity. The average hydraulic conductivity of the sample extracted from the pumping water (sample IV) is a factor ~ 15 larger than the conductivity of the other samples. However, the standard deviation of the hydraulic conductivity of sample IV is large, such that the minimum conductivity almost overlaps with conductivity of the other samples and the maximum conductivity is a factor ~ 48 larger than the other samples (Figure 21).

Discussion

Since initial division of all samples into 5 representative groups was only based on colour and texture classification in the field, the hydraulic conductivity of the representative sample cannot be generalized to its group. It only indicates that similar material was found at different locations.

The actual hydraulic conductivity of the second layer potentially deviates from the results of the grain size analysis, due to the presence of gravel in this layer. The content of gravel of the originating layer of sample IV was unknown, the gravel content of the originating layer of sample V was $> 50\%$ (Appendix H). The effect of the presence of gravel in a sandy matrix on the hydraulic conductivity, has been reported to be both positive (Wang et al., 2017) and negative (Bouwer & Rice, 1984) for the same range of gravel content. This further adds to the uncertainty of the hydraulic conductivity of the sample. In conclusion, the data is too limited to draw any conclusion upon for the hydraulic conductivity of the second layer.

The three samples from the top layer are quite similar regarding the hydraulic conductivity. Moreover, the standard error of the hydraulic conductivity was small. Therefore, the data was used to estimate the rainwater infiltration in the lower Terai as explained below. However, this is only an indication as infiltration capacity is also impacted by other factors - among them saturation and vegetation (Eagleson, 1978).

Table 4. Infiltration calculations from average hydraulic conductivity and rainfall data (Jha, 2000; Talchabhadel et al., 2019).

Hydraulic conductivity [mm/min]	Rainfall intensity [mm/min]	Infiltration [%]	Annual rainfall [mm]	Annual infiltration [mm]
0.36	1.53	23%	1000-1500	230-350

The rainfall intensity (Jha, 2000) and annual rainfall (Talchabhadel et al., 2019) were derived from a monitoring station slightly south of the study area: Gulariya (28°10', 81°21'). I estimated the percentual infiltration based on this data (Table 4), which corresponds well to previous estimations of 15% and 22.2 % (Shresta et al., 2018). The annual infiltration (Table 4) was somewhat lower than the rainfall infiltration of 460 mm and 635 mm according to previous research (Shresta et al., 2018). This may be explained by the higher rainfall in some parts of the Terai (Talchabhadel et al., 2019).

The grain size analysis is a useful tool for a first estimation of rainwater infiltration through the top layer. To improve our knowledge regarding the infiltration in the Terai, I recommend to perform infiltration tests rather than additional grain size analysis. Infiltration tests are more time consuming in the field but also cheaper and less time consuming afterwards since it does not require laboratory analysis. Moreover, infiltration tests provide information about the complete infiltration system instead of just one influential factor. I am especially interested in infiltration test in the upper Terai, as one-third of the total recharge of the Terai is thought to infiltrate through this zone (Shresta et al., 2018).

3.4 Pumping tests

Results

General

At location 1, the pump turned on and off a couple of times before the pumping test started. The pumping discharge was $1.3 \cdot 10^{-2} \text{ m}^3/\text{s}$. During the pumping, the water head in the first monitoring well dropped. The water head in the second monitoring well did not change. Semi-steady state was reached, after 50 minutes of continuous pumping. The first measurement took place 44 seconds after cessation of pumping and I continued monitoring until the water head returned to its initial state. The well is 10 m deep.

At location 2, the well was pumped for 4.5 hours with a pumping discharge of $0.24\text{-}0.25 \text{ m}^3/\text{s}$. The first measurement took place more than 4 minutes after cessation of pumping. The last measurement was before the water head returned to its initial state. The well has a depth of 113 m.

Recovery test

The recovery time exceeded the pumping time of 3000 seconds for location 1. Furthermore, the relation between the negative residual drawdown (s') and the time since cessation of pumping (t') was not linear for location 1 (Figure 22A). The relatively steep slope of the first 2 data points was assumed to result from the partial penetration of the well or from well-bore storage. Furthermore, I ascribed the deflection of slope beginning at the 10th datapoint (Figure 22A) to leakage from semi-permeable layers. In that case, the middle section (Figure 22A, filled circles) of the drawdown curve reflects the effect of the transmissivity of the aquifer. For this section, s' was linearly related to $\log(t'/t)$ ($R^2 = 1.00$; Figure 22C). The transmissivity was calculated from the slope. For location 2, plotting s' vs. t' resulted in a straight line (Figure 22B). Thus, all the data points were taken into account for the calculation of the transmissivity (Figure 22D). The correlation between s' and $\log(t'/t)$ was slightly less ($R^2 = 0.97$) than for location 1.

The transmissivities were $2.1 \cdot 10^3 \text{ m}^2/\text{day}$ and $2.3 \cdot 10^3 \text{ m}^2/\text{day}$ at respectively location 1 and location 2 (Table 5). The value of $\Delta s'$ is equal to the slope of the residual drawdown plots (Figure 22), as described by eq. 3. (chapter 2.5). The condition $\Delta s' > 0.1$ was nearly met for location 1 and amply met for location 2. The condition regarding the pumping time for partial penetrating wells is dependent on the layer thickness. The condition was met for a layer thickness up to 212 m at location 1 and up to 318 m at location 2, implying that the hydraulic conductivity should be at least 8.9 m/day and 2.1 m/day respectively (Table 5)

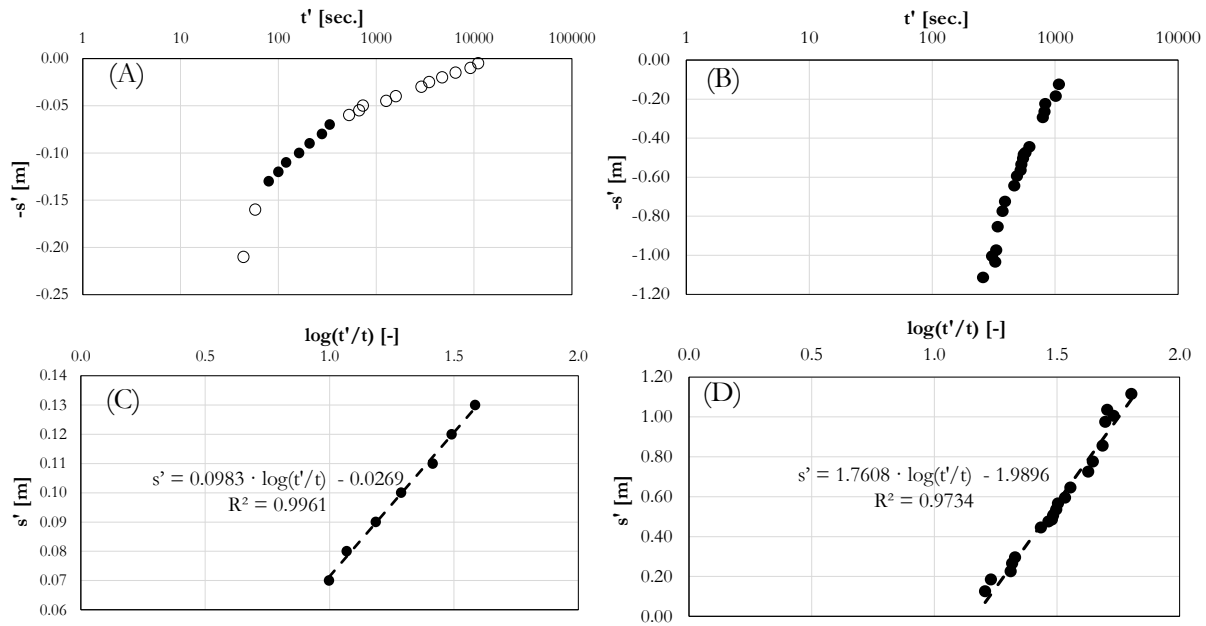


Figure 22. above: Plot of the negative residual drawdown versus the time after the cessation of pumping on a logarithmic axis, to determine which data points may be used for the calculation of the transmissivity (filled circles) and which not (open circles), for (A) location 1 and (B) location 2. below: The residual drawdown plotted vs. $\log(\text{time after start of pumping } (t)/\text{time after cessation of pumping } (t'))$, where slope of the trendline reflects $\Delta s'$ [-], for (C) location 1 and (D) location 2.

Table 5. Results and validation

Location:	Transmissivity [m ² /day]	$\Delta s'$ [m]	Max. layer thickness [m]	Min. K [m/day]
1: Dalla	$2.1 \cdot 10^3$	0.1	212	8.9
2: Betahanni	$2.3 \cdot 10^3$	1.7	381	2.1

Steady state test

I also calculated the transmissivity based on the steady state drawdown difference (S_m) between all possible combinations of the wells at location 1 using eq. 6 (chapter 2.5). The resulting transmissivity is $2.6 \cdot 10^3$ m²/day for all well combinations (Table 6). This is a factor ~ 1.2 larger than the transmissivity derived from the recovery test at the same location (Table 5). The validation of the assumptions of the recovery test are also applicable for the steady state test (Table 5).

Table 6. Results steady state test.

	Input		Transmissivity [m ² /day]		
	S_m [m]	r [m]	well 1	well 2	well 3
well 1	0.62	0.04	-	$2.3 \cdot 10^3$	$2.3 \cdot 10^3$
well 2	0.075	40	$2.3 \cdot 10^3$	-	$2.3 \cdot 10^3$
well 3	0	105	$2.3 \cdot 10^3$	$2.3 \cdot 10^3$	-

Sensitivity analyses

The sensitivity analysis for the pumping discharge at location 2 shows that the transmissivity is completely within the range of uncertainty for the transmissivity of the recovery test at location 1 – which is from $1.9 \cdot 10^3$ to $2.3 \cdot 10^3$ m²/day (Figure 23A). The pumping time at location 2 was also uncertain. However, a sensitivity analysis for the pumping time up to a deviation of an hour, demonstrated that the resulting transmissivity remained $2.3 \cdot 10^3$ m²/day. The results of the recovery test and the steady state test overlap for transmissivities between 2.1 and $2.4 \cdot 10^3$ m²/day (Figure 23A).

There was an additional limitation for the steady state test. The groundwater head of the pumping well in steady-state was uncertain as the first measurement took place 44 after the cessation of pumping. Therefore, I performed a sensitivity analysis for the steady-state drawdown of the pumping well (S_m) (Figure 23B). If the groundwater head in steady-state would have been equal to the groundwater head of the measurement 44 seconds after cessation of pumping, the transmissivity would be a factor 4 higher than for the extrapolated drawdown (Figure 23B). However, if I use a drawdown (S_m) smaller than 0.52 m for the pumping well (well 1) in the calculation of the transmissivity by eq. 6 (chapter 2.5), the calculated transmissivities of the different well combinations do no longer correspond, regardless of the value of the distance between the pumping well 1 and well 3 (r_3). Therefore, the steady-state drawdown must be larger than 0.52 m - corresponding to a transmissivity of $2.8 \cdot 10^3$ m²/day. Furthermore, the sensibility of the transmissivity for changes in S_m decreases for higher S_m values.

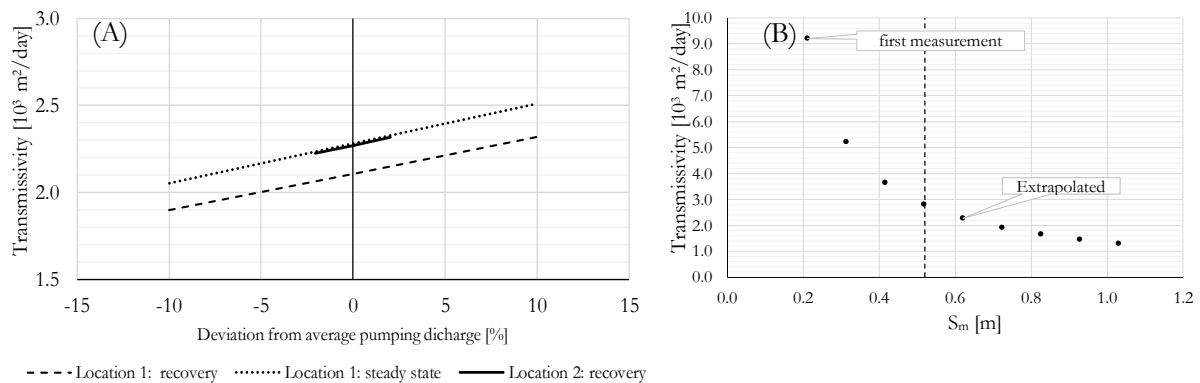


Figure 23. Sensitivity analysis for (A) the pumping discharge and (B) the difference between the initial water level and the water level in steady state (S_m).

Discussion

For location 1, the resulting transmissivity is dependent on which data points are included in the analyses. The data points were selected based on which processes I identified from the drawdown curve. At location 1, I interpreted that the drawdown curve reflected well-bore storage, partial penetration and leakage. Therefore, only the middle section was taken into account, giving a transmissivity of $2.1 \cdot 10^3 \text{ m}^2/\text{day}$. If I had assumed that leakage did not occur, I would only have selected the last section resulting in a transmissivity of $2.6 \cdot 10^3 \text{ m}^2/\text{day}$. However, judging by the various layers of finer material and the lack of clay as shown by the well log analysis, leakage through a semi-permeable layer is very likely process to occur.

For location 2, I was not able to identify processes from the drawdown curve as only a part of the recovery drawdown was monitored – resulting in a straight line. Judging by the monitoring times, this probably reflects the middle section of the total drawdown curve. Assuming that the same processes as at location 1 play a role in the recovery drawdown curve of location 2, this is the relevant section for the transmissivity calculations. However, the data is less reliable than if the complete recovery drawdown would have been monitored.

At location 1, the pumping time was shorter than the recovery time. This is associated with hysteresis processes in unconfined aquifers (Kruseman et al., 1970; Bunn, 2011). Interestingly, the drawdown curve does not reflect the effect of an unconfined aquifer. Differences in pumping and recovery time invalidates the principle of superposition, while this is the underlying principle of the analysis of the recovery test (Kruseman et al., 1970). However, the Theis recovery method is also applicable for unconfined aquifers if the early-time recovery data - which are affected by elastic storage - are excluded (Kruseman et al., 1970). Since I excluded the early-time recovery data for analysis, the results of this pumping test are valid, independent of the aquifer type. An other option is that the actual pumping time was slightly longer than reported, as the pump turned on and off a couple of time before the pumping test started. However, the effect was small: for the period where the recovery time exceeded the pumping time, the water head increased only 2 centimetre, which is only 3-4% of the total drawdown.

For the recovery test at location 1, the slope of the drawdown was slightly too small to meet the additional condition. However, this does not greatly impact the result as this condition only ensures the accuracy of determination of the slope. The drawdown curve suggested that the well at location 1 was only partially penetrating the aquifer, for location 2 it is yet unknown whether the well is fully penetrating the aquifer. The results of the pumping test are not valid for partially penetrating wells, unless the pumping time is sufficiently long. The required pumping time depends on the depth of the well and the thickness of the aquifer. For location 1 and location 2 the condition regarding the partial penetration of the well was met if the pumped aquifer has a thickness of respectively 212 and 318 m or less.

I expect the aquifer to be sufficiently small as the well log analysis showed that the subsurface consisted of many alternating layers of different permeabilities. Furthermore, the hydraulic conductivities corresponding to the maximum thicknesses of 212 and 318 m are respectively 8.9 m/day and 2.1 m/day. These hydraulic conductivities are within the range of hydraulic conductivity as estimated by the well log analysis (chapter 3.2).

The recovery test at location 1 shows that the transmissivity of location 1 ranges between $1.9 - 2.3 \cdot 10^3$ m²/day. The findings of the recovery test are supported by the results of the steady state test, which are in the same order of magnitude but less accurate but. The transmissivity of the well at location 2 was between the 2.2 and $2.3 \cdot 10^3$ m²/day. In other words, the transmissivities of the shallow well of location 1 and the deep well of location 2 are equal. Thus, it is possible that the tube wells pumped from the same aquifer. The most striking thing about the results is that the transmissivity was higher than was found in previous research in Bardiya: for shallow tube wells (~30 m) the transmissivity ranged between $2.6-6.1 \cdot 10^2$ m²/day and for deep wells (~16 m) between: $0.9-9.1 \cdot 10^2$ m²/day (Onta, 2004). However, the range of transmissivity in the whole Terai is large: it ranges between 5 m²/day and $1.6 \cdot 10^2$ m²/day (Onta, 2004). It was not specified in this report how many wells were tested and where they were located. Also, the original articles are not available. The differences regarding the transmissivity between the previous findings and our results may potentially be explained by the difference in locations, as the well log analysis (chapter 3.2) showed that the permeability of the subsurface was higher in the study area than southeast of the study area, where the highest permeabilities were measured close to the Karnali river within in the study area. However, this explanation only applies if the previous research was conducted at a considerable distance from the Karnali river or outside the study area.

To verify the above hypothesis and to get a robust understanding of the subsurface, I suggest to require more information about the previously performed pumping tests. Moreover, I suggest to perform additional pumping tests – especially at shallow wells further away from the river. Pumping tests in shallow wells only take a few hours and are easy and cheap to perform since wells for irrigation are usually equipped with a diesel pump. Using automatic pressure transducers instead of manual measurements will improve the accuracy of the data. I recommend to install the pressure transducer just after releasing the vacuum, as the automatic pressure transducer, which I installed before pumping at location 1, was pumped up with the water and broke.

3.5 Field observations water dynamics

Results and discussion

There are three main rivers in the study area: the Karnali river, the Babai river and the Aurahi river (Figure 24A). Besides these main rivers there are multiple monsoon rivers, which partially fall dry after the monsoon. The Karnali river splits up in two branches in the north of the park. The bulk of the water flows towards the western branch of the Karnali river. The Karnali river is braided and both branches exist of multiple smaller branches. From the most eastern subbranch, the Karnali river water was led to various irrigation channels – controlled by small dams (Figure 24B). Additionally, some of the irrigation water originated from the monsoon rivers. If the water in the irrigation channels is not used for irrigation, it flows to the Aurahi river, which ends in the Karnali river close to the border with India.



Figure 24. Overview of the area. (A) map study area, (B) small dam controlling an irrigation channel flowing towards Aurahi river (C) iron oxyhydroxides in Aurahi river and (D) Babai dam.

In the area between the Karnali river and the Aurahi river, the water from the channels was the main source of irrigation. Between the Aurahi river and the Babai river, groundwater was the main source for irrigation. Groundwater irrigation was usually not applied between September and December.

The Aurahi river originates from the spring in the hills, but it falls dry before it reaches the plain. The Aurahi river reappears downhill (Figure 24A) as the result of groundwater exfiltration – marked by bubbling water and iron oxyhydroxides (Figure 24C). These indications of groundwater exfiltration were also observed in the Karnali river in the south of the study area but not in the Babai river. There was a large dam in the Babai river (Figure 24D.). In the period of the field visit it only rained once at the 4th of November.

3.6 Groundwater heads

Results

General

The water head was monitored in 16 shallow wells, 1 middle deep and 2 deep wells. The monitoring locations are shown in Figure 25, where every location is labelled with a letter. This location label corresponds to the labels of the hydrographs (Figure 29). The depth of the shallow wells (wells B-K, wells M-Q) ranged between 4.4 and 11.6 m and the middle deep well was ~27m deep (well A). The deep wells were ~100 m deep (wells L and R) and were located near the shallow wells at location B and N. Refer to Appendix H for the well depth and pressure transducer type per location. The data of 4 pressure transducers were lost due to physical damage of the devices – all were Divers in active wells (wells F, G, H and K). At one of these locations, I did not measure the water head manually at the end of the monitoring period due to technical difficulties with opening the pump (well K). The data of pressure transducers in active wells (wells D, M and Q) were more scattered than in the inactive well but the general trend is clear. In deep well Q, the groundwater head varied 30 cm within a single day. This well was the drinking water source for the community and was constantly active.

The first day that the water heads were monitored in all locations was at October 30th 2018. For that day, I visualized the groundwater head below the surface (Figure 26) and relative to mean sea level (Figure 25). For the locations where the monitoring data was lost, I used the first manual monitoring point. The depth of the groundwater head at the shallow wells ranged from 1.54 m to 5.09 m below the surface (Figure 26). The depth of the groundwater head at the middle deep well was deeper: 7.39 m. The groundwater head was generally shallower close to the Babai river than close to the Karnali river. The deepest groundwater heads were found close to the foothills and relatively far away from the Karnali river and the Babai river.

Aquifer geometry

The groundwater head below the surface was compared with the depth of the top layer to determine where the aquifer was confined and where it was unconfined (Figure 26). However, the data on the depth of the top layer was limited. Close to the Karnali river in well E, the top layer was relatively thin (Figure 26). Here, the groundwater head was deeper than the top layer. Whereas in well C, the top layer reached deeper than the groundwater head. Furthermore, the results of the pumping test suggested that the aquifer was confined (chapter 3.4). The pumping test was executed in the south, at a distance of approximately 2 km from the Karnali river (Figure 26). I compared the hydrographs of the deep wells with the nearby shallow wells, to determine whether they were monitoring the same aquifer. The groundwater head at location B for both the shallow and the deep well dropped with a constant rate. However, the slope was steeper in the shallow well than in the deep well. While at location Q, the groundwater head dropped faster in the deep well than in the shallow well. For the middle deep well A, there was no corresponding shallow well. The slope of the hydrographs of the nearest shallow wells were gentler than in middle deep well A.

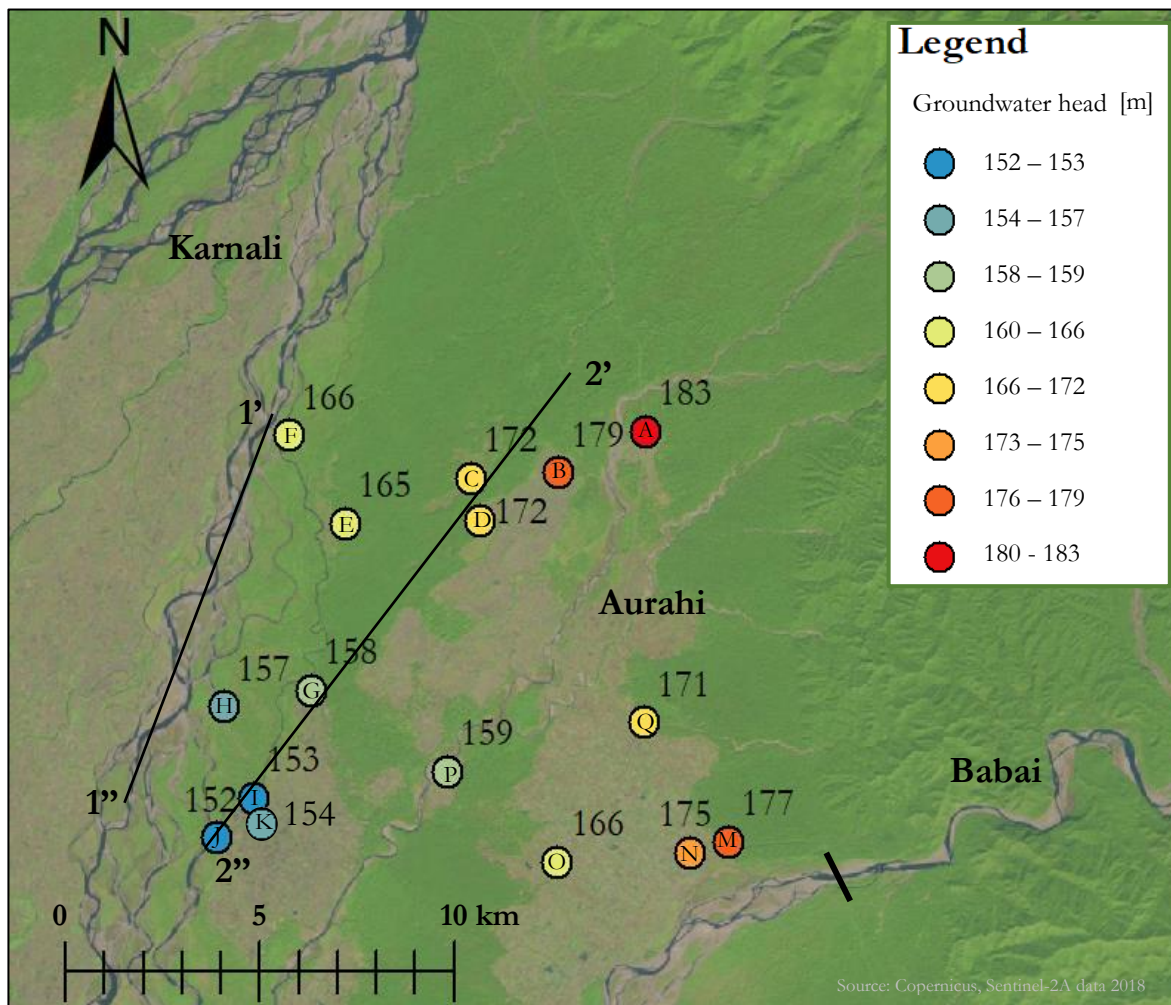


Figure 25. Groundwater heads [m] with respect to mean sea level of shallow wells and the middle deep well (well A) at October 30th 2018. The transects 1'-1'' and 2'-2'' correspond to respectively Figure 27A and Figure 27B.

Flow direction

The groundwater head relative to the mean sea level (Figure 25) demonstrated that the groundwater head was lowest in the south, near the Karnali river. Towards the foothills and towards the Babai river, the groundwater head relative to mean sea level was higher. The water level and gradient of the Karnali river was plotted with the gradient of the groundwater head in the wells near the river to further examine the flow direction (transect 1' – 1'', Figure 25). The water level of the Karnali river was found by using the minimum value from 10 parallel transects in the Karnali floodplain. Yet there was a large variation in the altitude of the Karnali floodplain, but the groundwater head was often higher than the Karnali water level. Also, the gradient of the Karnali river (-0.0017 m/m) was slightly steeper than of the groundwater (-0.0016) (Figure 27). Furthermore, I determined the hydraulic gradient of the groundwater between the Karnali river and the Aurahi river along transect 2'-2''. The hydraulic gradient parallel to the surface gradient (transect 2'-2'', Figure 25) was higher (-0.0021 m/m) (Figure 27) than the hydraulic gradient of the groundwater parallel to the Karnali river.

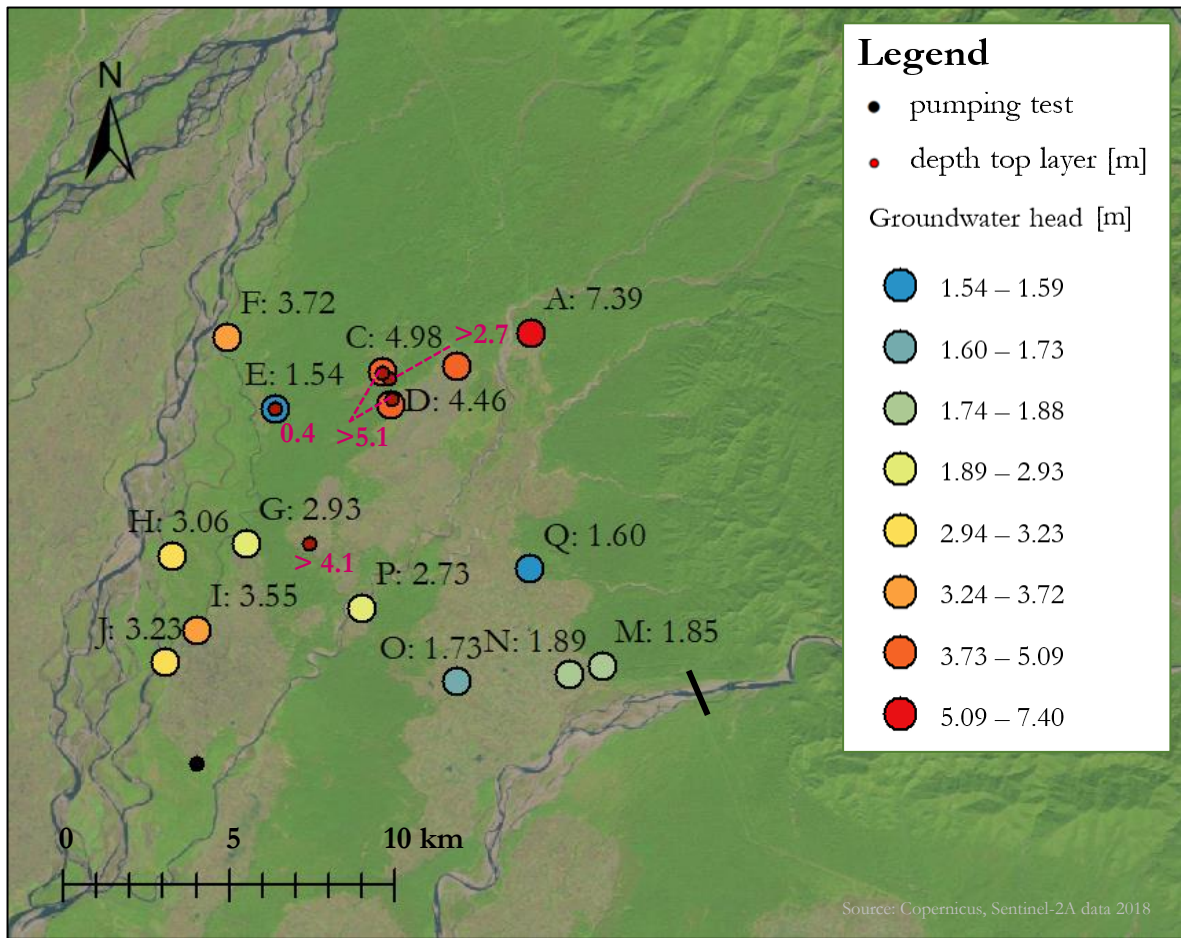


Figure 26. Groundwater heads below the surface [m]. The locations of the hand auger drillings and its corresponding top layer depth are given in pink. The location of the pumping test is also indicated.

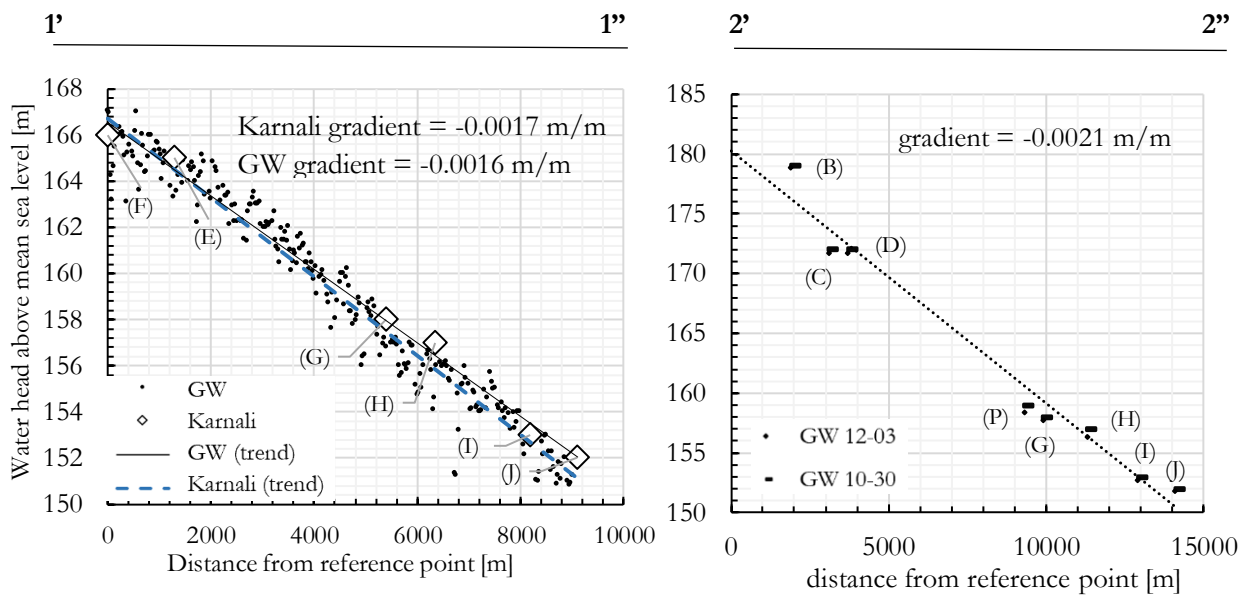
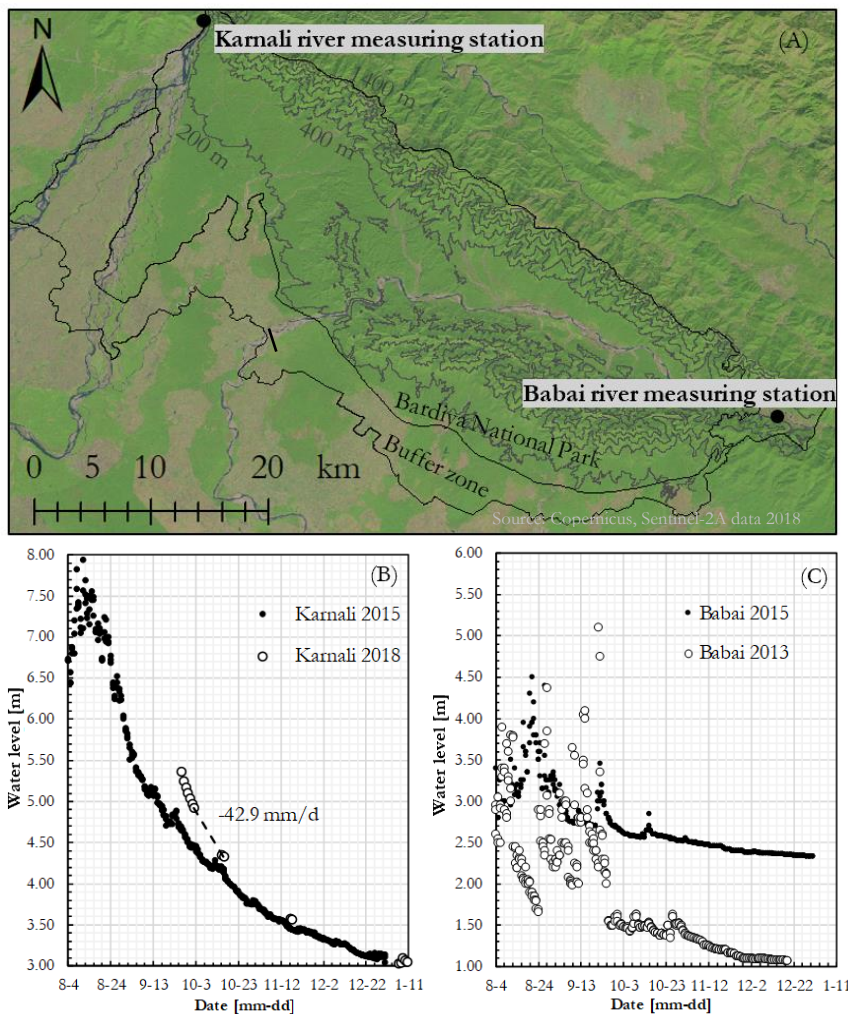


Figure 27. Groundwater heads at Oct. 30th 2018 in the wells parallel to the transects (Figure 25). For transect 1'-1'' only the wells near the Karnali river were included and compared to the river bed transect based on the DEM (JAXA, 2015) (A). In transect 2'-2'' the shallow wells near the transect were included (B).

Temporal trends rivers

The fluctuations in the groundwater head with time may potentially be related to the water level of the Karnali river and the Babai river. Therefore, I will first describe the curves of the water level in these river and subsequently compare them with the groundwater hydrographs. The Karnali river was monitored just upstream of the bifurcation of the river (Figure 28A; DHM, 2017). The water level of the Karnali river dropped 5 m in the period between August and December in 2015 (Figure 28B). The slope of the hydrograph was the steepest at the end of the rain season and decreased with time. In the beginning of October, the water level dropped with a rate of approximately 4 cm per day. The water level occasionally raised a few decimetres. In 2018, the water level was initially higher than in 2015. Nonetheless, the water level was similar to 2015 from half October on.



The monitoring station of the Babai river was located just upstream the eastern border of Bardiyia National Park (Figure 28A; DHM, 2017). The Babai dam is located downstream the monitoring station. The range of the water level in the Babai river (Figure 28C) between August and December was less than for the Karnali river (Figure 28B). The total drop of water level in this period was approximately 4 m in 2013 and only 2 m in 2015 (Figure 28C). Occasional rises in water level occurred more frequently and more pronounced in the Babai river than in the Karnali river.

Figure 28. The locations of DHM monitoring stations of the Karnali river and the Babai river (A). Hydrographs of the Karnali river in 2015 and 2018 (B) and of the Babai river in 2013 and 2015 (C). The water level was measured relative to the river bed. Data acquired from DHM.

Temporal trends groundwater

The hydrographs of the groundwater monitoring wells (Figure 29) are labelled with the letters A - R. These labels correspond to the labels in the other figures (Figure 25; Figure 26). Well L is the deep well near well B and well R is the deep well near well Q. The monitoring locations are divided into two groups: the Karnali river side and the Babai river side. The boundary between these groups is based on the distance to both rivers. I will start to describe the fluctuations in groundwater in the wells on the Karnali river side. Thereafter, I will do the same for the Babai river side.

The monitoring locations in the south of the study area on the Karnali river side (wells G, H, I and J) are all located at a distance of maximum 300 m from a branch of the Karnali river. The curves of these hydrographs (well G, I and J) are similar to the curve of the water level in the Karnali river: the slope was initially steep but decreased with time. From the 27th of November the groundwater in wells G, I, and J started to rise. There was no data available on the water level in the Karnali river for this period. However, the data of the Karnali river of 2015 demonstrates that the water level of the river does occasionally rise in this period of the year. The slope of the hydrograph of well I in the first week of October is similar to the slope of the Karnali river hydrograph in the first two weeks of October (2018). In well G, this initial slope is smaller. The slope in the first weeks of November is also larger in well I than in well G, but note that well G is located at a greater distance from the Karnali river than well I. At approximately the same altitude as well G, there was also a monitoring well at even a larger distance from the river (well P). I plotted the groundwater head of well G in the hydrograph of well P, such that the groundwater head of both wells overlap at the first measurement of well P, to compare the shape of the curves. This shows that at this altitude, the groundwater head drops slower near the river.

The monitoring wells A, B and C are located on the Karnali side, but relatively far from the river (> 5 km). Here, the drop of the groundwater head with time was linear. The slope of the hydrograph in well B was equal to the slope in well C. In middle deep well A, the slope was steeper. The average drop of groundwater head was smaller in wells B and C than in the wells close to the Karnali river in the south (well G, H and I), except for the location where the groundwater monitoring started later in the year (well J). The shape of the hydrograph of well D, which was located 500 metres downslope from well C, was slightly bended. Furthermore, the groundwater head dropped more than the groundwater head northeast of the well (well B and C), but less than southwest of the well near the river (well G, H and I). For the wells near the Karnali river in the north (well E and F), the average drop in groundwater head was less than in all other shallow wells. More specifically, well E was located between well D and well G in terms of altitude but the slope of the hydrograph of both well D and G was steeper than in well E.

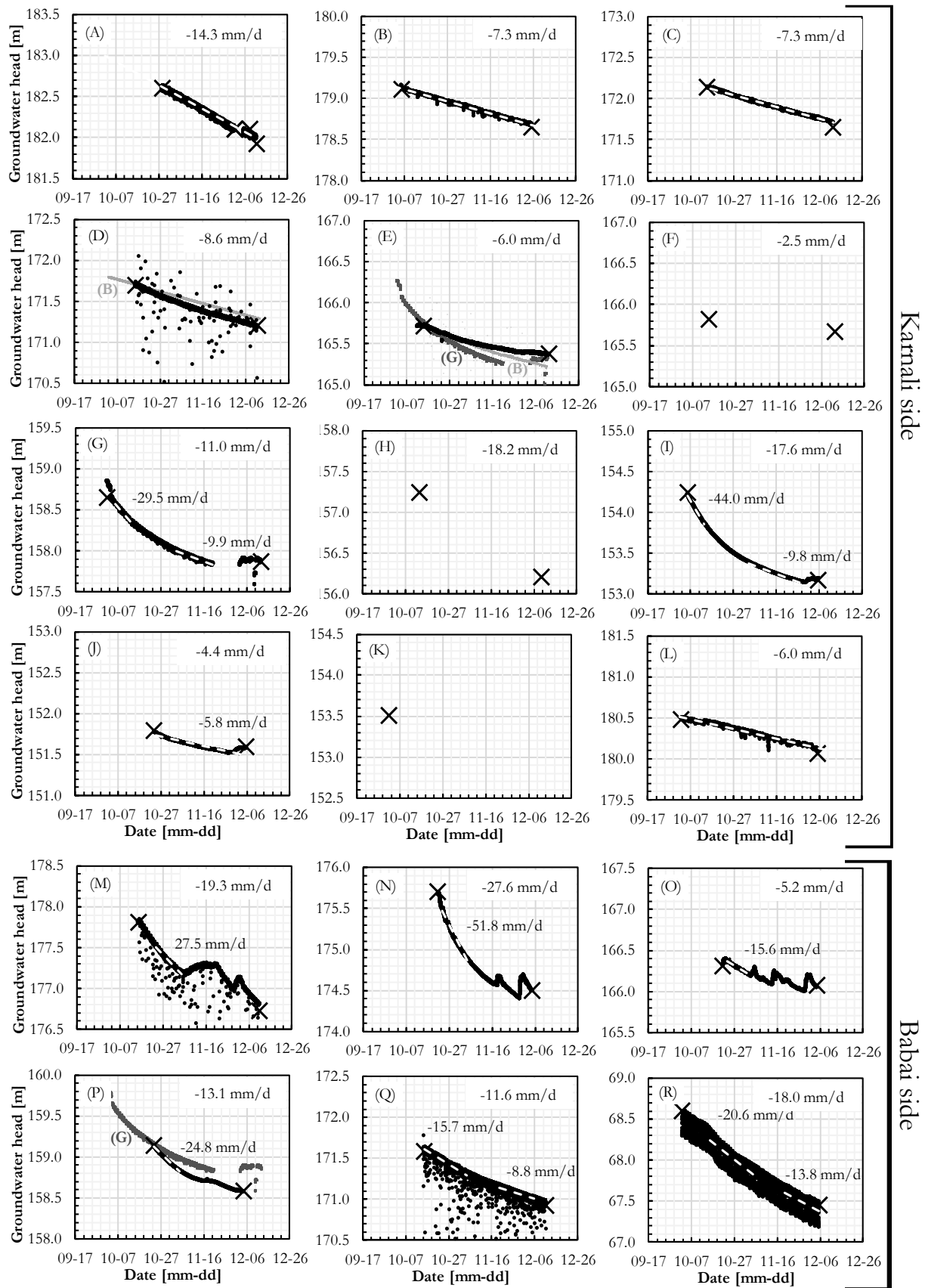


Figure 29. Hydrographs of groundwater monitoring wells. The well labels correspond to the well locations (Figure 25). The dots represent automatic monitoring, the crosses mark manual data points. The white, broken lines are trendlines. Their slopes are provided in the figures. The grey lines are data points of other wells, where the well is marked with a letter in brackets. The average daily drop of water level is given in the upper right corner.

On the Babai river side, the groundwater head in the wells near the Babai river (wells M, N and O) alternately raised and fell. This occasional rise in water level was also observed in the Babai river in 2013 and to a lesser extent in 2015. The rise and fall of the groundwater head at different wells did not occur simultaneously. Furthermore, the groundwater head in well O raised more often than in the other wells. This well was located at a relatively large distance from the Babai river. Also, the groundwater head at this location dropped with approximately the same rate as at the shallow well close to the foothills (well Q). While the drop in groundwater head in other wells near the Babai river (well M and N) was considerably higher.

Discussion

There are four obstacles for interpreting the groundwater head data. Firstly, the lack of knowledge about the geometry of the subsurface. This entails the depth, thickness and type of aquifers. This is problematic since it implies that the different wells may have monitored the groundwater head of different aquifers. I evaluated this possibility by comparing the fluctuations in groundwater head of the deep and middle deep wells with the shallow wells. The fluctuation in groundwater head in deep wells deviated from the nearby shallow wells. Thus, there are at least two aquifers in the first 100 m from the surface. The groundwater head of the deep wells probably represent a mixture of the heads of different aquifers as the screens of the deep wells were usually placed at multiple depths, judging by the borehole descriptions (Appendix AAppendix). The data of the deep wells were therefore not used for the interpretation of the flow in the shallow aquifer. The middle deep well is located more than 2 km from the nearest shallow well, thus I could not directly determine whether the head differences between these wells were due to the depth of the wells. I will further discuss this below. For the shallow wells, I assumed that they all penetrated the same aquifer. This assumption is not invalidated since the differences in groundwater head fluctuations could always be explained by other factors.

For most monitoring locations it is also unknown whether the aquifer is confined or unconfined. This is essential for the interpretation because the groundwater head in an unconfined aquifer represents the groundwater table whereas in an confined aquifer it represents the pressure level (Goulburn-Murray Water, 2015). The change pressure level is larger than the change in water table if the same amount of water is released. In other words, the changes in groundwater head are more pronounced in confined aquifers (Goulburn-Murray Water, 2015). At two locations, the type of aquifer is derived based on the comparison between the thickness of the top layer and the groundwater head with respect to the surface. In well E, near the Karnali river, the aquifer is unconfined. Whereas inland, in well C, the aquifer is confined. The pumping test in the south, at approximately 2 km from the Karnali river, also indicated that the aquifer is confined (chapter 3.4). I have concluded before that the loamy top layer may have eroded near the Karnali river (chapter 3.1), which suggests that the aquifer may be unconfined along the Karnali river. I have taken this possibility into account during the interpretation of the groundwater dynamics.

The second obstacle is the uncertainty regarding the altitude of the monitoring locations of the groundwater and the rivers. The vertical error of the digital elevation model (6.75 m) sometimes exceeded the altitude differences between the monitoring points. For the river beds, the DEM is even less reliable as the satellites cannot measure the altitude of the river bed underneath the water. Since the interpretation of the flow direction is based on the relative altitude differences, this should only be regarded as a first indication.

Thirdly, the data of the hydraulic head in the rivers is limited: there is no data available of the Babai river for the monitoring period and there is no data available at all about the Aurahi river. This complicated the interpretation of the groundwater heads. Fortunately, there is some data available on the water levels in the Karnali river during the monitoring period. However, there were only a few data points. Also, the measuring station of the Karnali river is upstream from the groundwater monitoring locations. Downstream from the Karnali river monitoring station, the fluctuations in hydraulic head may have been different due to differences in the width and the depth of the river. Because of these limitations, the relation between the Karnali river and the groundwater could not be determined quantitatively. However, the river data is helpful for the explanation of some trends in the groundwater.

Fourthly, the monitoring time is short. The flow of the Karnali river and the groundwater are dependent on precipitation, which varies per year and per season. Therefore, the conclusions only apply for the measuring period.

To the best of my knowledge, this is the first groundwater monitoring research in Bardiya National Park and its surroundings. However, there are 3 similar researches in the Ramganga sub-basin (Surinaidu et al., 2016), the Ilam district (Pathak, 2016) and the Rupandehi district (Rao et al., 1996). For the latter only the abstract is available. All districts are located in the Nepalese or Indian Terai and are at a distance of respectively 170 km west, 670 km east and 250 km east from Bardiya National Park. Where possible I will compare my findings with the results of these studies.

The flow direction is generally from northeast to southwest, judging by the gradient of the groundwater. In other words, the water flows from the hills and from the Babai river towards the Karnali river. According to other studies in the Terai, the groundwater also flows from the hills towards the south, due to the recharge in the Bhabar zone (Rao et al., 1996; Pathak, 2016; Surinaidu et al., 2016). Furthermore, in the Ramganga sub-basin, the groundwater flows towards both rivers in the area (Surinaidu et al., 2016). Whereas Rao et al. (1996) found that the piezometric surface had a wavy shape, due to recharge by rain water infiltration in present and former river beds. This may also apply for the piezometric surface in Bardiya National Park, as I observed multiple riverbanks where the poorly permeable top layers has eroded (chapter 3.1). However, the density of the monitoring wells is too low to verify this expectation.

For the altitude transect of the Karnali river, I took the local minimum of 10 parallel transects in the floodplain. Nevertheless there was still a large variation. Assuming that again only the local minima represent the river beds, the groundwater head was indeed higher than the river bed. Furthermore, the gradient of the river bed is slightly steeper than the gradient of the groundwater head. This suggest that the gradient between the Karnali river and the groundwater is larger downstream. The field visit supports this observation: there was groundwater exfiltration in the Karnali river in the southern part of the study area, whereas there were no indications for groundwater exfiltration in the north of the study area (chapter 3.5).

The groundwater head below the surface in the shallow wells ranged between 1.54 and 5.09 m just after the monsoon. This is comparable to the groundwater heads in other parts of the Terai at the same elevation. In the Ramganga sub-basin the groundwater heads were between 2.51 and 8.50 m deep in the pre-monsoon (Surinaidu et al., 2016) and in the Ilam district between 0.00 and 8.53 m deep, where the measuring period is not specified (Patak, 2016). In the southern part of the study area, the groundwater head below the surface gets deeper near the Karnali river, up to a depth of 3.55 m. While it was expected that the grasslands prevailed near the river because of the shallow groundwater head below the surface. Perhaps a groundwater head of 3.55 m deep is sufficiently shallow for the survival of the grasslands.

Towards the Siwalik foothills, the groundwater head below the surface became deeper. This is also found in other parts of the Terai (Pathak, 2016; Surinaidu et al., 2016). However, near the river the groundwater heads were still comparable to the groundwater heads in the south near the river. Based on these results, it is possible that the deep groundwater head below have been the limiting factor for the survival of the grasslands at a great distance from the Karnali river in the north. However the reason for the shallow groundwater heads below the surface near the Karnali river is different than expected. The hypothesis was that the groundwater head would be shallower near the river due to recharge of the Karnali river, but the flow direction derived from the groundwater heads relative to mean sea level suggested the opposite. Therefore, the relatively shallow groundwater head near the river in the north may rather result from the relatively low surface elevation near the river.

The groundwater head at the most northern monitoring locations dropped 7.3 mm per day. In the south, it dropped between the 11.0 and 18.2 mm per day. This is strikingly fast in comparison with the groundwater head in Ramganga sub-basin of the Terai. In that area, the groundwater head dropped with only 0.6 mm/day during the post-monsoon period (Surinaidu et al., 2016). Besides, it is interesting that the drop of the groundwater head was more pronounced downstream than upstream, the few exceptions will be discussed below. I assume that the drop of groundwater head in the post monsoon is either induced by a drop of the *upstream boundary condition* or a drop of the *downstream boundary condition*. A drop of the *upstream boundary condition* means the drop of the groundwater head at the water divide located at the Siwalik Hills. This may occur as the subsurface flow to areas with a lower groundwater head is not compensated by rain water infiltration during the post-monsoon. A drop of the *downstream boundary conditions* means a drop of the water level of a large water body during the post monsoon— for example the Karnali river

The above mentioned trend that the groundwater head drops faster downstream than upstream, implies that the changes in hydraulic head were mainly induced by a drop of the downstream boundary condition instead of a change in the upstream boundary condition. The drop of downstream boundary condition was most likely induced by groundwater discharge to the Karnali river, judging by the flow direction of the groundwater. This is also supported by the shape of the hydrograph curves of the wells near the Karnali river, which were similar to the hydrograph curve of the Karnali river.

The groundwater head at greater distances from the river, in north-eastern direction, showed similar bended curves but less pronounced. This indicates that the groundwater heads at these locations were also influenced by the Karnali river. Interestingly, the groundwater head in all the monitoring wells near the Karnali river raised a few centimetres at the end of November. The rise in groundwater head did not coincide with a rain event in BNP or surroundings during the study period. Hence, it must have been caused by the rise of the water level of the Karnali river. It is not possible to confirm this hypothesis since there was no data available of the Karnali river in this period. However, the data of 2015 does suggest that occasional rises in water level of the Karnali river are common during the post monsoon period.

The influence of the Karnali river reached up to well D, judging by the hydrographs. In well C, which is only 500 meters northward and at the same distance from the Karnali river as well D, the influence of the Karnali river is no longer reflected in the hydrograph. If the groundwater head in well D is directly influenced by the nearest branch of the Karnali river, I would expect a similar drop of groundwater head in well C. Therefore, the Karnali river rather indirectly influenced the groundwater head in well D by changing the groundwater gradient. This also supports the preliminary conclusion that the gradient between the Karnali river and the groundwater is larger downstream. In the eastern direction, the influence of the Karnali river reached up to somewhere between well G and well P. Well G and well P were approximately at the same altitude but well G is closer to the river. The groundwater head dropped faster in well P, suggesting that the drop of the groundwater head at this location was largely governed by processes other than the fluctuations in the hydraulic head of the Karnali river.

The drop of the groundwater head of some wells deviated from the general trend. Firstly, the groundwater head in the most upstream, middle deep well (well A) dropped faster than in the nearest wells downstream. This does not comply with the observation that the drop of the groundwater head was mainly induced by the drop of the downstream boundary condition. It is therefore likely that this middle deep well has monitored a deeper aquifer. Secondly, the drop of the groundwater head in the wells near the upper Karnali river is less than in the wells at a large distance from the river at the same altitude.

This may indicate that the groundwater near the Karnali river in the north of the study area becomes recharged by the river. In that case, the groundwater head near the northern part of the Karnali river must have been deeper than the water level of the Karnali river itself whereas the groundwater head near the Karnali river in the south of the study area was higher than the water level of the Karnali river. This is possible as the gradient of the Karnali river is larger than the hydraulic gradient of the groundwater along the Karnali river. On the other hand, exfiltration in the upstream areas is opposed by the preliminary conclusion regarding the flow direction, based upon the spatial distribution of the groundwater head relative to the mean sea level. Moreover, the reduced drop of the groundwater head can also be caused by an other process: the shallow aquifer penetrated by the well near the river (well E), is in all probability unconfined whereas the aquifer further inland (well C) is confined – as explained above. This means that the reduced drop in groundwater head near the river relative to well C, may still have reflected a larger release of

groundwater. This explanation is more likely. In line with this reasoning, well F must also have been monitoring an unconfined aquifer. Furthermore, I previously suggested that the aquifer may be unconfined along the entire Karnali river. However, the large drop of groundwater head near the Karnali river in the south of the study area does not support this suggestion.

The groundwater head at the Babai river side dropped generally faster than at the Karnali river side. This suggests that the groundwater head was mainly controlled by the drop of the hydraulic head of the groundwater in the hills or of the Babai river, instead of by the drop in the hydraulic head of the Karnali river. Furthermore, the groundwater head near the Babai river alternately raised and fell. Since the rise and drop of the hydraulic head also occurred in the Babai river in 2013 and 2015, this phenomena may be ascribed to influence of the Babai river – implying that the hydraulic head in the Babai river was often higher than of the nearby groundwater. However, the alternating rises and falls of the groundwater head at different locations do not exactly correspond, meaning that the relation between groundwater and river is slightly more complex than on the Karnali river side of the study area. I cannot explain these differences since there is no data available of the Babai river in 2018 but I expect it to be governed by the interaction of heterogeneities of the subsurface, the effect of the dam in the Babai river and influences of other small rivers or channels. To summarize, the Babai river does influence the groundwater head but the exact dynamics between groundwater and the Babai river are yet unclear.

The water head differences between the different monitoring locations determine the flow path of the water. Therefore, the groundwater heads relative to mean sea level potentially contains interesting information. However, the full potential of the water head data is not reached due to errors in the DEM. I therefore recommend to improve the DEM. I strived to improve the elevation model by converting the differences in air pressure between various locations to differences in altitude. However, the error of the relative altitude calculated by differences in air pressure proved to be larger than the error of the DEM. There are three other options to improve the DEM. Firstly, by purchasing a DEM with better accuracy. Secondly, by mapping the relative altitude using a levelling rod. Since measuring altitude differences with a levelling rod is time consuming, I recommend to focus on the altitude difference between the hydraulic head of the river and the groundwater at a transect parallel to the Karnali river.

Furthermore, I have a few suggestions to further examine the extent of the impact of the Karnali river on the groundwater head land inwards. The first suggestion is to add monitoring points between location (NTNC) and location P. I recommend to use an inactive well for the monitoring to reduce the risk on data loss. The second suggestion is to monitor the water head of the Aurahi river. This way, the effect of the Karnali river may be distinguished from the effect of the Aurahi river. Finally, it would be interesting to know how the fluctuations in the groundwater head evolves in other periods of the year.

3.7 Isotopic composition

Results

The average $\delta^2\text{H}$ were plotted versus the average $\delta^{18}\text{O}$ of the replicated samples (Figure 30). The data set is provided in Appendix K. The sampled groundwater, spring water and river water were $\delta^2\text{H}$ - and $\delta^{18}\text{O}$ relative to the VSMOW value. Furthermore, the samples were found to be approximately at the Global Meteoric Water Line (GMWL). Though most samples were slightly underneath this line. The samples from the Karnali river were lighter than almost all groundwater samples. The isotopic composition of the water from the Babai river and the Aurahi river were comparable to the groundwater. The deviation from the GMWL was more pronounced for the rain samples than for all the other samples. Also, the rain water was heavier than the groundwater. Furthermore, the samples from the single nocturnal rain event in November were isotopically enriched. In Figure 30, these samples are labelled with the time of sampling. The longer the time between the rain fall and the sampling, the lighter the sampled water. In contrast to the other rain samples, the differences between the rain water sample which was accumulated in the watch tower and the groundwater samples were small.

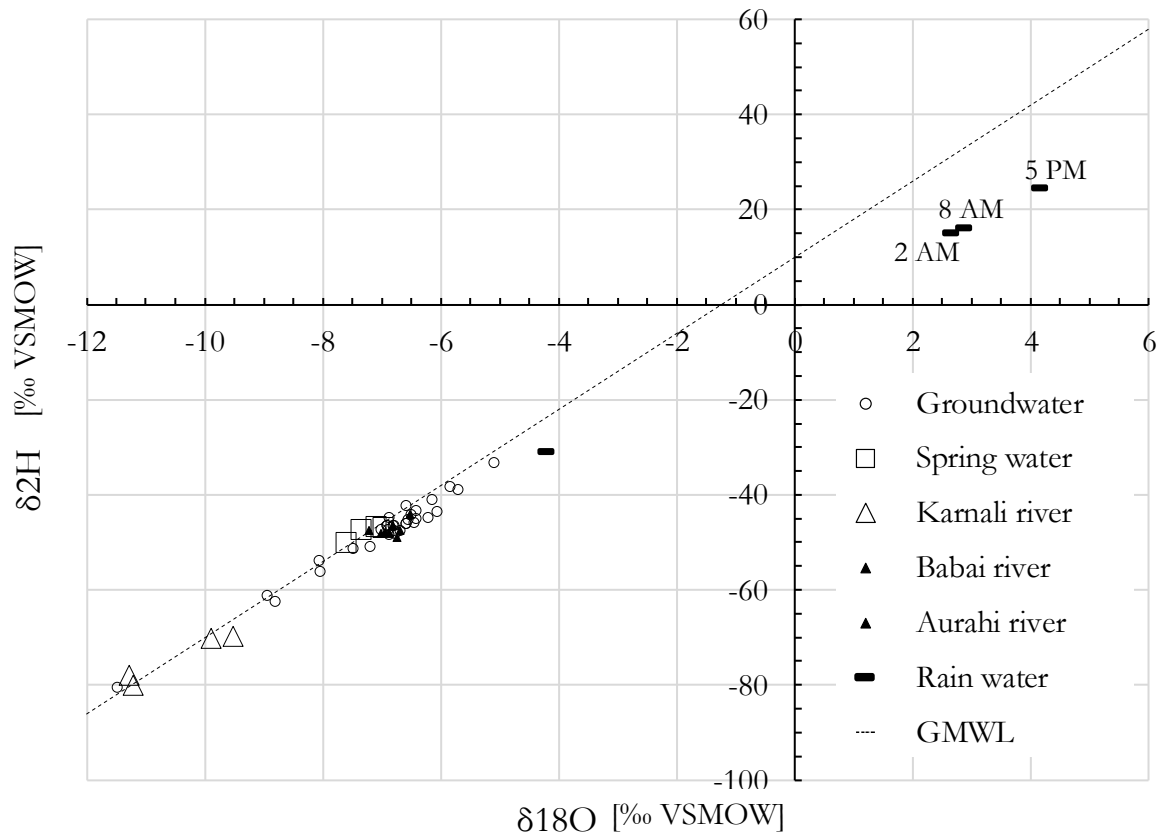


Figure 30. Isotope composition of samples from the study area.

We analysed the fluctuations in isotopic composition of rain water samples of the 5 nearest locations to Bardiya National Park (Figure 31). The rain water composition of the locations at highest altitude (Nainital and Rikikesh) were generally most $\delta^{18}\text{O}$ depleted. However, the fluctuations per month and per season were larger than the differences between the locations. The seasonal trends were analysed for New Delhi as most samples were available for this location. For New Delhi, the peak of $\delta^{18}\text{O}$ abundance in rain water was between February and March. The $\delta^{18}\text{O}$ isotopes were least abundant in the rain water between July and September. In New Delhi, the rain water of November was on average isotopically lighter than in the first month of the monsoon (June) and heavier than the last three months of the monsoon (July-September). It is uncertain whether the rain water at the other locations followed the same seasonal trend, due to a lack of data points. The isotopic composition of the rain water samples of New Delhi from November 1982 were comparable to composition of rain water for this study, which were also sampled in November. In other years, the rain water of New Delhi was lighter.

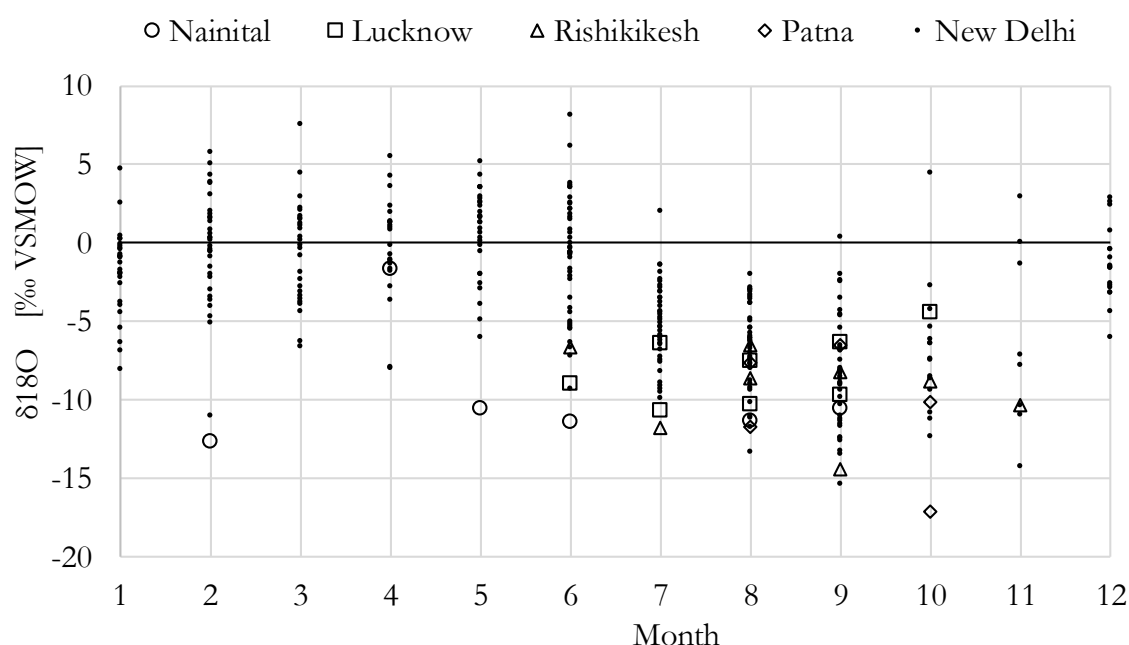


Figure 31. Isotope composition of precipitation of nearby monitoring points in India: Nainital 1995 (Kumar et al. 2010A), Lucknow 2003-2004, Rishikikesh 2005 -2006, Patna 2003-2005 (Kumar et al. 2010B) and New Delhi 1960-2012 (India Meteorological Dept., Safdarjung Airport, Delhi). Collected from: IAEA/WMO (2019).

The spatial distribution of the $\delta^{18}\text{O}$ value of the groundwater-, river-, and spring samples are shown in Figure 32. The water of the springs in the north of the park were more isotopically depleted than most of the groundwater samples. The $\delta^{18}\text{O}$ value of the Aurahi river- and Babai river samples was comparable to the spring water. The least isotopically depleted groundwater samples were all found at relative low altitudes. The isotopic composition of the most northern deep well was similar to the nearest shallow well.

For the other two deep wells, there was a difference between the deep and shallow well of 1.1 ‰ VSMOW and 1.4‰ VSMOW from west to east respectively. The most isotopically depleted groundwater samples were found in the buffer zone, along the Karnali river. Note that the other groundwaters samples along the Karnali river within the boundaries of BNP were all less isotopically depleted than the spring water samples. The water from the Karnali river was lighter upstream than downstream. However, besides a spatial difference between the samples, there was also a temporal difference: the upstream river water was sampled later in the year than downstream (Table 7). Furthermore, the upstream samples were slightly above the GMWL and the downstream samples slightly underneath (Figure 30).

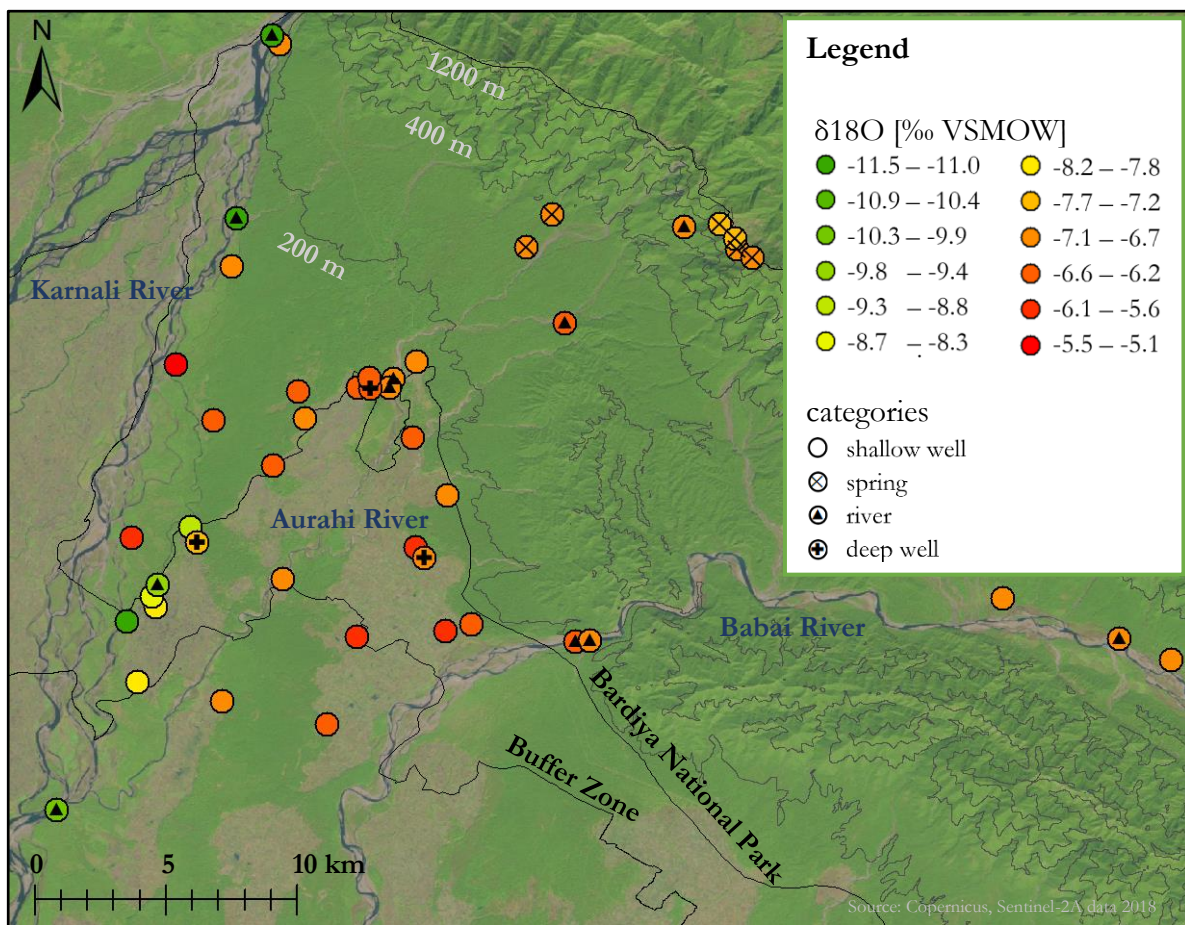


Figure 32. Spatial distribution of $\delta^{18}\text{O}$ in water samples

Table 7. $\delta^{18}\text{O}$ abundance in Karnali river samples.

no.	Distance from upstream sample [km]	Sample date [mm-dd-yyyy]	$\delta^{18}\text{O}$ [‰ VSMOW]	Channel type
1	0	10-15-2018	-11.23	Main channel
2	7	11-20-2018	-11.24	Main channel
3	23	10-05-2018	-9.53	Branch
4	31	10-07-2018	-9.90	Main channel

Discussion

The aim of the analysis of the isotopic composition of the water samples was to examine the extent of the influence of the Karnali river. I already concluded that the groundwater there infiltrates in the Karnali river instead of the other way around - at least during the post-monsoon of 2018 (chapter 3.6). However, the isotopic analysis of the groundwater and Karnali river water samples provide the opportunity to observe whether the Karnali infiltrated the subsurface during other periods. However, the sampling locations within BNP were limited.

I will first evaluate the reliability of the rain water samples by comparing the isotopic composition with GMWL, the groundwater samples and the composition of the precipitation of nearby monitoring points. Secondly, I will discuss the spatial variation in groundwater samples based on the composition of the spring samples, the rain samples and the Karnali river samples. Thirdly, I will examine the flow between the groundwater and the Karnali river based on the changes in the Karnali river from the north to the south of the study area. Where possible, I will compare the results and interpretation to a previous study in the Terai regarding the effect of a river on the groundwater composition, by Siegel and Jenkins (1987). They examined the groundwater composition along the Tinau river (Figure 33A). The Tinau river also flows through an alluvial fan in Rupandehi district, 200 km southeast of Bardiya National Park.

The majority of my samples plotted slightly under the GMWL. The deviation from the GMWL was most pronounced for the rain samples. This type of isotopic fractionation indicates kinetic evaporation (Dansgaard, 1964; Gat & Tzur, 1967). Kinetic evaporation entails that $\delta^{16}\text{O}$ and $\delta^1\text{H}$ do not evaporate in equilibrium ratio due to a high evaporation rate (Dansgaard, 1964). Evaporation may occur during precipitation, in open waters or during sampling. Once rain reaches the subsurface, changes in isotopic composition due to evaporation are prevented (Gat & Tzur, 1967). Therefore, the observed fractionation is only problematic for the interpretation if it has occurred during sampling. The fractionation of the rain samples has probably already taken place during precipitation, as the precipitation of the 5 locations near BNP is also generally underneath the GMWL. The Meteoric Water Line (MWL) of the Gangetic plains has a slope of approximately 7 (Lamb et al., 2005), whereas the GMWL has a slope of approximately 8. Moreover, the rain event was of low intensity – which usually results in kinetic evaporation and thereby in fractionation (Dansgaard, 1964).

On top of the fractionation, there was also a difference in isotopic composition between the samples from the same rain event, yet the samples were all fractionated to approximately the same degree. This indicates equilibrium or slow evaporation (Dansgaard, 1964). Two of the three samples have been in a collection bucket for a few hours before sampling. The slow evaporation has probably occurred in during this time as the $\delta^{18}\text{O}$ and $\delta^2\text{H}$ -values were positively related to the time that the water was exposed to air in the collection bucket before sampling. Thus, only the water which was directly sampled after the rain event was not disturbed by evaporation in the collection bucket.

Nonetheless, this sample does not represent the general isotopic composition of the rain water since there is a large variability in isotopic composition of precipitation (Gat & Tzur, 1967), as also demonstrated by the New Delhi samples. Moreover, the rain intensity of the monsoon is higher than during a small rain event in November as now sampled, resulting in less evaporation and thus in less isotopic enrichment. The sample that has accumulated in the watch tower before the field study is therefore more likely to represent the isotopic composition of the bulk of the rain water, as it has probably precipitated in the monsoon. This relatively light rain water sample indeed approximates the isotopic composition of the groundwater samples— in contrast to the other rain samples. Naturally, this sample is not completely reliable as the precipitation date and thereby the extent of evaporation is uncertain. However, it is the best available approximation.

Based on the assumption that the lightest rain sample represents the rain water of its sample location, in combination with the general trend that the $\delta^{18}\text{O}$ value of precipitation decreases 0.28‰ VSMOW per 100 m of increasing elevation (Hoefs, 2009), I expect an $\delta^{18}\text{O}$ value of approximately -7 ‰ VSMOW for the precipitation at the highest elevation in the park. This corresponds well with the observed isotopic composition of the sampled spring water. Thus, the isotopic composition of the rain fall in the park will roughly be between the rain sample and the spring samples— dependent on the location. Most groundwater samples were more isotopically depleted than the rain sample and equally or less depleted as spring water. Hence, these waters may purely exist of rain water, mixed from different altitudes. Whereas the groundwater samples which were lighter than the spring water reveal influence of the Karnali river.

The average $\delta^{18}\text{O}$ value of spring water in Bardiya and in the Rupendehi district (Figure 33B; Siegel & Jenkins, 1987) were equal (-7.2 ‰ SMOW). Whereas the range of isotopic composition of BNP samples (-5.1 to -11.5 ‰ SMOW) was larger than in the Rupendehi district (-6.4 to -10.3 ‰ VSMOW; Figure 33B). The large range in $\delta^{18}\text{O}$ value between the spring sample and the heaviest sample in BNP relative to the Rupendehi district samples, may be explained by the relatively large altitude differences in the study area which results in a large variation of isotopic composition of the precipitation. Furthermore, the difference between the spring water and the lightest groundwater sample was also larger for BNP than for the Rupendehi district. This may be ascribed by the difference in isotopic composition of the snow-fed Karnali river, with a $\delta^{18}\text{O}$ value of -9.5 to -11.3 ‰ VSMOW and the rain-fed Tinau river, which had a $\delta^{18}\text{O}$ value between -8.2 and -6.4 ‰ VSMOW.

The isotopic composition of the groundwater along the entire Karnali river did not reflect any influence of the Karnali river as their $\delta^{18}\text{O}$ values were all within the estimated range of rain water in the study area. This supports the conclusion that there was no infiltration of Karnali water into the subsurface chapter during the study period (chapter 3.6). Moreover, it indicates that there is also no infiltration of the Karnali river during the rest of the year. However, the samples only represent the groundwater at the depth of the filters of the well, which are at 5 to 6 m deep. Perhaps the Karnali river does infiltrate in the shallower groundwater.

In contrast to this study, all the groundwater samples of the Rupendehi district which were lighter than the spring water were found in the north of the study area (Siegel & Jenkins, 1987). Therefore, they concluded that groundwater was mainly influenced by the Tinau river in the north of the study area. However, their interpretation was different: they ascribed the lack of influence at the most southern groundwater sampling points to a low permeability instead of to the inflow of groundwater. Their explanation is not valid for BNP as the fluctuations in groundwater head proved that the river water level affected the groundwater head near the Karnali river in the south of the study area.

To further examine the interaction between the Karnali river and the groundwater, I will discuss the isotopic composition of the samples from the Karnali river. The isotopically enrichment of the river samples downstream relative to river samples upstream, may indicate the exfiltration of groundwater. However, the difference may as well be due to two other reasons: 1. Seasonal fluctuation or 2. Evaporation. Isotopic research of Indian rivers (Lamb et al., 2005) shows that there are indeed significant seasonal fluctuations (Figure 34). However, in the period when the Karnali river was sampled, between October and half November, the $\delta^{18}\text{O}$ -value in these rivers remained constant or slightly increased. This suggests that the difference in isotopic composition of upstream and downstream cannot be caused by seasonal fluctuations.

For the evaluation of the potential effect of evaporation, I compare the change of the upstream- and downstream Karnali river samples with the change of the morning- and afternoon rain water samples. The percentual change of $\delta^{18}\text{O}$ was similar. The arrival time of the Karnali from the upstream to the downstream sample is approximately 1 hour and maximally 8 hours (van Kooten, unpublished), meaning that the time of air exposure is lower or similar to the rain water samples. There is only one important difference: the amount of rain water was small thus practically all the water was exposed to air whereas for the Karnali river only the shallow surface water was exposed to air. Therefore, the change in isotopic composition of Karnali river water between upstream and downstream is probably partly caused by inflow of groundwater – supporting the preliminary conclusion that the groundwater is exfiltrating into the Karnali river.

If the changes between the upstream Karnali river samples were caused by inflow of groundwater, then isotopic composition of the samples is only expected to be changed in the area where the groundwater is exfiltrating into the Karnali river. The isotopic composition of the first two Karnali river samples from the north (no. 1 and no. 2), in the area where the groundwater is probably exfiltrating into the Karnali river to a lesser extent (chapter 3.6), were indeed almost equal. Whereas there was a large difference between the

second and third sample from the north (no. 2 and no. 3). Sample no. 3 was slightly less isotopically depleted than the fourth sample. This difference is probably due to the lesser amount of water in the branch of the Karnali of sample no. 2 than in the main channel, where sample no. 4 was taken. Because, if there is less water the effect of inflowing groundwater is more pronounced.

The trend in the Karnali river was also found in the Tinau river in the study of Siegel and Jenkins (1987): there was only a small change of 0.1 ‰ between the two most northern samples in the Tinau river, coinciding with the area where the Tinau was flowing towards the groundwater. While the third sample was 2.0 ‰ heavier than the most northern sample (Figure 33B). Siegel and Jenkins (1997) did not comment on this difference, but the results suggest that the groundwater was also exfiltrating into the river in the south of the study area in the Rupendehi district. This contradicts their conclusion that there was no impact of the Tinau river in the south due to a low permeability.

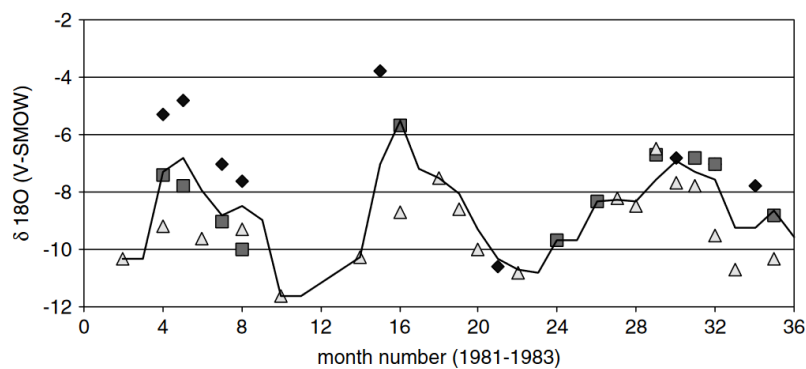


Figure 34. Visualisation of the seasonal effects of the $\delta^{18}\text{O}$ for the Himalayan rivers: Ganga (rhombus), Brahmaputra (square), Indus (triangle). The solid line is the moving average calculated from the average value per month. Derived from: Lambs et al., (2015).

The most interesting conclusion of the isotopic analysis is that irrigation of Karnali river water substantially recharges the groundwater in the buffer zone. Besides irrigation, there was no indication for infiltration of Karnali river water into the subsurface. However, the sampling locations within the boundaries of BNP were limited. It would be interesting to collect additional samples for analysis, but then new wells need to be installed. This is costly and unfeasible in most of the area due to a deep groundwater head. It could therefore also be interesting to sample over a period of time. Furthermore, the Karnali river samples suggested exfiltration of groundwater into the Karnali river. Future research may further examine the exfiltration of groundwater in the river by sampling Karnali river water in a transect from north to south at the same day.

3.8 Synthesis

This reconnaissance study to the groundwater system consists of multiple analyses, which all contribute to a better understanding of the system. The results of the various analyses are often complementary. In some cases, the results of an analysis change the interpretation of other analyses. In this section, I will highlight the results which in particular demonstrate the added value of analysing different components. Thereafter, I will return to the objective of the study and shortly discuss what the findings imply for the conservation of the wild tiger.

The well log analysis suggests that the permeability of the subsurface is higher within the study area than to the southeast of the study area. Also, the permeability was probably the largest near the Karnali river. This explains why I found a higher transmissivity with a pumping test near the Karnali river than was expected based on the previous pumping tests in Bardiya region. Furthermore, the relatively high transmissivity is in line with the results of the groundwater monitoring, which indicated a considerable influence of the Karnali river and the Babai river on the groundwater system.

I observed in the field that the sandy and gravelly subsurface is largely overlain by a loamy top layer. The grain size analysis demonstrated that the hydraulic conductivity of the top layer is relatively low. Implying that the shallow aquifer is confined, provided that the top layer reaches deeper than the groundwater head. The latter was tested by comparing the thickness of the top layer, according to hand auger drillings, with the depth of the groundwater head. This comparison appeared to be essential for the interpretation of the groundwater dynamics, in particular for two wells along the Karnali river in the north of the study area.

The relatively small drop in the groundwater head in those wells was initially ascribed to infiltration of the Karnali river. But, the comparison of the thickness of the top layer with the depth of the groundwater head demonstrated that the aquifer was unconfined in this area. Therefore, the reduced drop of the groundwater is rather the effect of the aquifer type, as the water table drops less in an unconfined aquifer than in a confined aquifer for the same amount of water released. The analysis of the isotopic composition of the water samples is also in accordance with this hypothesis, as there are no indications for the infiltration of Karnali river water in the groundwater samples of BNP. Whereas the composition of the groundwater samples from the buffer zone do reveal the influence of Karnali river water. The observation that the irrigation water largely originates from the Karnali river in this area was required to explain that finding.

Altogether, this study was the first step in the understanding of the groundwater system of the west part of BNP and surroundings. It demonstrates that the Karnali river plays a major role in the depth of the groundwater head along the Karnali river. On the one hand, it endorses the hypothesis that changes in the level of the Karnali river – for example due to the modernization and intensification of the irrigation system – may change the groundwater head. Thereby it potentially have problematic consequences for the tall grasslands, the deer and eventually also the wild tiger.

On the other hand, it creates the opportunity to manage the groundwater head with relatively simple interventions, for example by excavation of the east branch of the Karnali river at the bifurcation. However, this research is not sufficient for making quantitative predictions about the effect of potential changes or interventions. Therefore, I recommend to develop a geohydrological computer model of Bardiya National Park, based on the results of this study. The features of the subsurface may be used as input parameters and the groundwater measurements as calibration. Additionally, two groundwater monitoring locations in Bardiya National Park are still active. The data of these monitoring stations may be used to calibrate the model for other seasons.

4 Conclusion

4.1 What are the main characteristics of the subsurface?

a. How does the subsurface of BNP relate to the general geological setting of the Terai?

The Terai is subdivided into the upper, middle and lower Terai. The upper- and middle Terai consist of alluvial fan deposits. The boundaries between these geological zones in BNP were not mapped, but the width of the upper Terai was at most 6.5 km. This is small in comparison with other parts of the Terai where the upper Terai is 10 to 15 km wide. The lower Terai consists of Gangetic alluvium according to previous studies. However, I concluded that at least the top layer of the lower Terai is a limnological deposit.

b. What is the transmissivity of the shallow aquifer?

The first 100 m of the subsurface of the lower Terai consist of multiple layers ranging from clay to gravel, forming at least two distinct aquifers. The permeability of the subsurface seem to increase towards the Siwalik foothills. Near the Karnali river, the subsurface was found to be most permeable. The transmissivity was measured at one location in the shallow aquifer near the Karnali river, giving a transmissivity of $1.9 - 2.8 \cdot 10^3 \text{ m}^2/\text{day}$. This is a high value in comparison with previous studies. The increased permeability towards the Siwalik foothills and the Karnali river is in line with the theory that the first $\sim 1500 \text{ m}$ from the Terai subsurface was formed by coalescing alluvial fans from the Siwalik hills, including the Karnali mega-fan.

c. What is the hydraulic conductivity of the top layer?

The shallow aquifer is overlain by a less permeable top layer. This top layer consists of silt loam, with a hydraulic conductivity between 0.2 and 2.0 m/day.

d. What aquifer type is the shallow aquifer?

The aquifer generally seemed to be confined. However, at the locations where the groundwater table reaches deeper than the top layer, the aquifer may be considered as unconfined. This was only found once, near the Karnali river in the north of the park, where the top layer was relatively thin due to erosion. There may be more locations where the aquifer is unconfined, due to either a thin top layer or a deep water table.

4.2 What are the current groundwater dynamics?

- a. **What is the depth of the groundwater head along the Karnali river and in the rest of the study area in the post monsoon?**

The groundwater head below the surface in the shallow wells ranged between 1.54 and 5.09 m just after the monsoon. Near the Karnali river, the maximum groundwater head below the surface was only 3.72 m. This is in line with the argumentation that grasslands prevail near the Karnali river because of the shallow groundwater head.

- b. **What are the main zones of groundwater recharge and discharge?**

Groundwater recharge by rain water infiltration in the Terai is thought to occur largely in the upper Terai. Since the upper Terai in Bardiya National Park is smaller than in other parts of the Terai, the rain water infiltration will also be less. The bulk of the rain precipitates in the monsoon (June – September). In this period, only 23% of the rain water can directly infiltrate through the top layer in the lower Terai. This is comparable to previous estimations of rain water infiltration through the top layer in other parts of the lower Terai. However, the actual recharge by direct rain water infiltration in the lower Terai is larger, as the infiltration capacity of the soil is locally higher where the top layer is eroded. The density of the groundwater monitoring points was too low to determine whether the shape of the piezometric surface support locally increased infiltration from ephemeral brooks. Furthermore, the groundwater flows from the Siwalik Foothills and the Babai river in southeast direction towards the Karnali river – suggesting that groundwater is recharged by the Babai river and discharged by the Karnali river. Field observations supported this conclusion and also indicated that there is groundwater exfiltration in the Aurahi river. Finally, the groundwater from the buffer zone, where the land is irrigated with Karnali river water, seems to be a mixture of groundwater and Karnali water. Apparently, river water irrigation is also a substantial source of recharge.

- c. **How does the groundwater head change during the post-monsoon?**

In the post monsoon, the average drop of the groundwater head in the confined part of the shallow aquifer between the Karnali river and the Aurahi river was between the 7.3 mm/day and 18.2 mm/day. The smallest drop in groundwater head occurred in the north, far away from the river. It gradually increased in the direction of the Karnali river in the south of the study. The groundwater head of two wells in unconfined aquifers near the Karnali river dropped on average only 2.5 and 6.0 mm/day.

d. **What is the role of the Karnali river in the changes of groundwater head in the post monsoon?**

The drop of the groundwater head near the Karnali river was governed by the gradient between the water level of the Karnali river and the groundwater. The effect of the Karnali river was larger downstream than upstream. Probably because the gradient between the Karnali river and groundwater was larger in the south than in the north. The influence of the Karnali river on the groundwater head did not reach up to the Aurahi river. Furthermore, the isotopic composition of the groundwater samples did also not reveal infiltration of Karnali river water during other parts of the year.

In conclusion, the role of the Karnali river in the depth of the groundwater head is considerable. Thus alterations in the Karnali river may have problematic consequences for the depth of the groundwater head. On the other hand, it creates the opportunity to manage the groundwater head with relatively simple interventions in the Karnali river. However, this research is not sufficient for making quantitative predictions about the effect of potential changes or interventions. Therefore, I recommend to develop a geohydrological computer model of Bardiya National Park, based on the results of this study.

5 References

- Adhikari, B., Verhoeven, R., & Troch, P. (2009). Water rights of the head reach farmers in view of a water supply scenario at the extension area of the Babai Irrigation Project, Nepal. *Physics and Chemistry of the Earth, Parts A/B/C*, 34(1-2), 99-106.
- Bouwer, H., & Rice, R. C. (1984). Hydraulic Properties of Stony Vadose Zones a. *Groundwater*, 22(6), 696-705.
- Bunn, M. I., Rudolph, D., Endres, A. & Jones, J. (2011). Field observation of the response to pumping and recovery in the water table region of an unconfined aquifer. *Journal of Hydrology*, 403, 307-320.
- Chakraborty, R. N. (2001). Stability and outcomes of common property institutions in forestry: evidence from the Terai region of Nepal. *Ecological Economics*, 36(2), 341-353.
- Collier, H. A. (1993). *Borehole geophysical techniques for determining the water quality and reservoir parameters of fresh and saline water aquifers in Texas*. Dallas, Texas: University of Texas (Doctoral dissertation).
http://www.twdb.texas.gov/publications/reports/numbered_reports/doc/r343/r343vol1_1.pdf
- Copernicus, Sentinel-2A data 2019. Processed by ESA.
<https://landsatlook.usgs.gov/sentinel2/viewer.html>
- Crain, E. R., Eng, P. (1999). *Crain's Petrophysical Handbook. An Internet-based Worldwide eLearning Project for Petrophysics*. Available at: www.spec2000.net
- Dansgaard, W. (1964). Stable isotopes in precipitation. *Tellus*, 16, 436-468.
- DeCelles, P. G., & Cavazza, W. (1999). A comparison of fluvial megafans in the Cordilleran (Upper Cretaceous) and modern Himalayan foreland basin systems. *Geological Society of America Bulletin*, 111(9), 1315-1334.
- Dhital, M. R. (2015). *Geology of the Nepal Himalaya: regional perspective of the classic collided orogen*. Cham, Switzerland: Springer International Publishing AG,
- DHM (2017). *Observed Climate Trend Analysis in the Districts and Physiographic Regions of Nepal (1971-2014)*. Kathmandu, Nepal: Department of Hydrology and Meteorology.
- DNPWC & DFSC. (2018). *Status of Tigers and Prey in Nepal. Department of National Parks and Wildlife Conservation & Department of Forests and Soil Conservation*. Ministry of Forests and Environment, Kathmandu, Nepal.
- Domenico, P. A., & Mifflin, M. D. (1965). Water from low-permeability sediments and land subsidence. *Water Resources Research*, 1(4), 563-576.
- Domenico, P.A. and F.W. Schwartz (1990). *Physical and Chemical Hydrogeology*. New York, US: John Wiley & Sons, 824 p.
- Eagleson, P. S. (1978). Climate, soil, and vegetation: 3. A simplified model of soil moisture movement in the liquid phase. *Water Resources Research*, 14(5), 722-730.
- Fitts, C. R. (2013). *Groundwater science* (2nd ed.). Waltham, MA: Elsevier.
- Gat, J.R., and Tzur, Y. (1967). Modification of the isotopic composition of rainwater by processes which occur before groundwater recharge. *Isotope Hydrology, Proc. Symp. Vienna 1966*, IAEA, Vienna, 49-60.

Google. (n.d.). *Nepal*. Retrieved from:

<https://www.google.nl/maps/place/28%C2%B024'39.5%22N+81%C2%B013'47.9%22E/@28.4107404,81.2290908,179m/data=!3m1!1e3!4m5!3m4!1s0x0:0x0!8m2!3d28.410964!4d81.229981>

Goulburn-Murray Water (2015). *Groundwater Terms and definitions. Version 8*. Shepparton, Australia: Author. https://www.g-mwater.com.au/downloads/gmw/Groundwater/29012016-_2977263-v9-GROUNDWATER_TERMS_AND_DEFINITIONS_GLOSSARY_FOR_USERS.pdf

Hantush, M.S. 1961. Aquifer tests on partially penetrating wells. *J. Hydraul. Div., Proc. Amer. Soc. Civil Engrs.*, 87(HY5), 171-195.

Hartong, H., & Termes, P. (2009). *Handboek debietmeten in open waterlopen*. Utrecht, the Netherlands: STOWA.

His Majesty's Government of Nepal (HMGN) (2003). *Nepal population and environment, facts and figures*. Kathmandu, Nepal: Ministry of Population and Environment.

Hoefs, J. (2009). *Stable isotope geochemistry* (Vol. 285). Berlin, Germany: Springer.

Hugh, S., Sarah, B., Adhikari, B., Attak, M., Borthwick, A., Budimir, M., . . . Sharma, J. (2017). *Improving understanding of flooding and resilience in the Terai, Nepal*. Rugby, UK: Practical Action.

Huntley, D. (1986). Relations between permeability and electrical resistivity in granular aquifers. *Groundwater*, 24(4), 466-474.

IAEA/WMO (2019). Global Network of Isotopes in Precipitation. The GNIP Database. Accessible at: <http://www.iaea.org/water>

India Meteorological Dept., Safdarjung Airport, Delhi

ITTC (2011). Fresh Water and Seawater properties. Retrieved from: <https://ittc.info/media/4048/75-02-01-03.pdf>.

JAXA (2015). ALOS Global Digital Surface Model: ALOS World3D - 30m (AW3D30), *Japan Aerospace Exploration Agency*, <http://www.eorc.jaxa.jp/ALOS/en/aw3d3028>.

Jha, P. (2006). Estimation of hourly rainfall design intensity From 24 -hour maximum rainfall: the context of Nepal. *Journal of Hydrology and Meteorology*, 3.

Karki, R., Talchabhadel, R., Aalto, J., & Baidya, S. K. (2016). New climatic classification of Nepal. *Theoretical and applied climatology*, 125(3-4), 799-808.

Khatriwada, K., Panthi, J., Shrestha, M., & Nepal, S. (2016). Hydro-Climatic variability in the Karnali river basin of Nepal Himalaya. *Climate*, 4(2), 17.

Kim, S., Park, S., & Hamm, S. Y. (2013). Relationship between Hydraulic Conductivity and Electrical Resistivity of Standard Sand and Glass Bead. *Economic and Environmental Geology*, 46(3), 215-220.

Kosinski, W. K., & Kelly, W. E. (1981). Geoelectric soundings for predicting aquifer properties. *Groundwater*, 19(2), 163-171.

Kruseman, G. P., De Ridder, N. A., & Verweij, J. M. (1970). *Analysis and evaluation of pumping test data*. Wageningen, The Netherlands: International institute for land reclamation and improvement.

Kumar, U.S., Kumar, B., Rai, S. P., & Sharma, S. (2010a). Stable isotope ratios in precipitation and their relationship with meteorological conditions in the Kumaon Himalayas, India. *Journal of hydrology*, 391(1-2), 1-8.

- Kumar, B., Rai, S. P., Kumar, U. S., Verma, S. K., Garg, P., Kumar, S. V., Jaiswal, R., Purendra, B. K., Kumar, S. R. & Pande, N. G. (2010b). Isotopic characteristics of Indian precipitation. *Water Resources Research*, 46(12).
- Lambs, L., Balakrishna K., Brunet, F. & Probst, J. L. (2005). Oxygen and hydrogen isotopic composition of major Indian rivers: a first global assessment. *Hydrol. Process.* 19, 3345-3355.
- Lehner, B., Verdin, K., Jarvis, A. (2008): New global hydrography derived from spaceborne elevation data. *Eos, Transactions, AGU*, 89(10): 93-94.
- Mazáč, O., Kelly, W. E., & Landa, I. (1985). A hydrogeophysical model for relations between electrical and hydraulic properties of aquifers. *Journal of hydrology*, 79(1-2), 1-190.
- Nelson, S. T. (2000). A simple, practical methodology for routine VSMOW/SLAP normalization of water samples analyzed by continuous flow methods. *Rapid Communications in Mass Spectrometry*, 14(12), 1044-1046.
- Nichols, G., (2009). *Sedimentology and stratigraphy* (2nd ed.). Chichester, West Sussex: Wiley-Blackwell.
- Onta, I. R. (2004). *State of Nepal's Water, Research Report*. Los Clubes, Mexico: Third World Centre for Water Management. <https://thirdworldcentre.org/publication/state-of-nepals-waters/>.
- Pathak, D. (2016). Water Availability and Hydrogeological Condition in the Siwalik Foothill of Eastern Nepal. *Nepal Journal of Science and Technology*, 17(1).
- Peet, N. B., Watkinson, A. R., Bell, D. J., & Kattel, B. J. (1999). Plant diversity in the threatened sub-tropical grasslands of Nepal. *Biological Conservation*, 88(2), 193-206.
- Poesen, J., & Lavee, H. (1994). Rock fragments in top soils: significance and processes. *Catena*, 23(1-2), 1-28.
- Rana, M. (2018). *Modernization of Rani Jamara Kulariya Irrigation Scheme - Phase 1 - Procurement Plan (English)*. Washington, D.C.: World Bank Group.
<http://documents.worldbank.org/curated/en/882681560718185429/Nepal-SOUTH-ASIA-P158364-NP-Modernization-of-Rani-Jamara-Kulariya-Irrigation-Scheme-Phase-2-Procurement-Plan>
- Rao, G. K., Shrestha, R., & Vaidya, Y. L. (1996). Hydrogeological Conditions in the Terai Plain of Rupandehi District, Lumbini Zone, Nepal with Special Emphasis on Groundwater Recharge. In *Subsurface-Water Hydrology*, 131-149.
- Santillan, J. R., & Makinano-Santillan, M. (2016). VERTICAL ACCURACY ASSESSMENT OF 30-M RESOLUTION ALOS, ASTER, AND SRTM GLOBAL DEMS OVER NORTHEASTERN MINDANAO, PHILIPPINES. *International Archives of the Photogrammetry, Remote Sensing & Spatial Information Sciences*, 41.
- Seidensticker, J., Dinerstein, E., Goyal, S. P., Gurung, B., Harihar, A., Johnsingh, A. J. T., ... & Smith, J. D. (2010). Tiger range collapse and recovery at the base of the Himalayas. *Biology and conservation of wild felids*, 12, 305-324.
- Shrestha, S. R., Tripathi, G. N., & Laudari, D. (2018). Groundwater Resources of Nepal: An Overview. In *Groundwater of South Asia* (pp. 169-193). Singapore, Singapore: Springer.
- Siegel, D. I., & Jenkins, D. T. (1987). Isotopic analysis of groundwater flow systems in a wet alluvial fan, southern Nepal. *Isotope techniques in water resources development*. IAEA, Vienna, 475-482.
- Steiner, G., & Gautschi, M. (2014). *Logger 5.1: manual*. Winterthur, Germany: KELLER AG für Druckmesstechnik.

- Støen, O.G. & Wegge, P. (1996). Prey selection and prey removal by tiger (*Panthera tigris*) during the dry season in lowland Nepal. *Mammalia* 60, 363–373.
- Surinaidu, L., Muthuwatta, L., Amarasinghe, U. A., Jain, S. K., Ghosh, N. C., Kumar, S., & Singh, S. (2016). Reviving the Ganges water machine: accelerating surface water and groundwater interactions in the Ramganga sub-basin. *Journal of Hydrology*, 540, 207-219.
- Talchabhadel, R., Karki, R., Yadav, M., Maharjan, M., Aryal, A., & Thapa, B. R. (2019). Spatial distribution of soil moisture index across Nepal: a step towards sharing climatic information for agricultural sector. *Theoretical and Applied Climatology*, 1-14.
- Twarakavi, N. K., Šimůnek, J., & Schaap, M. G. (2010). Can texture-based classification optimally classify soils with respect to soil hydraulics?. *Water Resources Research*, 46(1).
- Uffink, G. J. M. (1982) Richtlijnen voor het uitvoeren van putproeven. *H2O* 9(15).
- USAID PAANI PROGRAM (2018). *Lower Karnali Watershed Health Report*. Kathmandu, Nepal: Author.
- Van Essen Instruments (2016). *TD-Diver™ & Baro-Diver® – DI8xx Series: product manual*. Giesbeek, the Netherlands: Author.
- Van Kooten, E. E. (unpublished). *The changes in the Lower Karnali river by human activities and its possible role on sub-tropical tall grasslands in Bardia National Park, Nepal. An assessment of the changes in spatial and temporal patterns of the Lower Karnali river flow by human activities with an 2D hydrodynamic model in HEC-RAS*. The Netherlands, Utrecht: Utrecht University (MSc Thesis).
- Wang, T. Y., Lin, L. L., & Tsai, Y. Z. (2017). Effect of gravel content on saturated hydraulic conductivity in sand. *Geotechnical hazards from large earthquakes and heavy rainfalls*, 163-169.
- Wegge, P., Odden, M., Pokharel, C.P. & Storaas, T. (2009). Predator–prey relationships and responses of ungulates and their predators to the establishment of protected areas: a case study of tigers, leopards and their prey in Bardia National Park, Nepal. *Biol. Conserv.* 142, 189–202.
- Wegge, P., & Storaas, T. (2009). Sampling tiger ungulate prey by the distance method: lessons learned in Bardia National Park, Nepal. *Animal Conservation*, 12(1), 78-84.

6 Appendices

Appendix A

Background information geophysical well logging

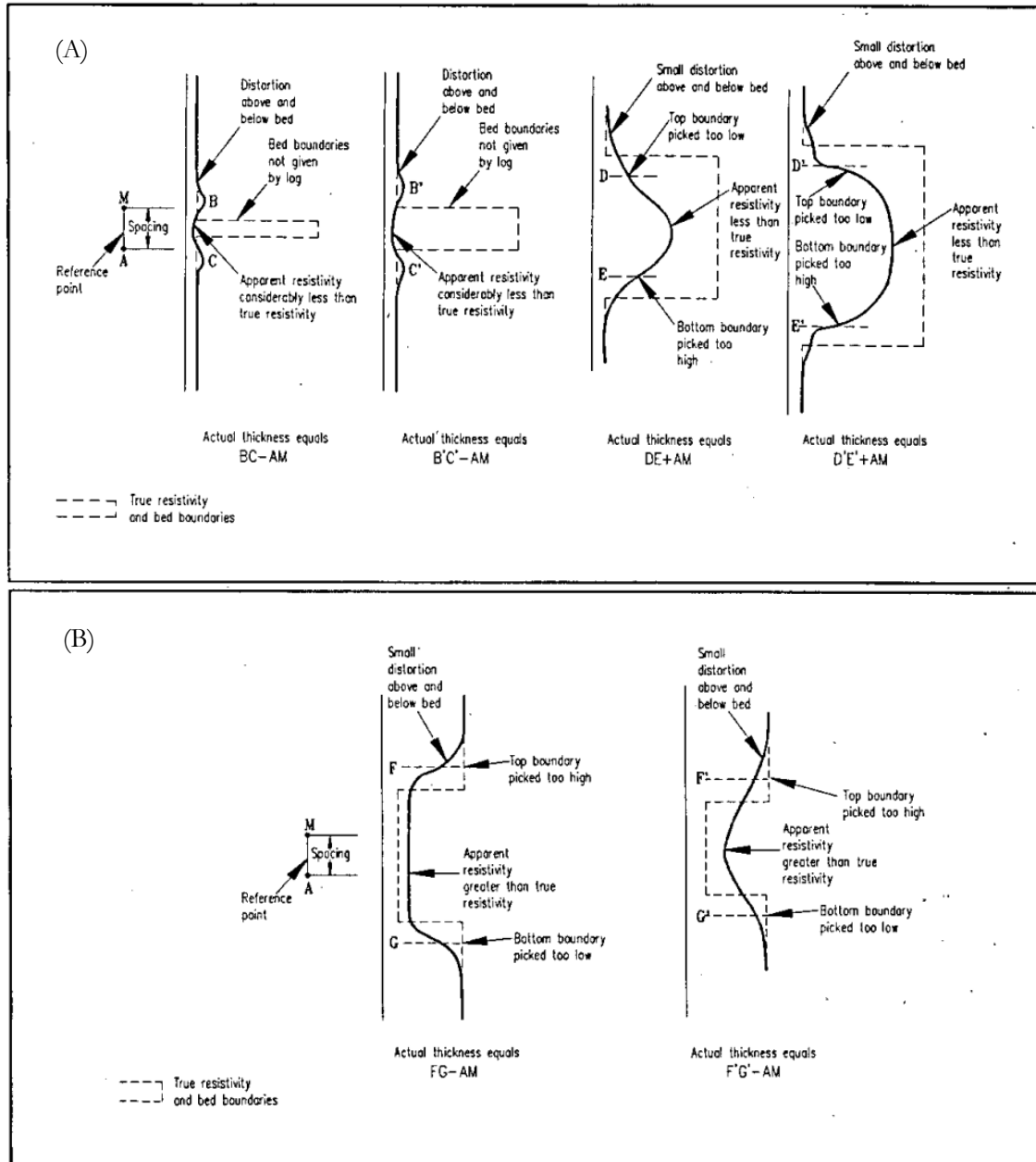


Figure 35. Typical normal curve responses for resistive beds (A) and for conductive beds (B) of varying thicknesses. From: Collier (1993).

Appendix B

Analysed well log data

no.	name location	longitude	latitude	source
1	Ramkrishna Tole, Sanoshree VDC, Bardiya	81.27	28.30	google maps: Sanoshree Taratal 21800
2	Kalika-6, Mayurbasti, Bardiya	81.44	28.19	https://satellites.pro/#G28.190650,81.442664,18
3	Mainapokhar, Bardiya	81.48	28.18	google maps: Mainapokhar
4	Tepari, Rampur-9, Bardiya	81.72	27.98	http://nepal.places-in-the-world.com/8008008-place-tepari.html
5	Madhuwan/Dalla	81.23	28.40	interview: Water Supply and Sanitation division office
6	Bagnaha, Tarkiya-05	81.30	28.41	interview: NTNC
7	Dharmabasti-9, Bardiya	81.28	28.25	http://www.worldpoi.com/nepal/mid-western/bheri/dharmabasti.html
8	Dodari, Madhuwan-4, Bardiya	81.27	28.34	coordinates provided
9	Asansneri-4	81.47	28.27	interview: NTNC
10	Bhuriguon-01, Thakurbaba VDC Bardiya	81.33	28.46	visited
11	Karmala-02, Thakurbaba municipality, Bardiya	81.34	28.47	visited
12	Ganeshpur, Gulariya, Bardiya	81.41	28.18	google maps: Ganeshpur
13	Jamuni-5 Badaiya, Gaupalika, Sitapur, Bardiya	81.50	28.09	google maps: Jamuni
14	Deudakala-7, Basgadi, Bardiya	81.46	28.19	google maps: Deudakala
15	Dasrath Basti	80.47	28.67	http://nepal.places-in-the-world.com/7958687-place-dashrathbasti.html
16	Khareni, Barbardiya, Bardiya	81.51	28.27	interview: NTNC
17	Betahni, Thakurbaba-9, Bardiya	81.25	28.46	visited

Figure 36. Overview of analysed well log data, including the coordinates of the location and the method of determination of the location.

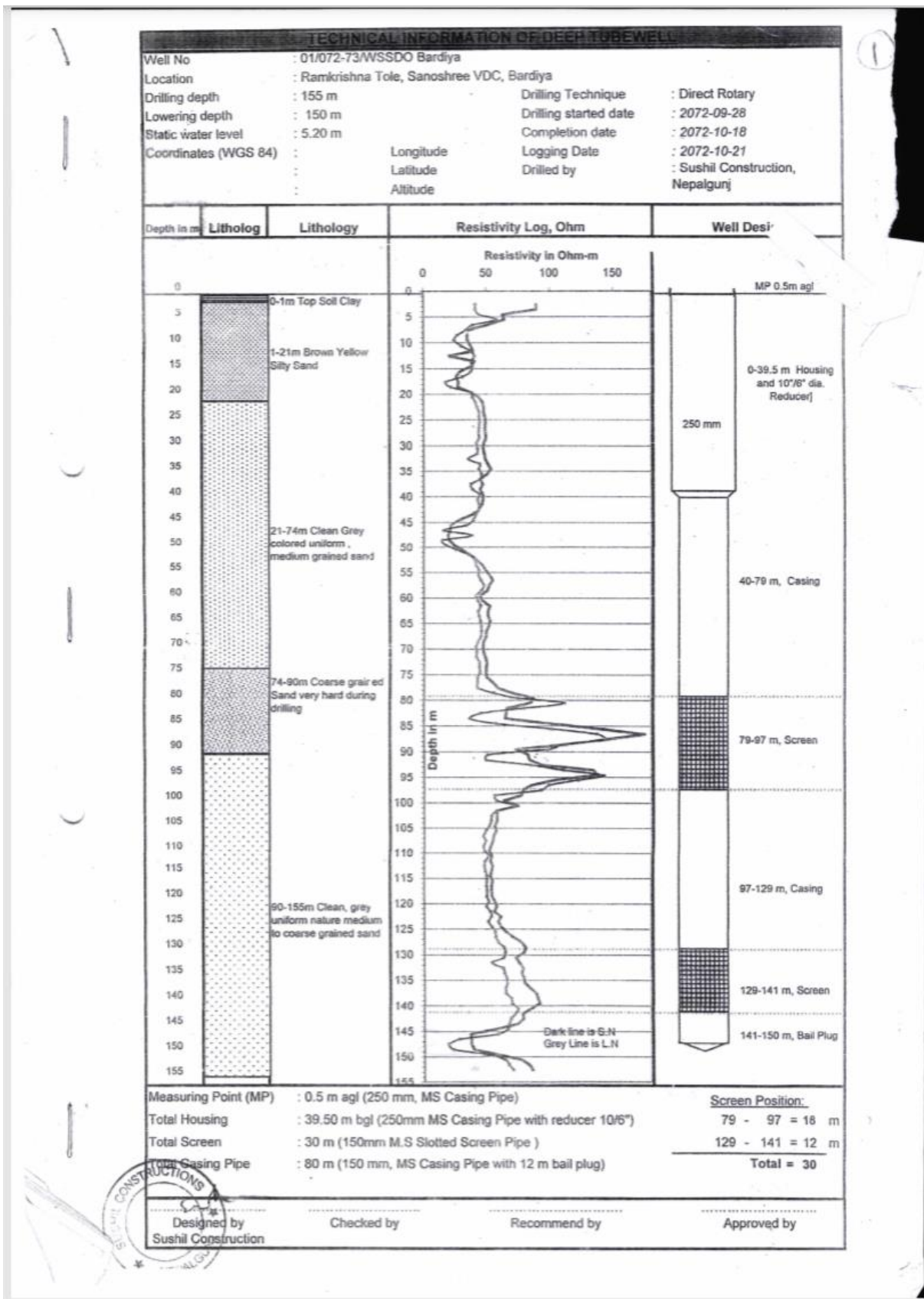


Figure 37. Well log 1: Ramkrishna Tole, Sanoshree VDC, Bardiya. Borehole description and resistivity curve.

Resistivity Record of Deep Tubewell			
Well No:	: 01/072-73/WSSDO Bardiya		
Location:	: Ramkrishna Tole, Sanoshree VDC, Bardiya		
Drilling Depth:	: 156 m	Logger:	: Minilog 300A, Indian
Logging Depth:	: 153 m	Logging Date:	: 2072-10-21

Resistivity Log						
Depth, m	Self Potential, mV	Resistivity, Ohm-m				Remarks
		S.N	S.Nx5	L.N	LNx20	
1	-	-	-	-	-	
2	-	-	-	-	-	
3	-30.00	8.53	42.65	4.68	93.60	
4	-30.00	8.29	41.45	4.48	89.60	
5	-31.00	8.91	44.55	3.15	63.00	
6	-37.00	11.63	58.15	3.22	64.40	
7	-42.00	7.87	39.35	2.53	50.60	
8	-46.00	6.72	33.60	1.80	36.00	
9	-46.00	5.37	26.85	1.73	34.60	
10	-45.00	4.91	24.55	1.74	34.80	
11	-45.00	5.99	29.95	1.87	37.40	
12	-47.00	7.50	37.50	1.97	39.40	
13	-47.00	8.1	40.50	1.02	20.40	
14	-49.00	7.59	37.95	2.02	40.40	
15	-50.00	7.78	38.90	1.88	37.60	
16	-49.00	7.51	37.55	1.43	28.60	
17	-46.00	6.09	30.45	1.28	25.60	
18	-41.00	3.54	17.70	1.38	27.60	
19	-44.00	4.29	21.45	1.35	27.00	
20	-48.00	7.50	37.50	1.87	37.40	
21	-49.00	7.80	39.00	2.19	43.80	
22	-49.00	8.27	41.35	2.35	47.00	
23	-49.00	8.52	42.60	2.40	48.00	
24	-48.00	8.87	44.35	2.39	47.80	
25	-49.00	8.86	44.30	2.45	49.00	
26	-48.00	8.9	44.50	2.46	49.20	
27	-49.00	8.81	44.05	2.43	48.60	
28	-48.00	8.78	43.90	2.46	49.20	
29	-48.00	8.83	44.15	2.48	49.60	
30	-48.00	8.41	42.05	2.39	47.80	
31	-48.00	8.56	42.80	2.37	47.40	

Figure 38. Well log 1: Ramkrishna Tole, Sanoshree VDC, Bardiya. Table with resistivities (1).

Resistivity Record of Deep Tubewell						
Well No:		: 01/072-73/WSSDO Bardiya				
Location:		: Ramkrishna Tole, Sanoshree VDC, Bardiya				
Drilling Depth:		: 156 m		Logger::Minilog 300A, Indian		
Logging Depth:		: 153 m		Logging Date: 2072-10-21		
32	-47.00	8.44	42.20	2.41	48.20	
33	-46.00	7.12	35.60	2.45	49.00	
34	-47.00	8.93	44.65	2.55	51.00	
35	-48.00	8.78	43.90	2.68	53.60	
36	-48.00	9.19	45.95	2.53	50.60	
37	-46.00	8.98	44.90	2.24	44.80	
38	-44.00	7.53	37.65	2.35	47.00	
39	-46.00	7.79	38.95	2.24	44.80	
40	-46.00	8.9	44.50	2.35	47.00	
41	-46.00	8.57	42.85	2.35	47.00	
42	-45.00	8.76	43.80	2.31	46.20	
43	-46.00	8.74	43.70	2.17	43.40	
44	-45.00	8.23	41.15	1.90	38.00	
45	-43.00	7.91	39.55	1.41	28.20	
46	-41.00	6.72	33.60	1.07	21.40	
47	-33.00	3.12	15.60	1.04	20.80	
48	-32.00	7.7	38.50	0.95	19.00	
49	-33.00	2.92	14.60	1.00	20.00	
50	-34.00	3.54	17.70	1.19	23.80	
51	-39.00	5.29	26.45	1.54	30.80	
52	-39.00	7.233	36.17	1.87	37.40	
53	-40.00	8.14	40.70	2.11	42.20	
54	-40.00	8.37	41.85	2.34	46.80	
55	-40.00	8.77	43.85	2.46	49.20	
56	-40.00	8.74	43.70	2.62	52.40	
57	-40.00	9.12	45.60	2.75	55.00	
58	-39.00	9.55	47.75	2.61	52.20	
59	-38.00	9.15	45.75	2.53	50.60	
60	-37.00	8.38	41.90	2.24	44.80	
61	-37.00	8.63	43.15	2.33	46.60	
62	-37.00	9.03	45.15	2.62	52.40	
63	-39.00	8.7	43.50	2.55	51.00	
64	-40.00	8.76	43.80	2.55	51.00	
65	-38.00	9.05	45.25	2.64	52.80	

Figure 39. Well log 1: Ramkrishna Tole, Sanoshree VDC, Bardiya. Table with resistivities (2).

Resistivity Record of Deep Tubewell						
Well No:		: 01/072-73/WSSDO Bardiya				
Location:		: Ramkrishna Tole, Sanoshree VDC, Bardiya				
Drilling Depth:		: 156 m		Logger::Minilog 300A, Indian		
Logging Depth:		: 153 m		Logging Date: 2072-10-21		
66	-37.00	9.12	45.60	2.58	51.60	
67	-37.00	9.155	45.78	2.48	49.60	
68	-36.00	9.06	45.30	2.48	49.60	
69	-35.00	8.6	43.00	2.37	47.40	
70	-34.00	8.28	41.40	2.35	47.00	
71	-33.00	8.4	42.00	2.37	47.40	
72	-33.00	8.37	41.85	2.44	48.80	
73	-33.00	8.84	44.20	2.51	50.20	
74	-33.00	8.86	44.30	2.48	49.60	
75	-33.00	8.91	44.55	2.47	49.40	
76	-33.00	8.5	42.50	2.50	50.00	
77	-32.00	8.52	42.60	2.77	55.40	
78	-35.00	8.58	42.90	2.93	58.60	
79	-33.00	11.13	55.65	3.51	70.20	
80	-42.00	15.01	75.05	4.36	87.20	
81	-49.00	22.38	111.90	4.24	84.80	
82	-42.00	15.96	79.80	3.31	66.20	
83	-26.00	9.08	45.40	3.28	65.60	
84	-20.00	7.33	36.65	3.24	64.80	
85	-25.00	11.50	57.50	5.04	100.80	
86	-40.00	20.30	101.50	7.04	140.80	
87	-46.00	27.54	137.70	8.74	174.80	
88	-48.00	28.72	143.60	7.21	144.20	
89	-42.00	22.35	111.75	5.66	113.20	
90	-38.00	19.67	98.35	3.65	73.00	
91	-15.00	10.16	50.80	4.14	82.80	
92	-21.00	9.84	49.20	4.18	83.60	
93	-34.00	17.00	85.00	4.69	93.80	
94	-37.00	22.19	110.95	6.73	134.60	
95	-41.00	28.58	142.90	6.91	138.20	
96	-37.00	24.57	122.85	5.22	104.40	
97	-33.00	19.79	98.95	4.27	85.40	
98	-32.00	18.59	92.95	3.93	78.60	
99	-15.00	11.32	56.60	3.87	77.40	

Figure 40. Well log 1: Ramkrishna Tole, Sanoshree VDC, Bardiya. Table with resistivities (3).

Resistivity Record of Deep Tubewell						
Well No:		: 01/072-73/WSSDO Bardiya				
Location:		: Ramkrishna Tole, Sanoshree VDC, Bardiya				
Drilling Depth:		: 156 m			Logger: Minilog 300A, Indian	
Logging Depth:		: 153 m			Logging Date: 2072-10-21	
100	-14.00	11.55	57.75	3.18	63.60	
101	-17.00	14.17	70.85	3.74	74.80	
102	-12.00	11.61	58.05	2.90	58.00	
103	-11.00	10.72	53.60	2.91	58.20	
104	-11.00	10.66	53.30	2.91	58.20	
105	-11.00	10.35	51.75	2.81	56.20	
106	-10.00	9.83	49.15	2.87	57.40	
107	-9.00	9.43	47.15	2.76	55.20	
108	-8.00	9.79	48.95	2.73	54.60	
109	-5.00	9.43	47.15	2.64	52.80	
110	-7.00	9.62	48.10	2.59	51.80	
111	-6.00	10.29	51.45	2.70	54.00	
112	-5.00	9.74	48.70	2.63	52.60	
113	-4.00	9.61	48.05	2.73	54.60	
114	-4.00	9.77	48.85	2.69	53.80	
115	-3.00	9.99	49.95	2.63	52.60	
116	-2.00	10.00	50.00	2.73	54.60	
117	-2.00	9.93	49.65	2.68	53.60	
118	-1.00	10.09	50.45	2.69	53.80	
119	1.00	10.03	50.15	2.71	54.20	
120	1.00	10.29	51.45	2.83	56.60	
121	2.00	9.96	49.80	2.89	57.80	
122	2.00	10.59	52.95	2.80	56.00	
123	4.00	10.70	53.50	3.06	61.20	
124	4.00	10.22	51.10	2.95	59.00	
125	5.00	10.82	54.10	3.06	61.20	
126	5.00	11.33	56.65	3.27	65.40	
127	6.00	11.43	57.15	3.53	70.60	
128	8.00	11.79	58.95	3.87	77.40	
129	8.00	12.71	63.55	4.03	80.60	
130	9.00	12.90	64.50	3.96	79.20	
131	10.00	12.62	63.10	3.64	72.80	
132	11.00	10.80	54.00	3.78	75.60	
133	12.00	12.54	62.70	3.94	78.80	

Figure 41. Well log 1: Ramkrishna Tole, Sanoshree VDC, Bardiya. Table with resistivities (4).

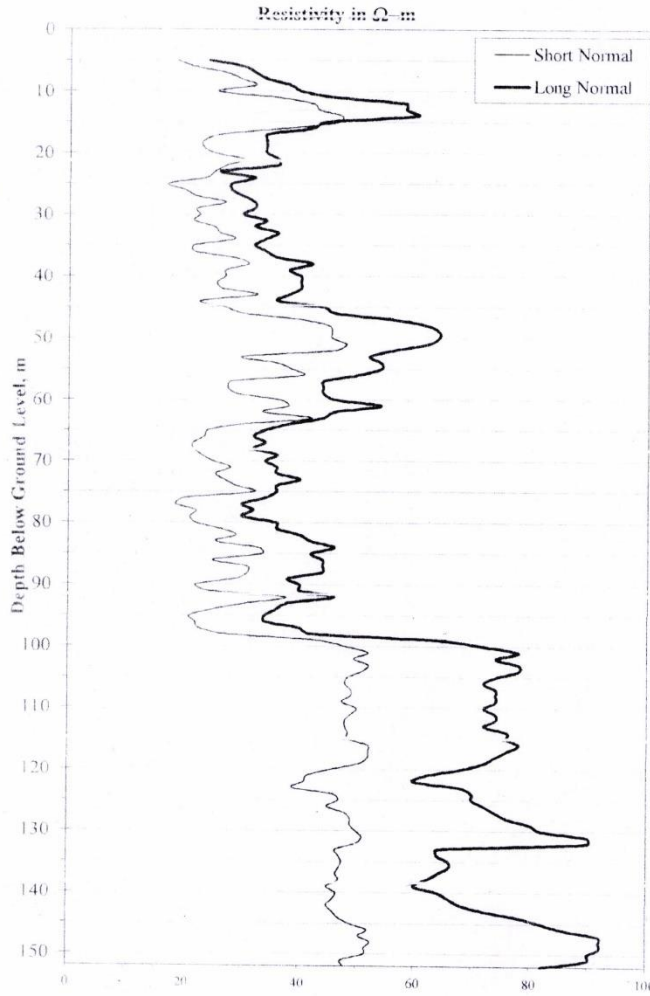
WATER SUPPLY & SANITATION DIVISION OFFICE
GULERIYA, BARDIYA

②

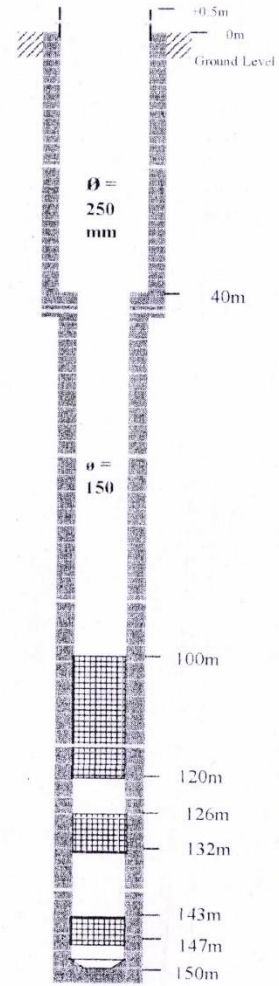
LOCATION : KALIKA-6, MAYURBASTI, BARDIYA

Date : 2072/11/29

ELECTRICAL LOG DATA



WELL ASSEMBLY DIAGRAM



Prepared by Hydrogeologist **Om kumar khadka**




 Casing Pipe
 Gravel Pack Envelope
 Slotted Screen Pipe

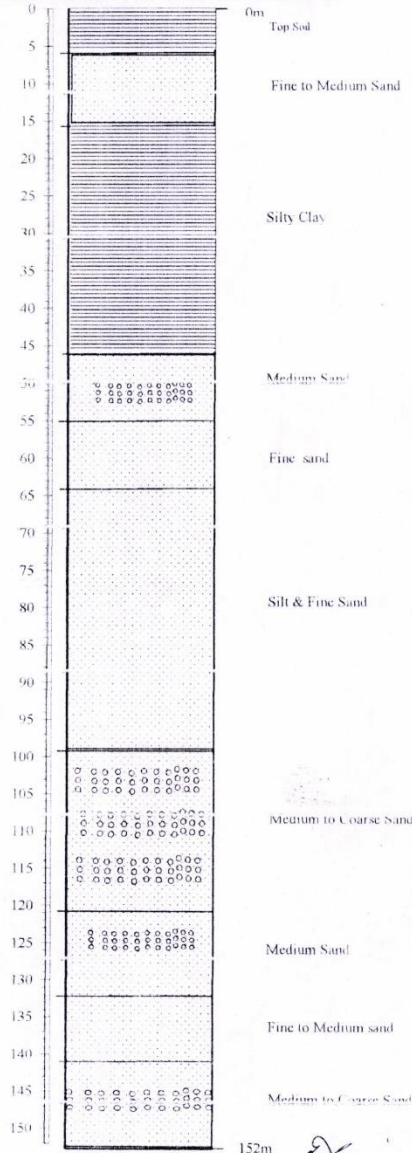


Figure 43. Well log 2: Kalika-6, Mayurbasti, Bardiya. Resistivity curve.

**WATER SUPPLY & SANITATION DIVISION OFFICE
GULERIYA, BARDIYA**

WATERWELL DRILLING AT KALIKA-6, MAYURBASTI, BARDIYA

DRILLER'S LITHOLOGICAL LOG



152m

Figure 44. Well log 2: Kalika-6, Mayurbasti, Bardiya. Borehole description.

**WATER WELL DRILLING AT KALIKA-6,
MAYURBASTI, BARDIYA
ELECTRICAL LOG DATA**

Depth (m)	Short Normal	long Normal		
1				
2				
3				
4				
5	3.7	18.5	1.2	24
6	4.3	21.5	1.5	30
7	5.4	27.0	1.6	32
8	5.9	29.5	1.7	34
9	6.4	32.0	1.9	38
10	5.1	25.5	2	40
11	7.2	36.0	2.3	46
12	8.4	42.0	2.9	58
13	8.6	43.0	2.9	58
14	9.4	47.0	3	60
15	9.3	46.5	2.2	44
16	7.4	37.0	2.1	42
17	5.2	26.0	1.7	34
18	4.6	23.0	1.7	34
19	4.6	23.0	1.7	34
20	5.0	25.0	1.7	34
21	6.0	30.0	1.8	36
22	5.4	27.0	1.8	36
23	5.0	25.0	1.3	26
24	4.7	23.5	1.6	32
25	3.4	17.0	1.4	28
26	4.0	20.0	1.4	28
27	4.4	22.0	1.5	30
28	5.4	27.0	1.6	32
29	4.4	22.0	1.6	32
30	4.5	22.5	1.5	30
31	4.3	21.5	1.7	34
32	5.0	25.0	1.6	32
33	5.2	26.0	1.8	36
34	5.7	28.5	1.7	34
35	4.3	21.5	1.6	32
36	4.3	21.5	1.7	34
37	5.7	28.5	1.8	36
38	6.2	31.0	2.1	42
39	5.4	27.0	1.9	38
40	5.4	27.0	2	40
41	5.1	25.5	2	40
42	5.3	26.5	2	40
43	6.5	32.5	1.9	38
44	4.5	22.5	1.8	36
45	5.4	27.0	2.2	44
46	6.0	30.0	2.3	46
47	8.0	40.0	2.8	56
48	9.0	45.0	3.1	62
49	9.1	45.5	3.2	64
50	9.1	45.5	3.2	64
51	9.6	48.0	3.1	62
52	9.2	46.0	2.8	56
53	6.0	30.0	2.6	52
54	7.2	36.0	2.7	54
55	7.7	38.5	2.7	54
56	8.1	40.5	2.5	50
57	5.6	28.0	2.2	44
58	5.5	27.5	2.2	44



Figure 45. Well log 2: Kalika-6, Mayurbasti, Bardiya. Table with resistivities (1).

59	5.8	29.0	2.2	44
60	7.3	36.5	2.3	46
61	7.6	38.0	2.7	54
62	6.7	33.5	2.3	46
63	8.4	42.0	2.2	44
64	6.0	30.0	1.9	38
65	4.8	24.0	1.7	34
66	4.7	23.5	1.6	32
67	4.3	21.5	1.7	34
68	4.3	21.5	1.6	32
69	4.6	23.0	1.8	36
70	5.0	25.0	1.7	34
71	5.6	28.0	1.8	36
72	5.1	25.5	1.8	36
73	5.4	27.0	2	40
74	5.8	29.0	1.8	36
75	6.4	32.0	1.8	36
76	4.0	20.0	1.7	34
77	3.7	18.5	1.5	30
78	4.4	22.0	1.6	32
79	4.2	21.0	1.5	30
80	4.4	22.0	1.8	36
81	5.3	26.5	1.8	36
82	5.8	29.0	2	40
83	5.1	25.5	2.1	42
84	6.6	33.0	2.3	46
85	6.7	33.5	2.1	42
86	5.0	25.0	2.2	44
87	6.2	31.0	2.2	44
88	6.2	31.0	2.2	44
89	5.8	29.0	1.9	38
90	4.4	22.0	2	40
91	4.9	24.5	2	40
92	7.5	37.5	2.3	46
93	6.2	31.0	1.9	38
94	5.6	28.5	1.8	36
95	4.2	21.0	1.7	34
96	4.4	22.0	1.7	34
97	4.5	22.5	2	40
98	5.4	27.0	2.1	42
99	8.6	43.0	3.2	64
100	9.6	48.0	3.6	72
101	10.4	52.0	3.9	78
102	9.9	49.5	3.7	74
103	10.4	52.0	3.9	78
104	10.2	51.0	3.9	78
105	9.7	48.5	3.7	74
106	9.6	48.0	3.6	72
107	9.8	49.0	3.7	74
108	9.8	49.0	3.7	74
109	9.5	47.5	3.7	74
110	10.0	50.0	3.6	72
111	9.8	49.0	3.7	74
112	9.6	48.0	3.7	74
113	9.6	48.0	3.6	72
114	9.7	48.5	3.8	76
115	9.7	48.5	3.8	76
116	10.4	52.0	3.9	78
117	10.4	52.0	3.8	76
118	10.4	52.0	3.7	74
119	10.1	50.5	3.6	72
120	9.1	45.5	3.4	68
121	8.3	41.5	3.1	62
122	8.2	41.0	3	60
123	7.8	39.0	3.4	68
124	9.2	46.0	3.5	70
125	9.4	47.0	3.5	70
126	9.0	45.0	3.6	72



Figure 46. Well log 2: Kalika-6, Mayurbasti, Bardiya. Table with resistivities (2).

127	9.6	48.0	3.7	74
128	9.8	49.0	3.8	76
129	9.8	49.0	4	80
130	10.0	50.0	4.1	82
131	10.2	51.0	4.5	90
132	10.0	50.0	4.5	90
133	9.5	46.5	3.2	64
134	9.4	47.0	3.2	64
135	9.5	47.5	3.3	66
136	9.4	47.0	3.3	66
137	9.3	46.5	3.2	64
138	9.4	47.0	3.1	62
139	9.0	45.0	3	60
140	9.3	46.5	3.2	64
141	9.2	46.0	3.3	66
142	9.0	45.0	3.4	68
143	9.2	46.0	3.6	72
144	9.4	47.0	3.9	78
145	9.8	49.0	4.1	82
146	10.4	52.0	4.3	86
147	10.1	50.5	4.6	92
148	10.5	52.5	4.6	92
149	10.3	51.5	4.6	92
150	10.3	51.5	4.5	90
151	9.5	47.5	4.5	90
152	9.6	48.0	4.1	82

[Handwritten signature]



Figure 47. Well log 2: Kalika-6, Mayurbasti, Bardiya. Table with resistivities (3).

WATER SUPPLY & SANITATION SUB DIVISION OFFICE

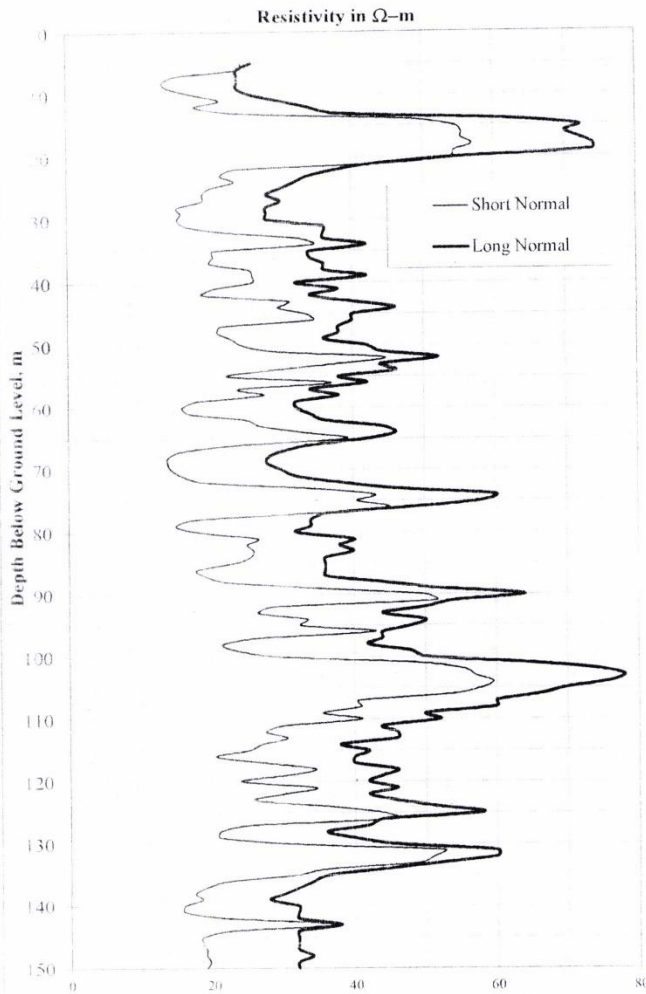
GULERIYA, BARDIYA

(Mainapokhar Water Supply Project)

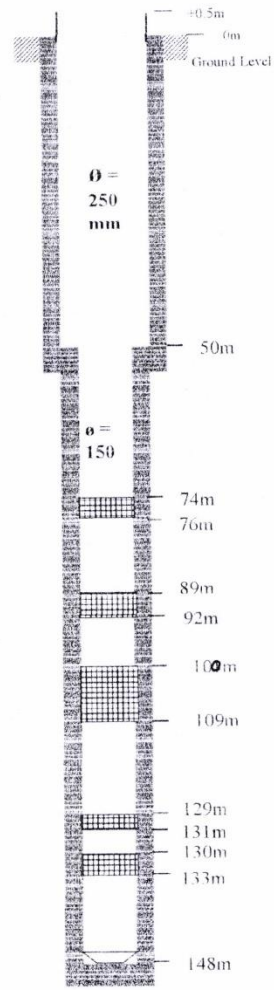
Date : 2072/12/18

KHAR, BARDIYA (Hole No.2)

ELECTRICAL LOG DATA



WELL ASSEMBLY DIAGRAM



Prepared by Hydrogeologist *Om kumar khadka*

□ Casing Pipe
▨ Gravel Pack Envelope
▧ SS Johnson Screen Pipe



Figure 48. Well log 3: Mainopokhar, Bardiya. Resistivity curve.

WATER SUPPLY SANITATION SUB DIVISION OFFICE

GULERIYA, BARDIYA

(Mainapokhar Water Supply Project)

WATERWELL DRILLING AT MAINAPOKHAR, BARDIYA (Hole No. 2)

DRILLER'S LITHOLOGICAL LOG

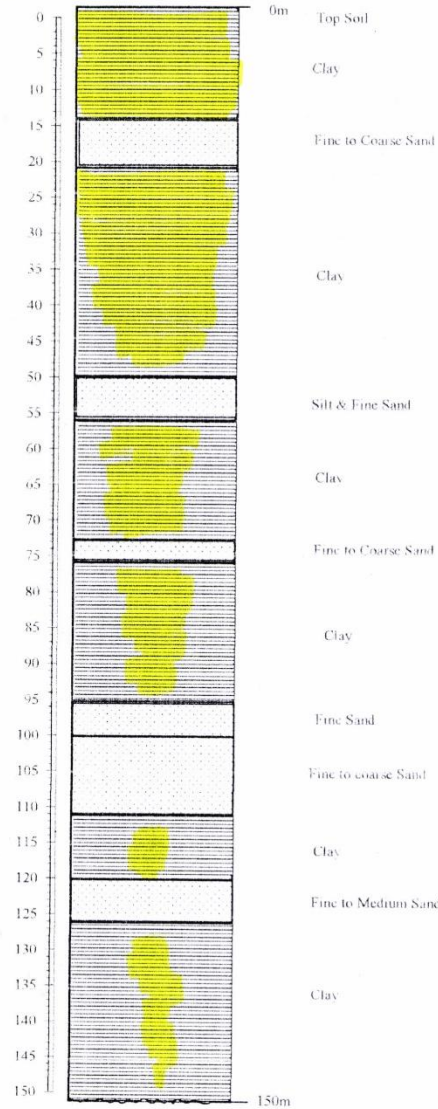


Figure 49. Well log 3: Mainopokhar, Bardiya. Borehole description.

**WATER DRILLING AT
BARDIYA, MAINAPOKHAR (HOLE NO. 2)
ELECTRICAL LOG DATA**

Depth (m)	Short Normal		long Normal	
2				
3				
4				
5	4.9	24.5	1.3	26
6	4.9	24.5	1.2	24
7	3.1	15.5	1.2	24
8	2.7	13.5	1.2	24
9	2.9	14.5	1.2	24
10	3.6	18.0	1.3	26
11	4.3	21.5	1.5	30
12	3.6	18.0	1.7	34
13	4.8	24.0	1.9	38
14	9.6	48.0	3.1	62
15	10.9	54.5	3.6	72
16	11.1	55.5	3.5	70
17	11.1	55.5	3.6	72
18	11.4	57.0	3.7	74
19	10.9	54.5	3.7	74
20	10.8	54.0	2.8	56
21	9.3	46.5	2.2	44
22	4.7	23.5	1.9	38
23	4.3	21.5	1.7	34
24	4.7	23.5	1.6	32
25	4.0	20.0	1.5	30
26	3.8	19.0	1.4	28
27	3.8	19.0	1.5	30
28	3.1	15.5	1.4	28
29	3.2	16.0	1.4	28
30	3.1	15.5	1.4	28
31	3.3	16.5	1.8	36
32	4.4	22.0	1.8	36
33	6.5	32.5	1.8	36
34	6.9	34.5	2.1	42
35	4.1	20.5	1.7	34
36	4.1	20.5	1.7	34
37	4.0	20.0	1.8	36
38	5.1	25.5	1.8	36
39	5.2	26.0	2.1	42
40	5.2	26.0	1.6	32
41	4.1	20.5	1.9	38
42	3.8	19.0	1.7	34
43	6.2	31.0	2	40
44	5.9	29.5	2.3	46
45	6.7	33.5	2	40
46	6.9	34.5	2	40
47	4.3	21.5	1.9	38
48	4.2	21.0	1.9	38
49	4.6	23.0	1.8	36
50	4.9	24.5	2.1	42
51	5.8	29.0	2.2	44
52	8.9	44.5	2.6	52
53	7.5	37.5	2.2	44
54	5.7	28.5	2.3	46
55	4.5	22.5	1.9	38
56	7.4	37.0	2.1	42
57	4.8	24.0	1.7	34
58	5.5	27.5	1.9	38
59	3.6	18.0	1.6	32
60	3.2	16.0	1.6	32
61	3.4	17.0	1.7	34
62	5.0	25.0	1.8	36

Figure 50. Well log 3: Mainopokhar, Bardiya. Table with resistivities (1).

63	5.4	27.0	2.2	44
64	6.6	33.0	2.3	46
65	7.8	39.0	2.1	42
66	4.8	24.0	1.7	34
67	3.2	16.0	1.5	30
68	2.8	14.0	1.4	28
69	2.8	14.0	1.4	28
70	2.9	14.5	1.5	30
71	3.2	16.0	1.6	32
72	3.8	19.0	1.9	38
73	6.8	34.0	2.3	46
74	8.6	43.0	3	60
75	8.1	40.5	2.9	58
76	9.0	45.0	2.4	48
77	6.7	33.5	1.8	36
78	3.5	17.5	1.7	34
79	3.0	15.0	1.7	34
80	3.7	18.5	1.6	32
81	5.3	26.5	2	40
82	5.0	25.0	1.9	38
83	5.2	26.0	2	40
84	5.1	25.5	1.8	36
85	4.6	23.0	1.8	36
86	3.6	18.0	1.8	36
87	3.8	19.0	1.8	36
88	4.4	22.0	2.2	44
89	7.0	35.0	2.6	52
90	10.0	50.0	3.2	64
91	10.3	51.5	2.7	54
92	5.7	28.5	2.5	50
93	5.3	26.5	2.2	44
94	6.7	33.5	2.5	50
95	6.5	32.5	2.4	48
96	8.6	43.0	2.2	44
97	5.3	26.5	2.2	44
98	4.3	21.5	2.1	42
99	4.7	23.5	2.4	48
100	5.9	29.5	2.5	50
101	9.8	49.0	3.2	64
102	11.1	55.5	3.7	74
103	11.4	57.0	3.9	78
104	11.9	59.5	3.8	76
105	11.6	58.0	3.5	70
106	10.7	53.5	3.3	66
107	8.1	40.5	3.0	60
108	8.2	41.0	3.0	60
109	7.1	35.5	2.5	50
110	8.2	41.0	2.6	52
111	6.0	30.0	2.2	44
112	5.5	27.5	2.3	46
113	6.1	30.5	2.3	46
114	5.4	27.0	1.9	38
115	5.0	25.0	2.1	42
116	4.1	20.5	2.0	40
117	5.5	27.5	2.0	40
118	6.9	34.5	2.3	46
119	6.1	30.5	2.2	44
120	4.8	24.0	2.1	42
121	6.9	34.5	2.3	46
122	6.0	30.0	2.1	42
123	5.2	26.0	2.3	46
124	7.3	36.5	2.6	52
125	8.8	44.0	2.9	58
126	9.2	46.0	2.3	44
127	5.0	25.0	2.1	42
128	4.2	21.0	1.8	36
129	4.5	21.0	2.0	40
130	6.3	31.5	2.3	46
131	10.3	52.5	3.0	60
132	10.2	51.0	3.0	60

Figure 51. Well log 3: Mainopokhar, Bardiya. Table with resistivities (2).

133	9.8	49.0	2.6	52
134	7.2	36.0	2.2	44
135	6.3	31.5	1.8	36
136	4.4	22.0	1.7	34
137	3.8	19.0	1.6	32
138	3.5	17.5	1.5	30
139	3.7	18.5	1.4	28
140	3.2	16.0	1.6	32
141	3.2	16.0	1.6	32
142	4.4	22.0	1.6	32
143	7.5	37.5	1.9	38
144	4.5	22.5	1.6	32
145	3.7	18.5	1.6	32
146	3.7	18.5	1.6	32
147	3.8	19.0	1.6	32
148	3.8	19.0	1.7	34
149	3.9	19.5	1.6	32
150	3.8	19.0	1.6	32



Figure 52. Well log 3: Mainopokhar, Bardiya. Table with resistivities (3).

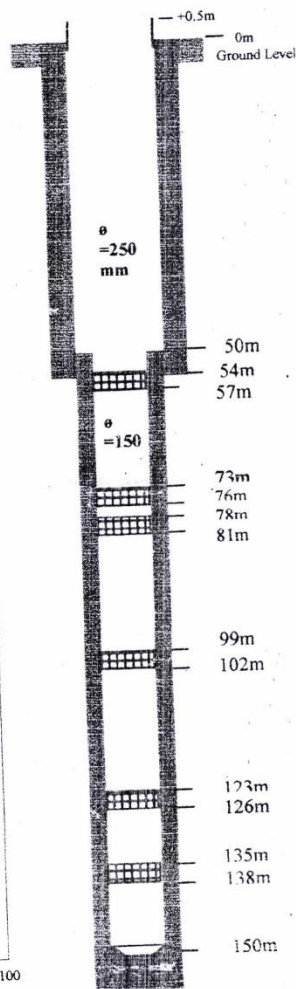
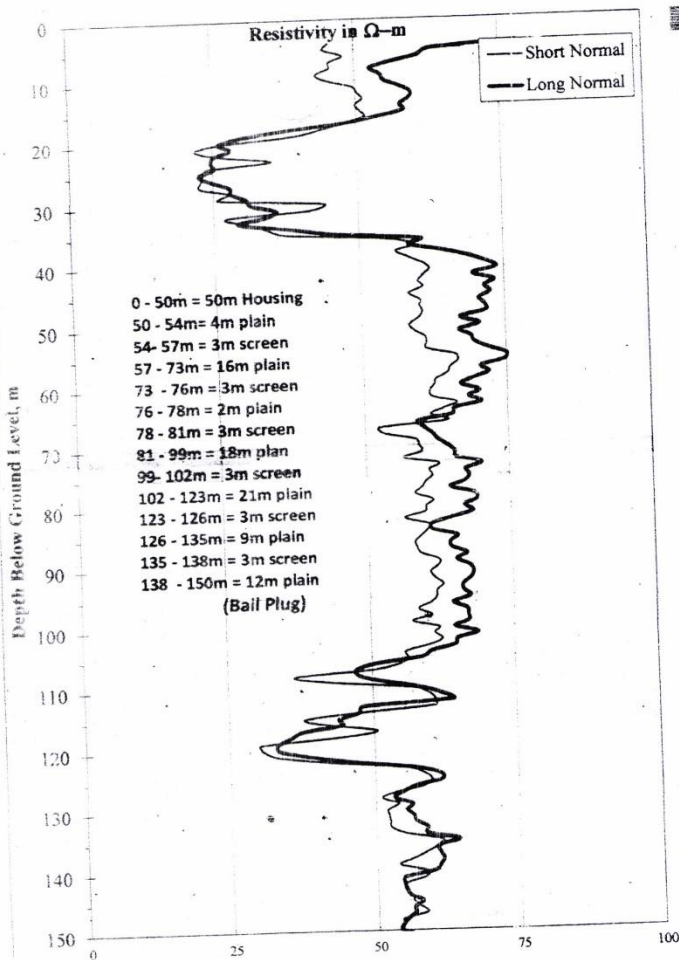
WATER SUPPLY AND SANITATION DIVISION OFFICE
GULARIYA BARDIYA *Gulariya-12*
Ist

LOCATION : Tepari, Rampur-9, Bardiya

Date : 2074/8/29

WELL ASSEMBLY DIAGRAM

ELECTRICAL LOG DATA



Prepared by

Hydrogeologist *Bikash Rana Bhat*

- Casing Pipe
- Gravel Pack Envelope
- Jhonson SS Screen pipe

Figure 53. Well log 4: Tepari, Rampur-9, Bardiya. Resistivity curve.

Dalla

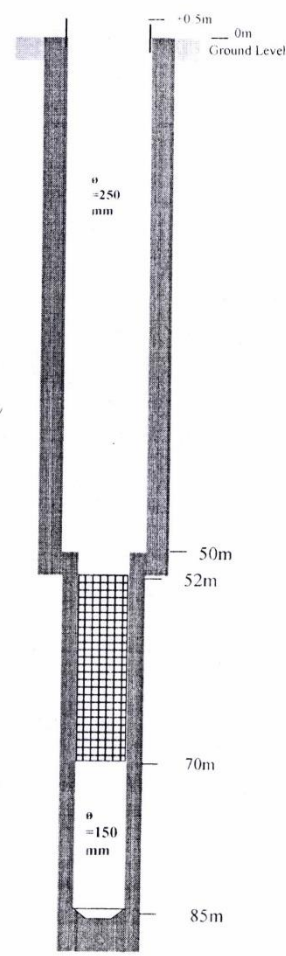
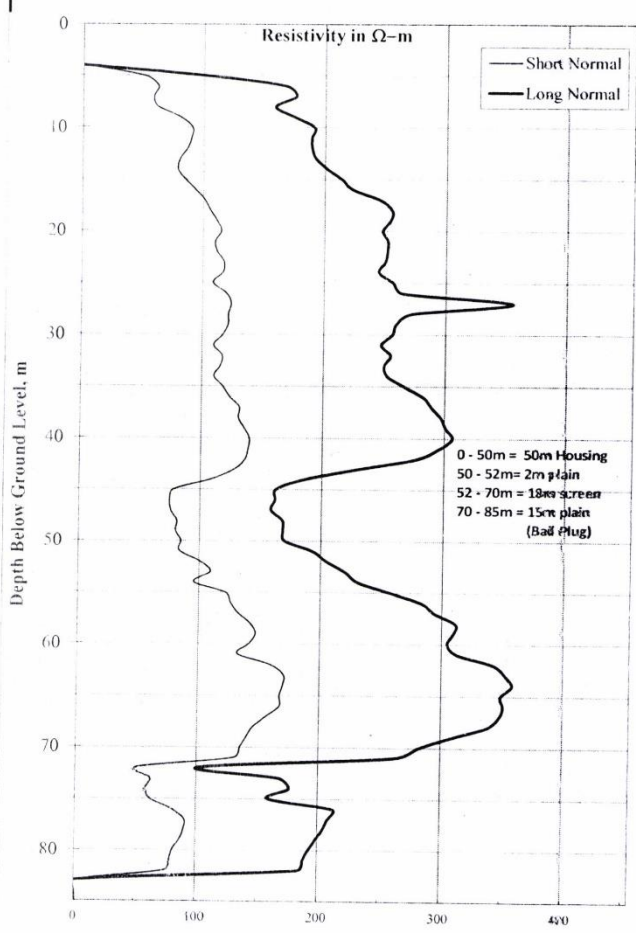
KAILASHI WATER SUPPLY PROJECT BARDIYA

LOCATION : MADHUWAN, BARDIYA

Date : 2074/2/18

WELL
ASSEMBLY
DIAGRAM

ELECTRICAL LOG DATA



- Casing Pipe
- Gravel Pack Envelope
- Jhonson SS Screen pipe

5

Figure 54. Well log 5: Madhuwan/Dalla, Bardiya. Resistivity curve.

WATER SUPPLY AND SANITATION DIVISION OFFICE

GULARIYA BARDIYA

Babai - 67 ID
 WSP
 Baganaha

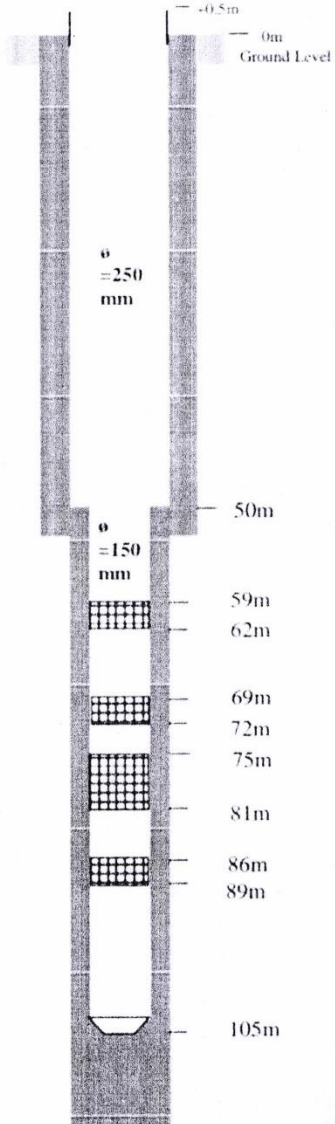
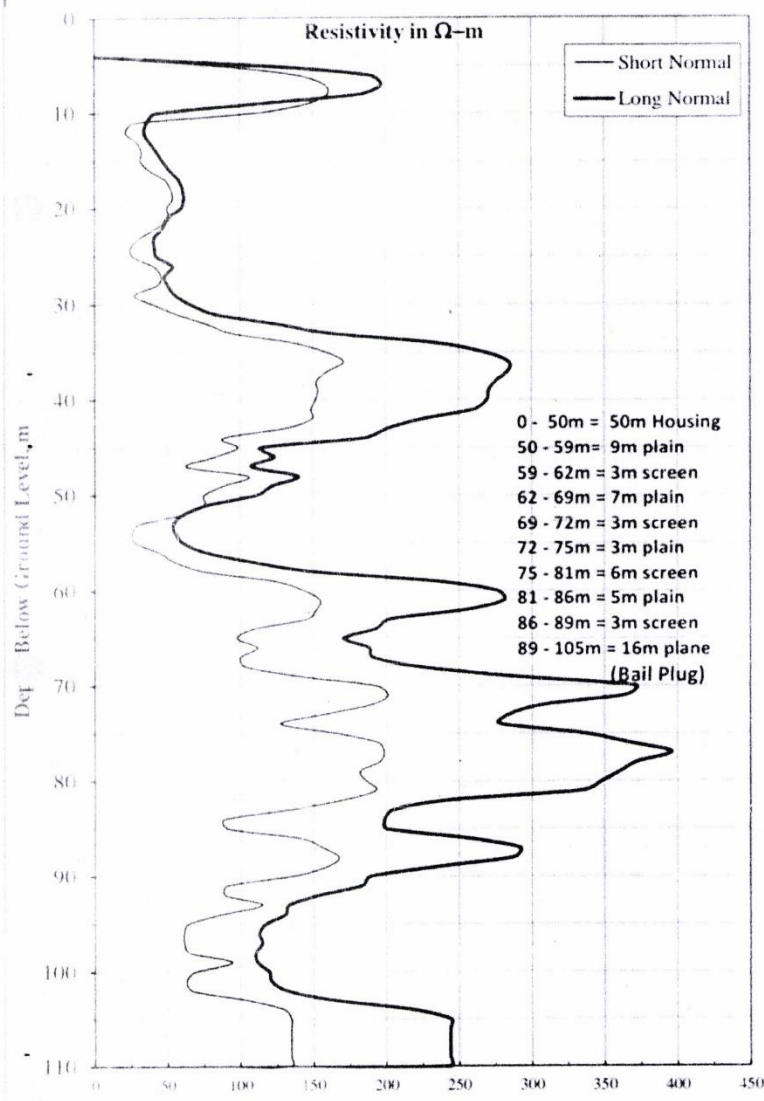
Baganaha

LOCATION : BAGNAHA, TAKIYA-05, BARDIYA

Date : 2074/9/27

WELL ASSEMBLY DIAGRAM

ELECTRICAL LOG DATA



Prepared by

 Hydrogeologist Bikash Rana Bhat

□ Casing Pipe
 ▨ Gravel Pack Envelope
 ▩ Johnson SS Screen pipe

Bhargava/Nalopre

Figure 55. Well log 6: Baganaha, Takiya-05, Bardiya. Resistivity curve.

2

सुनी ४५

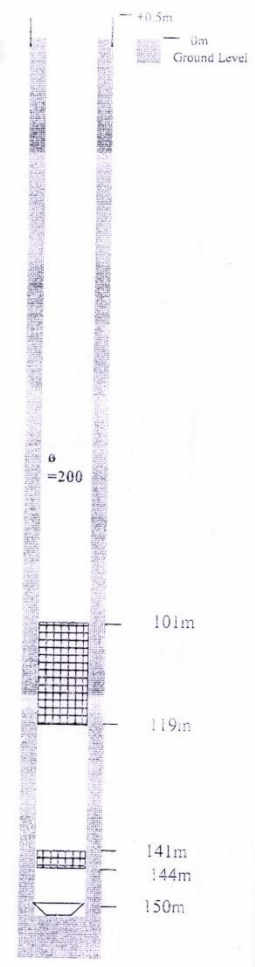
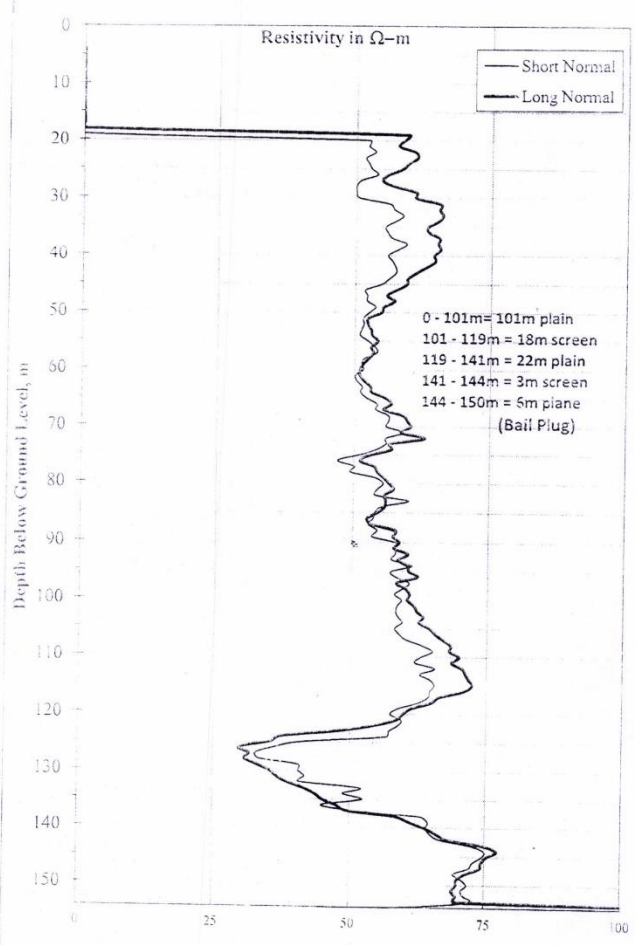
WATER SUPPLY AND SANITATION DIVISION OFFICE GULARIYA BARDIYA

LOCATION : DHARMABASTI-9, BARDIYA

Date : 2074/11/01

WELL
ASSEMBLY
DIAGRAM

ELECTRICAL LOG DATA

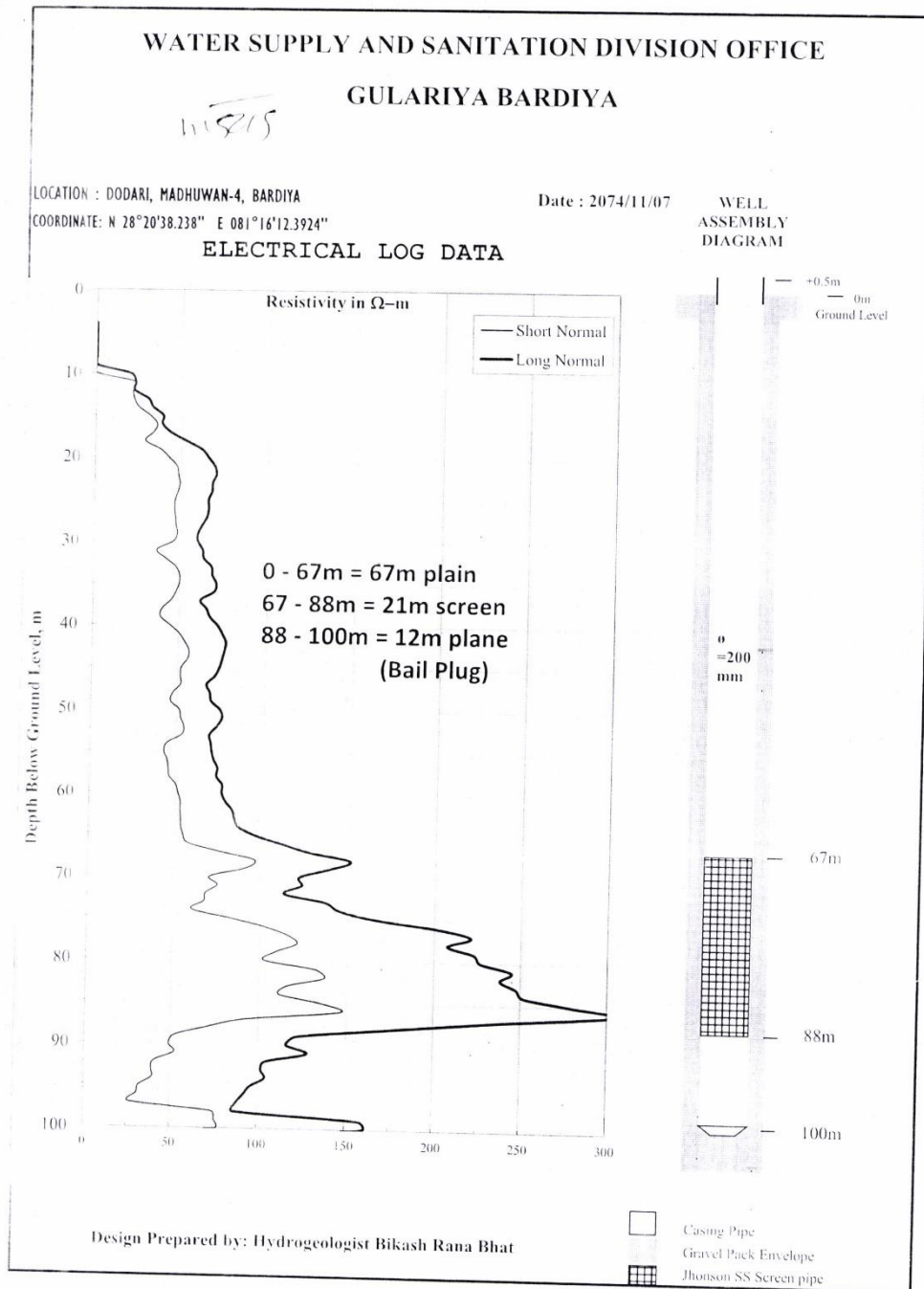


Prepared by
[Signature]
Hydrogeologist Bikash Ram Bhat



- Casing Pipe
- ▨ Gravel Pack Envelope
- ▧ Jhonson SS Screen pipe

Figure 56. Well log 7: Dharmabasti-9, Bardiya. Resistivity curve.



Dhodhari

(19) (20)

Figure 57. Well log 8: Dodari, Madhuwan-4, Bardiya. Resistivity curve.

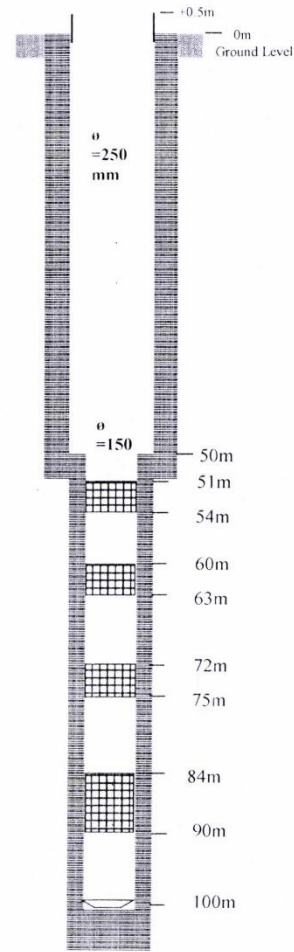
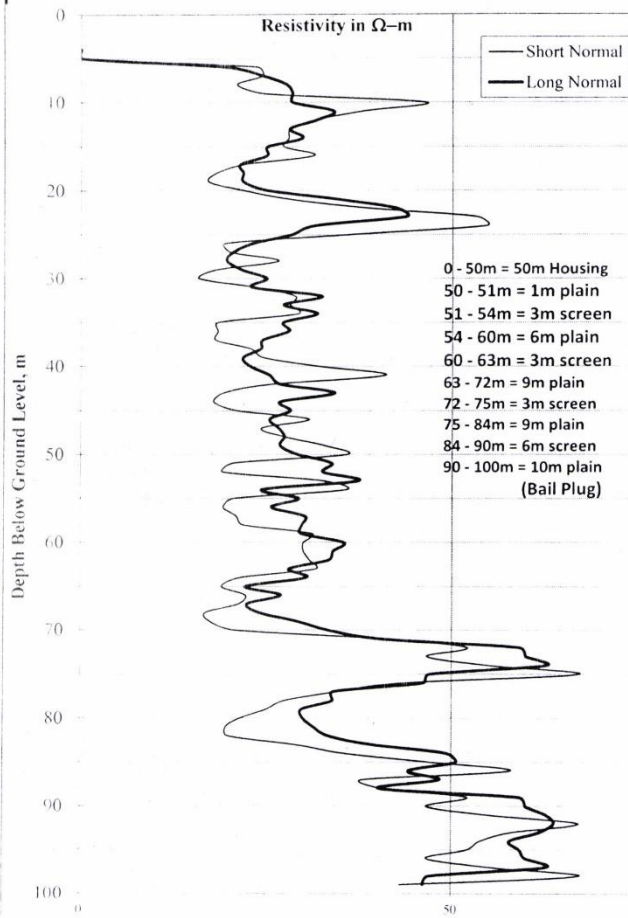
**WATER SUPPLY AND SANITATION SUB-DIVISION OFFICE
BARDIYA**

LOCATION : Sansneri-4, Bardiya
COORDINATE:

Date : 2075/1/8

WELL
ASSEMBLY
DIAGRAM

ELECTRICAL LOG DATA



Casing Pipe
 Gravel Pack Envelope
 Jhonson SS Screen pipe

Prepared By : Hydrogeologist Om Kumar Khadka

32

?

Figure 58. Well log 9: Asansneri-4, Bardiya. Resistivity curve.

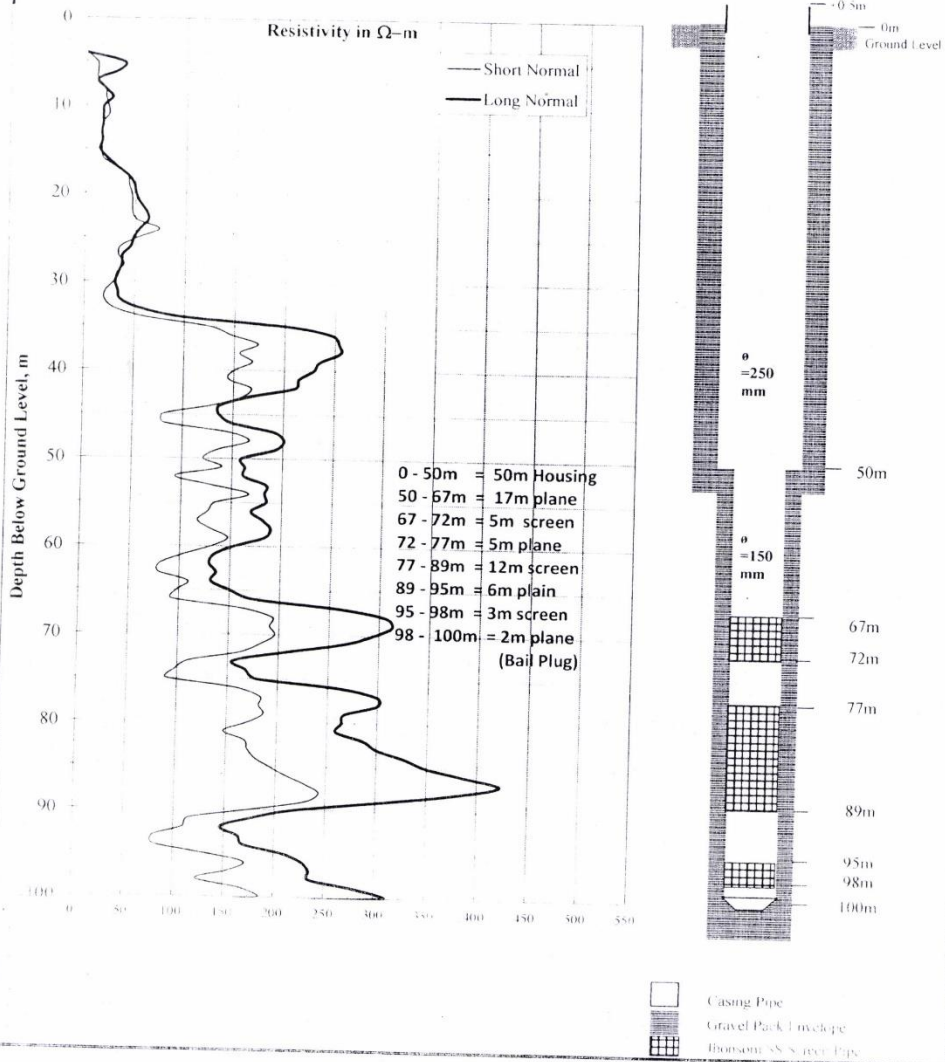
WATER SUPPLY AND SANITATION DIVISION OFFICE
GULARIYA, BARDIYA

LOCATION : Bhuriguon-01, Thakurbaba vdc, Bardiya

Date : 2074/08/12

WELL
ASSEMBLY
DIAGRAM

ELECTRICAL LOG DATA



18

Figure 59. Well log 10: Bhuriguon-01, Thakurbaba VDC Bardiya. Resistivity curve.

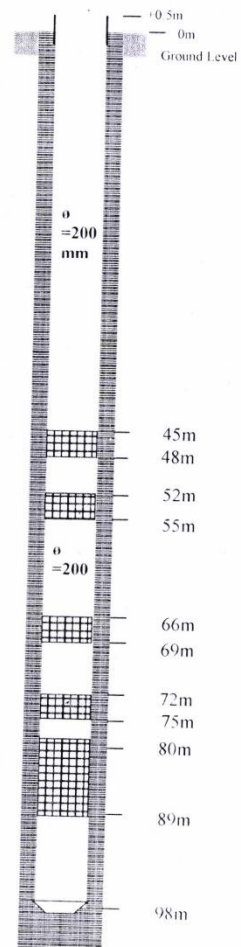
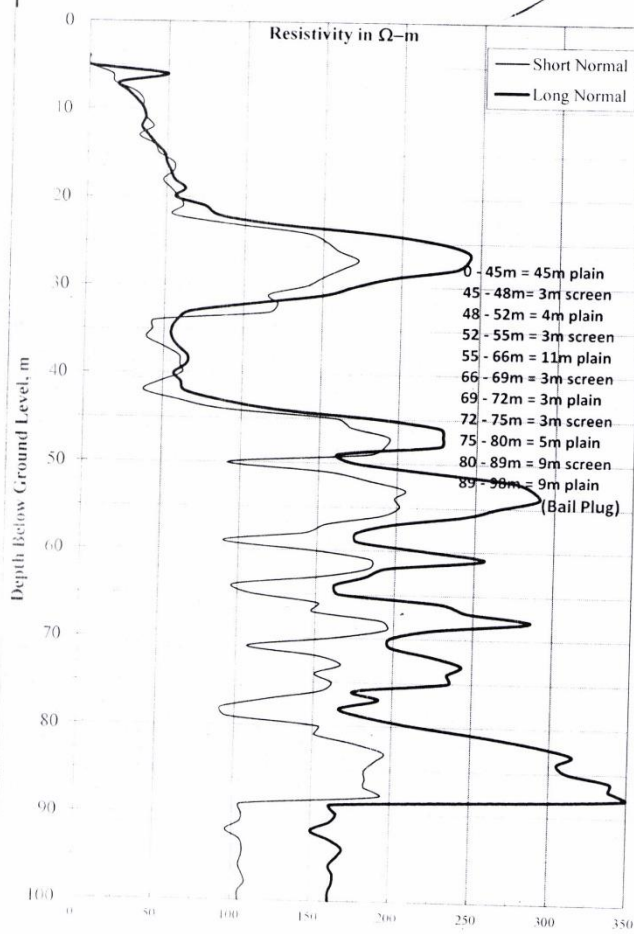
WATER SUPPLY AND SANITATION DIVISION OFFICE
GULARIYA BARDIYA

LOCATION : KARMALA -2, THAKUR BABA MUNICIPLAITY, BARDIYA

Date : 2074/9/27

WELL ASSEMBLY DIAGRAM

ELECTRICAL LOG DATA



□ Casing Pipe
▨ Gravel Pack Envelope
▧ Johnson SS Screen pipe

Close to Pratapur.

19

Figure 60. Well log 11: Karmala-02, Thakurbaba municipality, Bardiya. Resistivity curve.

WATER SUPPLY AND SANITATION DIVISION OFFICE
GULARIYA BARDIYA

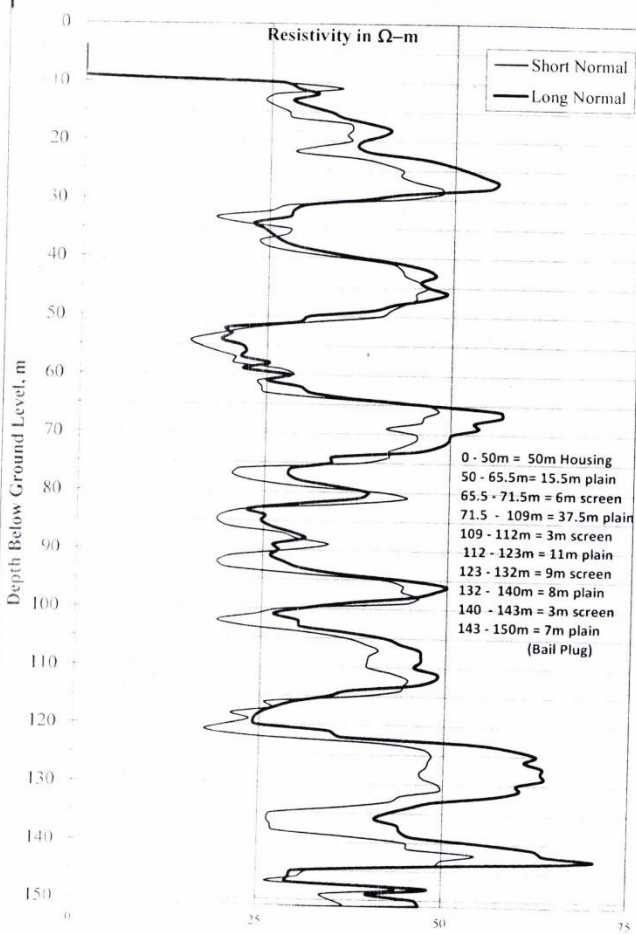
W.D. 10/1/14

LOCATION : GANESHPUR, GULARIYA, BARDIYA

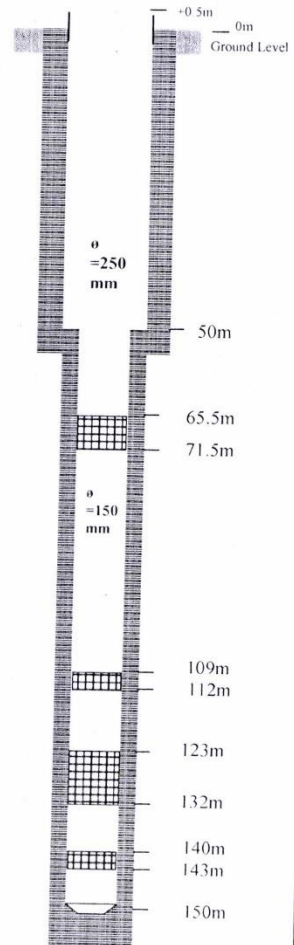
Date : 2074/1/14

WELL ASSEMBLY DIAGRAM

ELECTRICAL LOG DATA



0 - 50m = 50m Housing
50 - 65.5m = 15.5m plain
65.5 - 71.5m = 6m screen
71.5 - 109m = 37.5m plain
109 - 112m = 3m screen
112 - 123m = 11m plain
123 - 132m = 9m screen
132 - 140m = 8m plain
140 - 143m = 3m screen
143 - 150m = 7m plain
(Bail Plug)



Prepared by *[Signature]*

Hydrogeologist **Bikash Rana Bhat**

- Casing Pipe
- Gravel Pack Envelope
- Jhouson SS Screen pipe

on the map

[Signature]

Figure 61. Well log 12: Ganeshpur, Gulariya, Municipality, Bardiya. Resistivity curve.

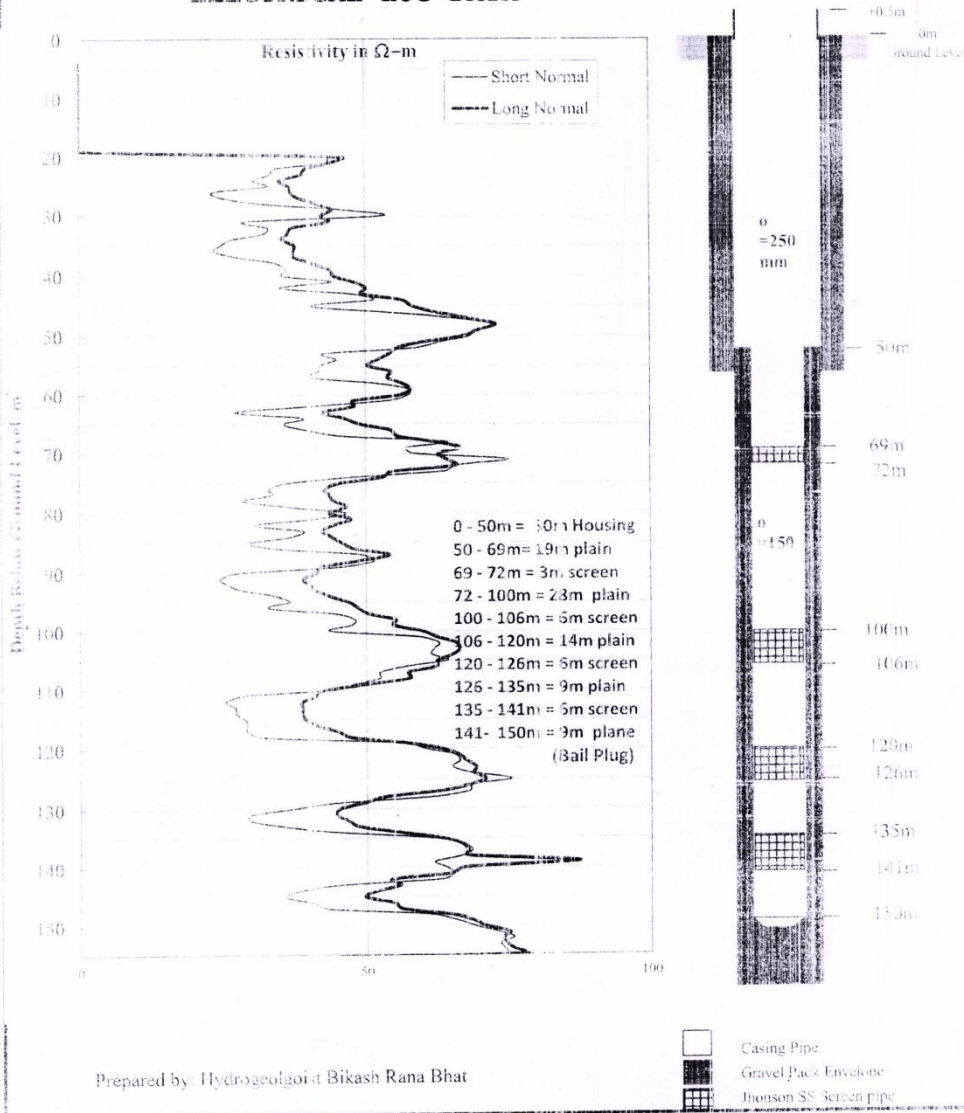
**WATER SUPPLY AND SANITATION DIVISION OFFICE
GULERIYA, BARDIYA**

LOCATION : JAMUNI-5, BADAIYA GAUPALIKA, SITAPUR, BARDIYA

Date : 2074/12/20

WELL
ASSEMBLY
DIAGRAM

ELECTRICAL LOG DATA



Bahaiya Lake
(30)

Figure 62. well log 13: Jamuni-5, Badaiya, Gaupalika, Sitapur, Bardiya. Resistivity curve.

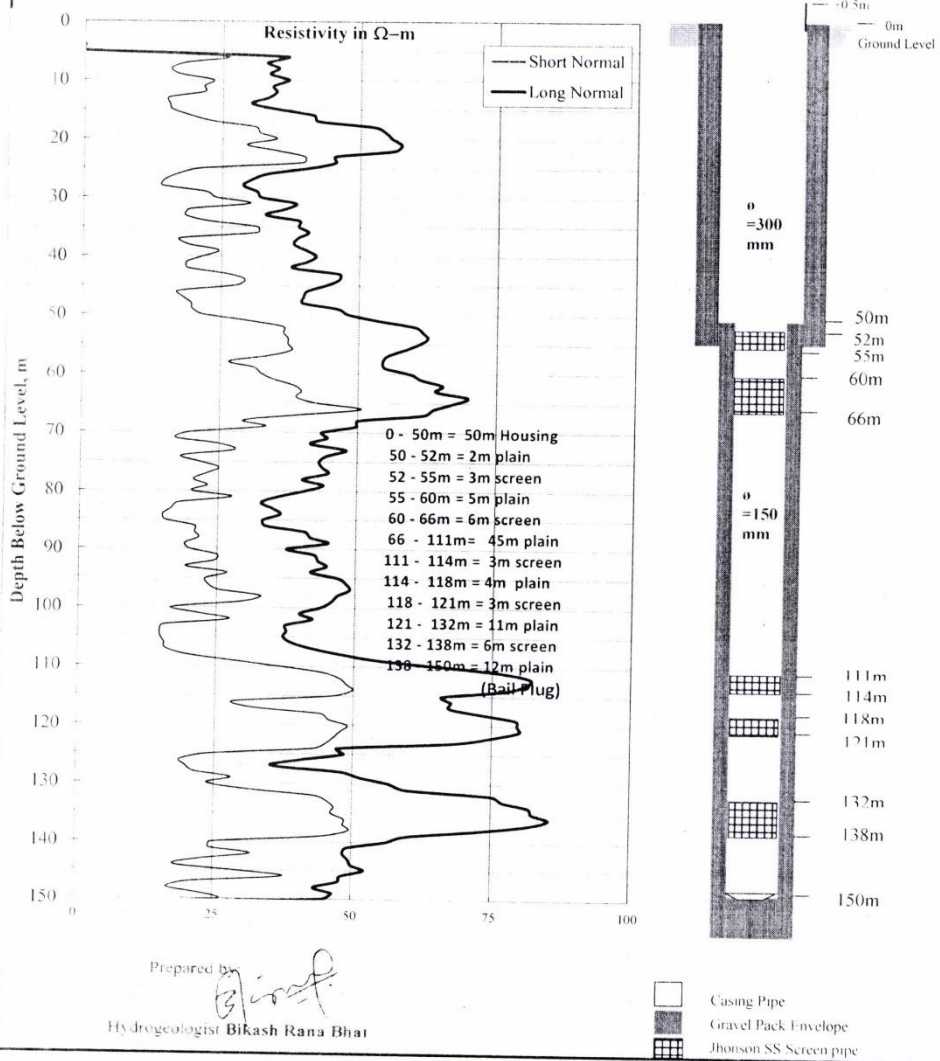
**WATER SUPPLY AND SANITATION DIVISION OFFICE
BARDIYA**

LOCATION : Deudakala-7, Basgadi, Bardiya

Date : 2075/2/11

WELL ASSEMBLY DIAGRAM

ELECTRICAL LOG DATA



Deudakala on map

Figure 63. Well log 14: Deudakala-7, Basgadi, Bardiya. Resistivity curve.

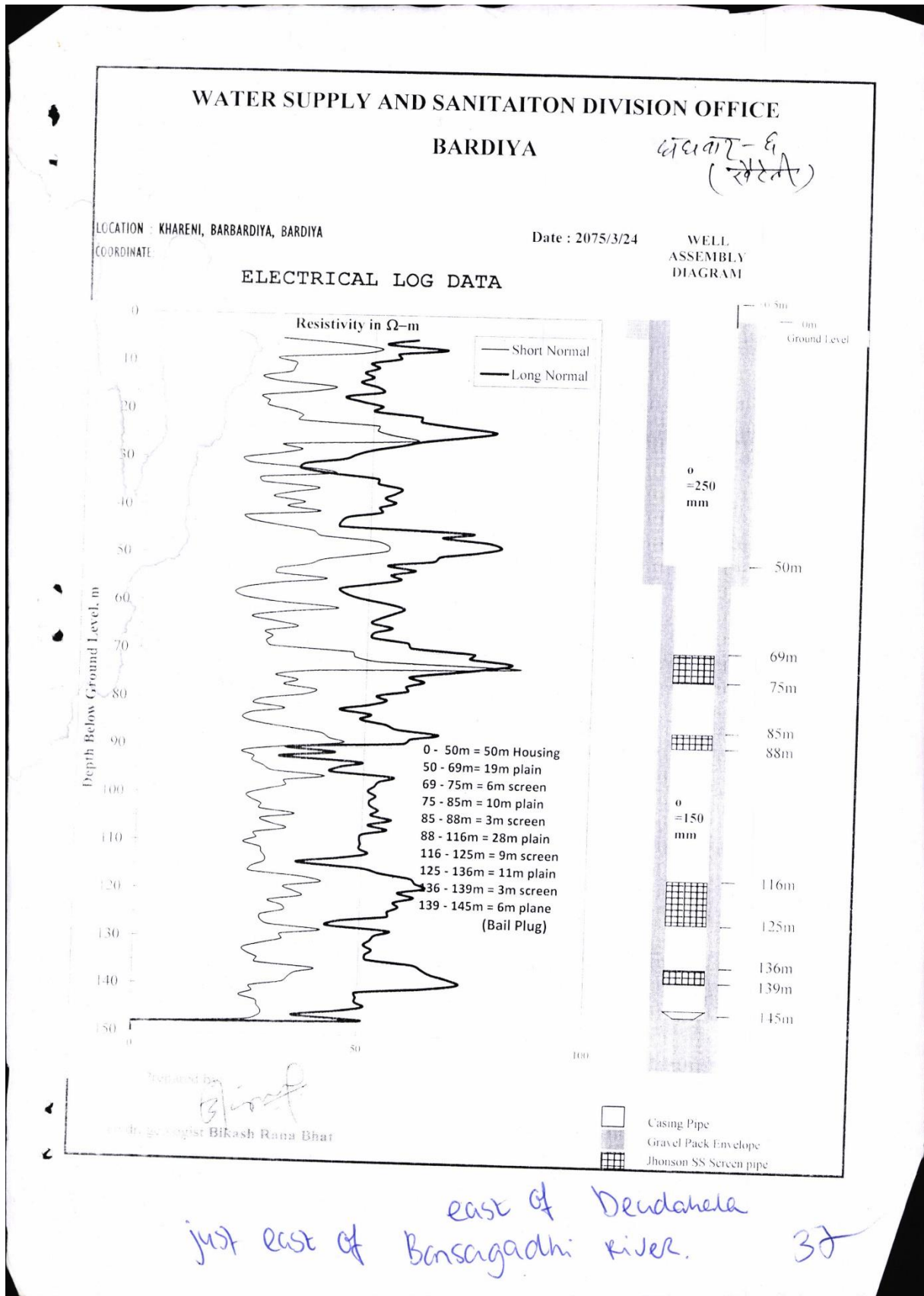


Figure 64. Well log 16: Khareni, Barbardiya, Bardiya. Resistivity curve.

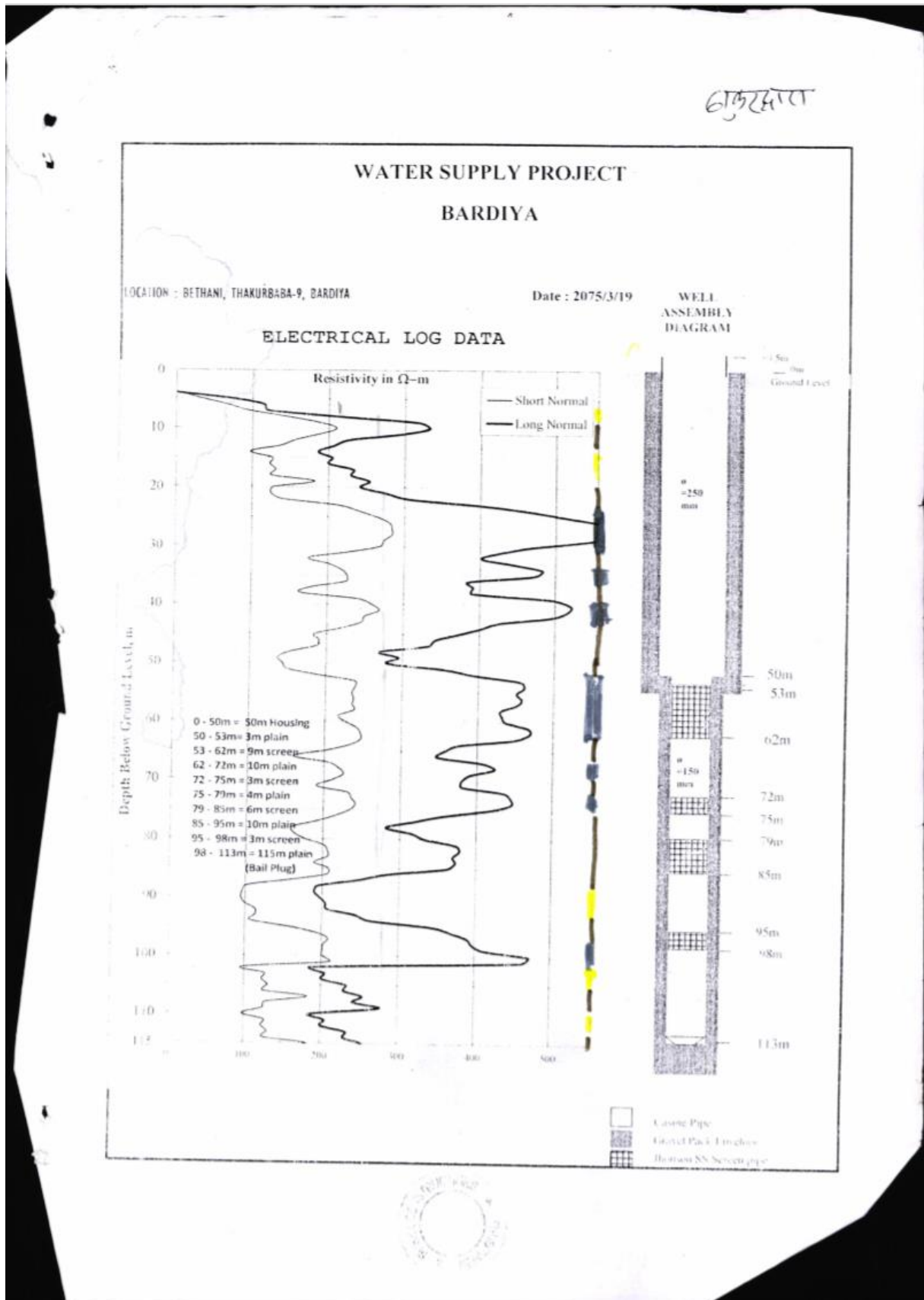
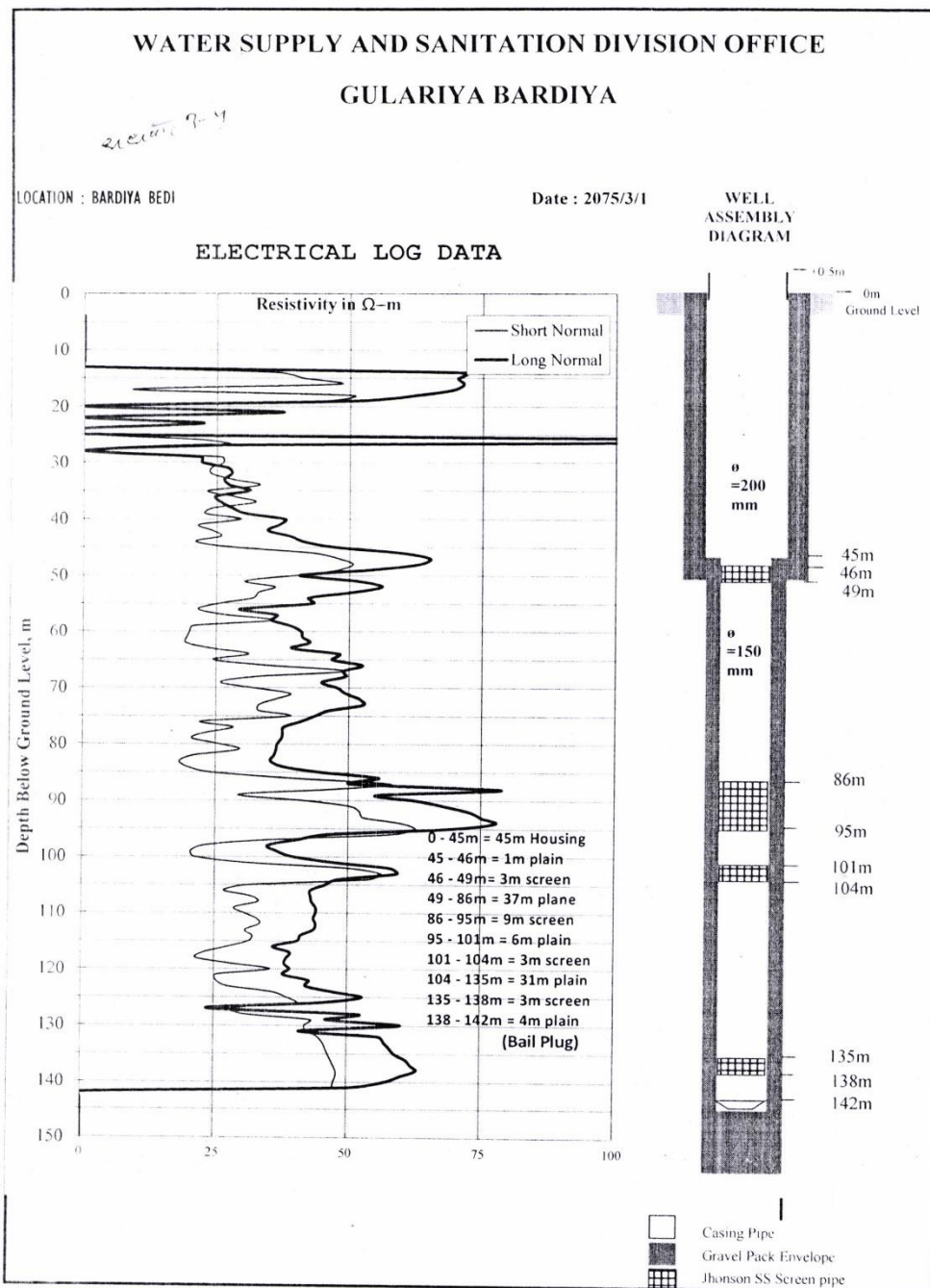


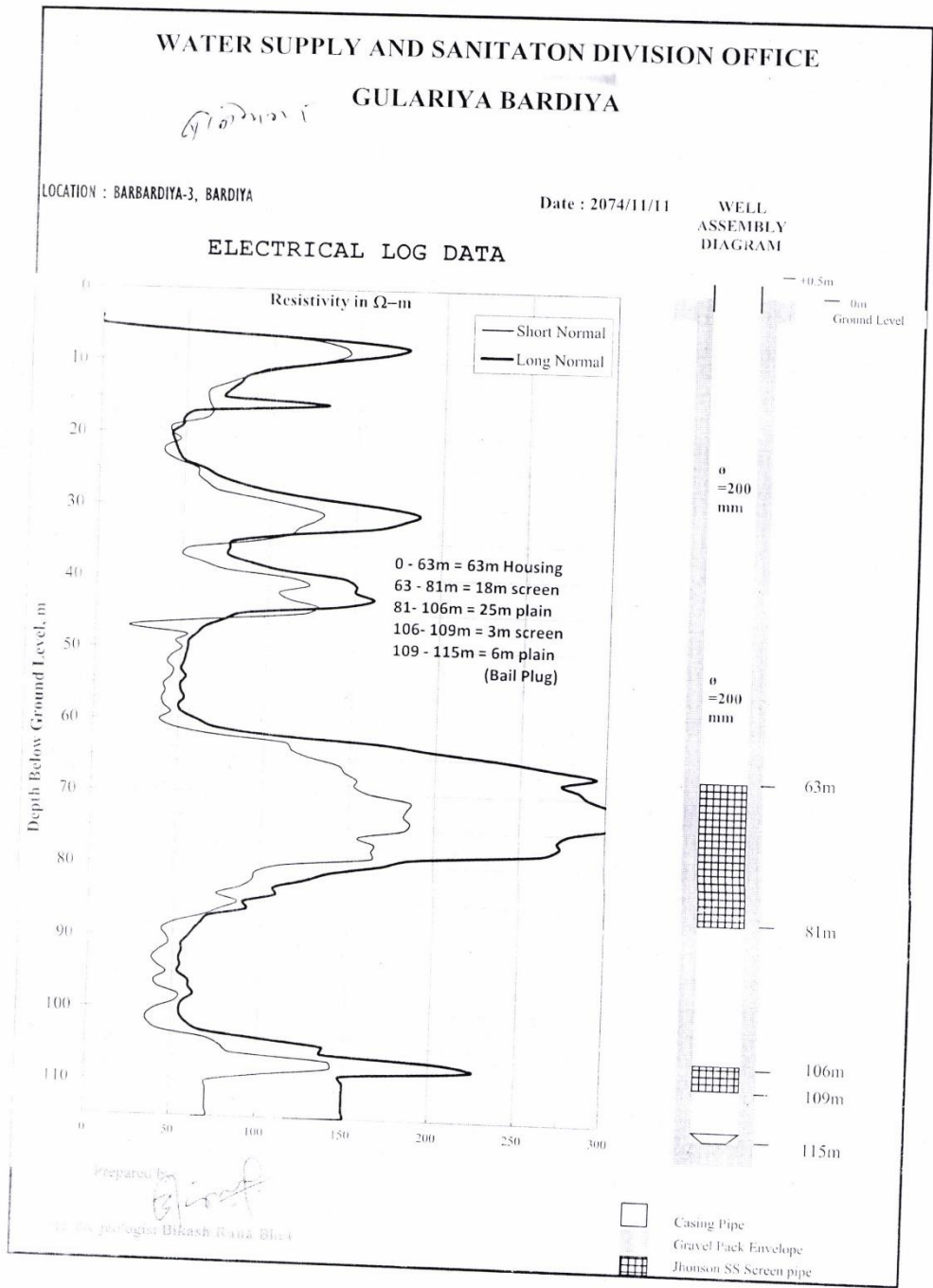
Figure 65. Well log 17: Bethani, Thakurdbaba-9, Bardiya. Resistivity curve.

Appendix C
Unused well log data



32

Figure 66. Unused resistivity curve 1: uncertainty regarding the location.



near Banigabhar.



Figure 67. Unused resistivity curve 2: location unknown.

WATER SUPPLY AND SANITATION DIVISION OFFICE

621915

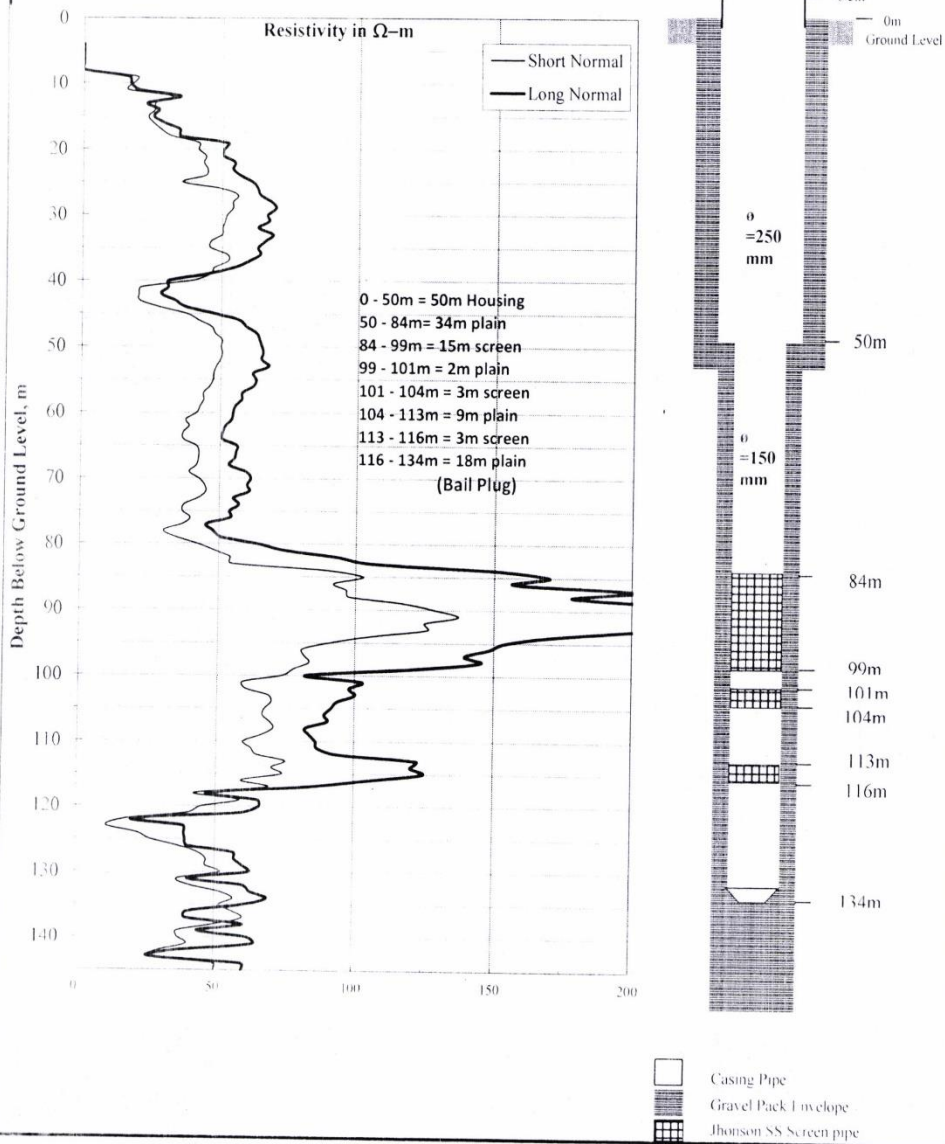
GULARIYA BARDIYA

LOCATION : DASHRATH BASTI-7, MADHUWAN, TARATALL, BARDIYA

Date : 2074/9/27

WELL ASSEMBLY DIAGRAM

ELECTRICAL LOG DATA



bl

Sanashree taratall

Figure 68. Well log 15: Dasrath Basti-7, Madhuwan, Taratell, Bardiya. Resistivity curve.

Appendix D

Pumping discharge measurements pumping test 1

All the water that was pumped up was transported to the rice fields through a small irrigation channel. The irrigation channel was trapezium shaped. The dimensions of the of the irrigation channel were measured. The flow velocity was measured with an electromagnetic flow meter in the horizontal centre of the irrigation channel, at a depth of 60% of the depth from the water head (V_{measured} , Figure 69). This flow velocity approximates the average flow velocity over the depth at the horizontal centre (Hartong & Termes, 2009). The average flow velocity was extended to the entire cross-section, by dividing the trapezium-shaped cross-section into a rectangle and two triangles (Figure 69). For the rectangle, the average flow velocity ($V_{\text{rectangle}}$) equals the average flow velocity at horizontal centre:

$$V_{\text{rectangle}} = V_{\text{measured}} \quad (7)$$

The decrease in flow velocity towards the banks of the irrigation channel is represented by a correction of the flow velocity in the triangles (V_{triangle}), which equals the average flow velocity at the horizontal centre multiplied with a factor of 0.5 (Hartong & Termes, 2009):

$$V_{\text{triangle}} = 1/2 \cdot V_{\text{measured}} \quad (8)$$

Then, the discharge (D) is calculated by multiplying the area (A) with the corresponding average flow velocity:

$$D = A_{\text{rectangle}} \cdot V_{\text{rectangle}} + A_{\text{triangle}} V_{\text{triangle}} \quad (9)$$

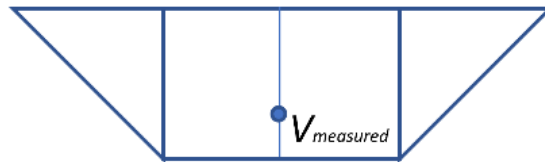


Figure 69. Shape irrigation channel and flow velocity measuring point

Appendix E

Assumptions pumping test

Eq. 2 (chapter 2.5) is only valid if u and $u' < 0.01$. This requirement is fulfilled if (Kruseman et al., 1970):

$$t > \frac{25 r^2 S}{KD}$$

where t = pumping time [s], r = filter diameter [m], s = storativity [-] and KD = transmissivity [m^2/s]. For this research this requirement is amply fulfilled.

Appendix F

Determination of storativity

$$S = S_b \cdot D \tag{11}$$

where S is storativity [-], S_b = specific storage [m^{-1}] and D = depth of the aquifer [m]. For the specific storage was assumed that the aquifer exists of dense sand, giving a specific storage of $1.5 \cdot 10^{-5} m^{-1}$ (Domenico & Mifflin, 1965).

Appendix G

Extrapolation of groundwater head to steady state groundwater head

The first three measurements after cessation of pumping were extrapolated to the steady state water head as follows:

$$\frac{slope0}{slope1} = \frac{slope1}{slope2} \tag{12}$$

where $slope0$ = slope between the steady state water head and the first measurement after cessation of pumping [m/s], $slope1$ = slope between the first and second measurement [m/s] and $slope2$ = slope between the second and third measurement [m/s]. Based on the estimated slope 0 and the first water head measurement, the water head at steady state was calculated.

Appendix H

Photo of soil profile



Figure 70. Profile of originating layer of sample IV.

Appendix H

Information of groundwater head monitoring locations

Table 8. Overview of well depth and pressure transducer type of groundwater monitoring locations.

Name	Loc.	Sample no.	Depth [m]	Pressure transducer	Type of well
Ambassa	A	26	27	Diver	Active handpump military post
Motipur	B	7	9.8	Keller	Inactive handpump
Lamkauli	C	13	11.6	Keller	Inactive handpump for drinking water pond
Bankhet	D	18	10.5	Diver	Active handpump military post
Bhagaura	E	11	5.1	Keller	Newly installed monitoring well
Gaida Machan	F	12	6.2	Diver	Active handpump military post
NTNC	G	54	5.7	Diver	Active handpump
Hatti Machan	H	10	5.2	Diver	Active handpump military post
Girwa Bank	I	6	4.4	Keller	Inactive handpump
Hattisar	J	24	5.0	Keller	Inactive handpump
Godhana	K	23	7.7	Keller	Inactive irrigation pump
Bhaurigon	L	15	7.4	Diver	Active handpump military post
Sainawar	M	14	7.0	Diver	Active handpump military post
Chotki	N	21	9.3	Keller	Inactive irrigation pump
Bawapur	O	20	10.2	Keller	Inactive irrigation pump
Bardiya Homestay	P	1	6.8	Diver	Active handpump
Bhaurigon deep	Q	3	100	Keller	Active deep well water tower
Motipur deep	R	53	100	Keller	Inactive deep well water tower

Appendix I
Groundwater heads at 12th December 2018

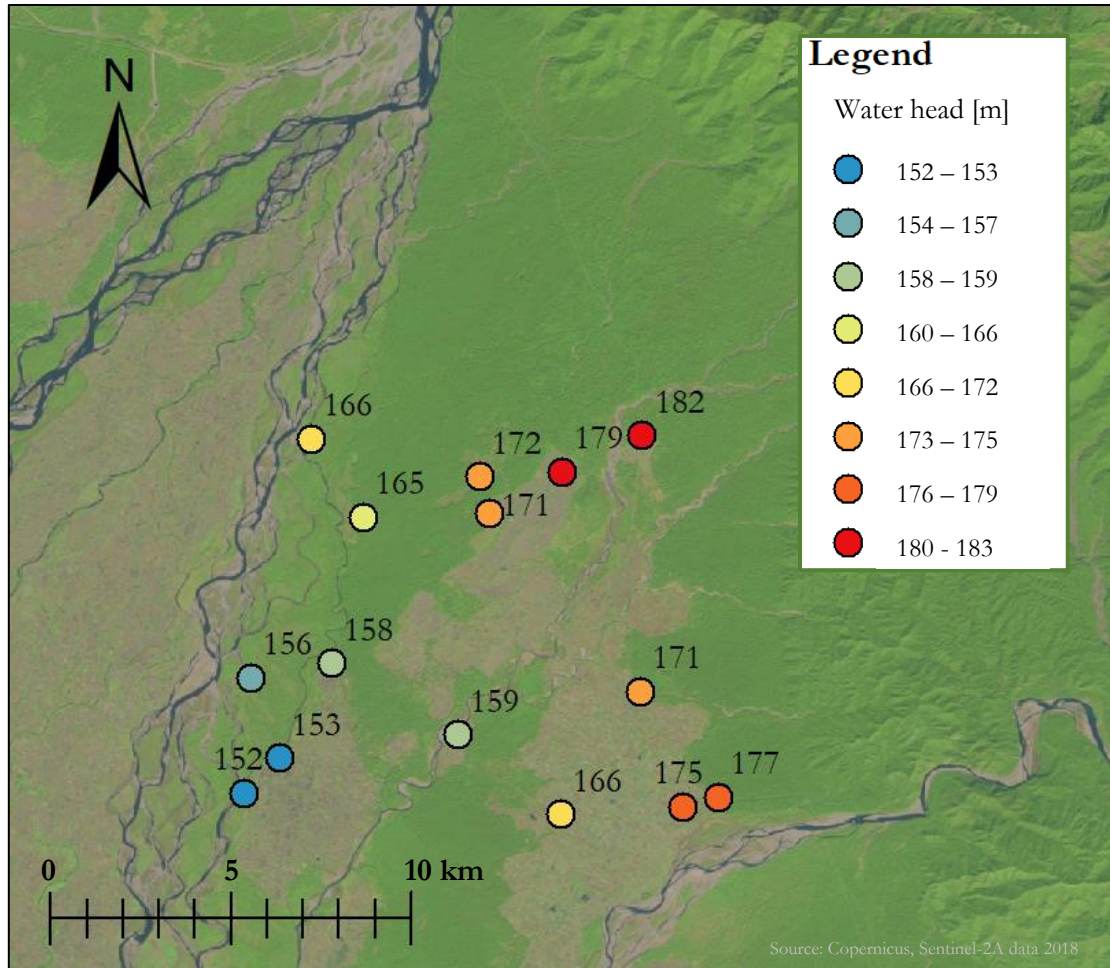


Figure 71. Spatial distribution groundwater head at 12th December 2018.

Appendix J
General information water samples

No.	Month	Day	Type	Lat. (DD)	Long. (DD)
1	9	28	shallow GW	28.4366	81.2363
2	9	29	Aurahi river	28.5119	81.3164
3	10	2	deep GW	28.4531	81.3294
5	10	4	accumulated rain	28.4641	81.2482
6	10	5	shallow GW	28.4404	81.2350
7	10	5	shallow GW	28.5119	81.3055
8	10	5	Karnali river	28.4407	81.2343
9	10	7	Karnali river	28.3670	81.2022
10	10	13	shallow GW	28.4605	81.2280
11	10	14	shallow GW	28.5006	81.2561
12	10	14	shallow GW	28.5200	81.2430
13	10	14	shallow GW	28.5107	81.2852
14	10	15	shallow GW	28.4308	81.3448
15	10	15	shallow GW	28.4571	81.3253
16	10	15	shallow GW	28.6301	81.2788
17	10	15	Karnali river	28.6329	81.2761
18	10	15	shallow GW	28.5014	81.2875
19	10	21	Babai river	28.4236	81.3802
20	10	21	shallow GW	28.4284	81.3358
21	10	21	shallow GW	28.4265	81.3053
22	10	22	shallow GW	28.5535	81.2622
23	10	23	shallow GW	28.4463	81.2797
24	10	23	shallow GW	28.4317	81.2264
25	10	28	shallow GW	28.4853	81.2766
26	10	28	shallow-deep GW	28.5210	81.3257
27	10	28	shallow GW	28.4949	81.3244
28	10	28	shallow GW	28.4750	81.3364
29	10	28	shallow GW	28.3962	81.2949
30	10	28	shallow GW	28.4043	81.2589
31	11	4	rain 2AM	28.4641	81.2482
32	11	4	rain 8AM	28.4641	81.2482
34	11	4	rain 5PM	28.4641	81.2482
36	11	5	Aurahi river	28.5149	81.3177
37	11	7	shallow GW	28.4110	81.2300
38	11	8	shallow GW	28.5714	81.3724
39	11	8	brook	28.5602	81.3634
40	11	10	brook	28.5671	81.4175
41	11	10	spring	28.5682	81.4299
42	11	11	spring	28.5600	81.4364
43	11	11	spring	28.5597	81.4357
44	11	11	spring	28.5565	81.4409
45	11	11	brook	28.5341	81.3767
46	11	14	deep GW	28.4587	81.2503
47	11	20	Karnali river	28.5701	81.2640
48	11	25	Babai river	28.4246	81.3803
49	12	1	Babai river	28.4256	81.5671
50	12	1	shallow GW	28.4186	81.5849
51	12	1	shallow GW	28.4396	81.5270
52	12	10	shallow GW	28.5118	81.3098
53	12	10	deep GW	28.5118	81.3098
54	12	12	shallow GW	28.4641	81.2482

Figure 72. Sample numbers and their sample date, sample type and sample location.

Appendix K
Isotope data

Table 9. Replications of isotope measurements.

no.	$\delta^{18}\text{O}$ [‰SMOW]	$\delta^2\text{H}$ [‰SMOW]	no.	$\delta^{18}\text{O}$ [‰SMOW]	$\delta^2\text{H}$ [‰SMOW]
1	-8.0804996896	-55.460503000	31	2.6432056000	15.254840788
	-8.0376630800	-56.615746990		2.6358803200	
	-6.8928601824	-47.246764627		2.9734536400	17.503008396
2		-48.519768611	32	2.7473873600	15.329187617
	-6.9360711952	-47.034600900		4.1359348800	26.240498665
3	-6.6155413600	-48.937238082	34	4.1745960800	23.181950271
	-4.2190760080	-29.775599579	36	-6.9472137600	-47.799491075
5		-31.552393453		-8.0689990000	-52.648503533
	-8.7681481408	-62.589914974	37		-54.918406371
6	-8.8613501200	-61.930189300		-6.8000000000	-47.524253442
	-6.2198378736	-45.472517895	38		-44.577292200
7		-44.103457300		-7.1150847600	-48.372443918
	-9.5309376864	-69.703589016	39	-6.9323597200	-47.812362500
9	-9.9872130992	-70.145290312		-7.2288300800	-45.422022887
	-9.8075321200				-47.364649460
	-6.1525022720	-41.366246679	40		-49.700887600
10		-40.327770000		-7.5330326800	-50.148851758
	-6.5856542176	-46.201985575	41	-7.6567485200	-50.173813900
11	-6.5544973600	-44.246561800		-7.3409475600	-45.791711164
	-5.1066313504	-31.866205389			-49.000500462
12		-34.361741496	42		-49.043969800
	-6.4213888832	-43.044955717		-6.9734626800	-45.578425273
13		-43.364311200			-48.182162700
	-6.5482301760	-45.894582438	43		-47.818722700
14	-6.3923238000	-45.714859400		-7.0564825200	-46.731430739
	-5.7128145488	-38.852239709	44	-7.1213926400	-46.799273500
15		-38.884004600		-6.5321145600	-43.156007736
	-6.9191172416	-44.949182656			-45.652501012
16		-47.820850980	45		-43.728659800
	-11.1982088547	-80.034064751		-7.6117794400	-49.982845965
17	-11.2587514800			-7.3885618800	-51.611459892
	-6.8005669958	-45.383221170	46		-52.103226000
18		-47.418171897		-11.2955813600	-77.288999001
	-6.8350252655	-48.951346389			-78.630012919
19	-6.6546095200		47		-77.789802300
	-5.7524805839	-35.901535929		-6.6786201600	-47.376513817
20	-5.9497548000	-40.417400210	48	-6.7123978400	-47.439382200
	-6.0785267110	-43.675378056		-6.8184109200	-45.340718792
21		-43.408378300			-45.856709671
	-6.8940444869	-47.192726177	49		-48.080399500
23	-7.2908736246	-51.720631148		-6.8926811200	-44.314320731
	-7.1181369600	-50.096128600	50		-45.049309900
24	-11.4940297066	-78.921827408		-7.0983994000	-45.597117540
		-82.030300444		-6.9435511200	-46.612076398
25	-6.6055981572	-48.044860740	51		-49.660909200
		-43.804073600		-6.6047569200	-42.858483094
26	-6.8935965765	-47.503826911		-6.4195901200	-44.524870371
	-6.7209440000				-45.330521600
27	-6.4290247246	-45.974673107	52		-43.559660200
		-43.765912400		-6.6035360400	-40.918862400
28	-6.8857090813	-48.287753374			-42.763726600
	-6.5918579667	-46.277552970	53		-42.585186700
29	-6.6057743200	-45.770284000		-9.1671805600	-60.327653185
	-6.9268657600	-45.030142993		-8.7244080800	-61.524499400
30		-47.725323741	54		-61.554937500

Appendix L

Cations content of water samples

Table 10. Cations content of water samples (1). If cation content < detection limit: result is unreliable. If cation content > 2 times the line-range, error is >10%. If cation content < BEC, error is >10%.

sample no.	Al	As	B	Ba	Be	Ca	Cd	Cl	Co	Cr	Cu	Fe	K	Li	Mg
<i>BEC</i>	0.339	0.105	0.178	0.012	0.005	0.238	0.015	21.9	0.039	0.019	0.052	0.04	3.75	0.063	0.019
<i>Line Range</i>	12.2	5.85	5.85	5.85	5.85	232	5.85	309	5.85	5.85	5.85	58.5	58.5	5.85	242
<i>Det. Lim.</i>	0.006	0.008	0.029	3E-04	2E-04	0.0043	2E-04	1.76	8E-04	8E-04	1E-05	3E-04	0.23	9E-04	4E-04
<i>Pract. Det. Lim.</i>	0.018	0.024	0.088	9E-04	5E-04	0.0128	7E-04	5.28	0.002	0.003	4E-05	9E-04	0.69	0.003	0.001
1	-0.048	0.001	-0.096	0.163	0.000	90.253	0.000	14.256	0.000	0.000	0.001	-0.004	2.391	0.005	27.285
2	-0.023	0.000	-0.108	0.230	0.000	78.810	0.000	-10.383	0.000	0.000	0.001	-0.004	1.856	0.002	13.630
3	-0.004	0.000	-0.107	0.014	0.000	12.468	0.000	1.361	0.000	0.000	0.002	0.004	0.659	0.002	12.162
5	-0.005	0.000	-0.111	0.008	0.000	14.918	0.000	9.892	0.000	0.000	0.001	0.021	21.737	0.002	3.579
6	-0.036	0.003	-0.099	0.243	0.000	102.403	0.000	-2.318	0.000	0.000	0.001	-0.005	14.105	0.007	19.588
7	-0.051	0.002	-0.101	0.304	0.000	108.803	0.000	1.975	0.000	0.000	0.001	-0.002	4.046	0.002	25.674
8	-0.030	0.004	-0.104	0.184	0.000	66.462	0.000	-8.678	0.000	0.000	0.000	-0.004	3.758	0.004	16.558
9	-0.013	0.004	-0.104	0.083	0.000	41.453	0.000	1.215	0.000	0.000	0.001	0.001	0.956	0.004	14.095
10	-0.047	0.000	-0.110	0.444	0.000	93.221	0.000	-4.939	0.000	0.000	0.000	-0.001	5.068	0.006	19.924
11	-0.110	0.004	-0.111	0.279	0.000	118.054	0.000	-16.718	0.000	0.000	0.000	0.103	0.923	0.002	27.695
12	-0.049	0.003	-0.110	0.361	0.000	92.189	0.000	-8.988	0.000	0.000	0.000	-0.004	7.577	0.003	18.736
13	-0.048	0.003	-0.112	0.083	0.000	117.336	0.000	-15.662	0.000	0.000	0.004	0.005	-0.714	0.002	14.660
14	-0.020	0.000	-0.108	0.019	0.000	54.477	0.000	-5.382	0.000	0.000	0.001	0.043	-0.243	0.001	15.946
15	-0.049	0.003	-0.114	0.179	0.000	92.213	0.000	1.263	0.000	0.000	0.000	0.006	-0.554	0.001	17.945
16	-0.045	0.003	-0.107	0.358	0.000	88.173	0.000	-12.485	0.000	0.000	0.001	-0.005	3.368	0.005	22.962
17	-0.006	0.002	-0.103	0.051	0.000	27.309	0.000	-5.247	0.000	0.000	0.001	0.001	0.053	0.005	9.107
18	-0.056	0.002	-0.108	0.104	0.000	111.806	0.000	-9.222	0.000	0.000	0.000	-0.005	1.464	0.002	17.209
19	-0.017	0.001	-0.105	0.075	0.000	43.350	0.000	-5.969	0.000	0.000	0.001	0.000	0.020	0.002	17.797
20	-0.027	-0.001	-0.102	0.029	0.000	69.356	0.000	6.503	0.000	0.006	0.001	0.015	1.031	0.001	19.173
21	-0.020	0.000	-0.105	0.036	0.000	61.922	0.000	-6.769	0.000	0.000	0.001	-0.004	1.298	0.000	12.825
22	-0.053	0.003	-0.113	0.108	0.000	99.172	0.000	-14.572	0.000	0.000	0.001	-0.003	0.370	0.004	40.143
23	-0.023	0.001	-0.107	0.038	0.000	72.557	0.000	-10.824	0.000	0.000	0.001	0.002	0.264	0.002	10.408
24	-0.047	0.008	-0.107	0.188	0.000	82.214	0.000	-12.139	0.000	0.000	0.001	-0.004	4.500	0.006	19.215
25	-0.044	0.000	-0.107	0.055	0.000	89.348	0.000	-3.428	0.000	0.000	0.000	-0.006	-0.487	0.002	16.396
26	-0.039	0.002	-0.112	0.129	0.000	96.253	0.000	-11.751	0.000	0.000	0.001	-0.005	1.389	0.002	14.767
27	-0.041	0.000	-0.108	0.079	0.000	80.998	0.000	-9.354	0.000	0.000	0.000	-0.005	1.714	0.000	13.112
28	-0.020	0.003	-0.109	0.020	0.000	54.005	0.000	-6.985	0.000	0.000	0.000	-0.005	-0.246	0.001	5.695
29	-0.047	0.001	-0.091	0.069	0.000	106.359	0.000	1.530	0.000	0.000	0.001	-0.005	3.485	0.001	18.019
30	-0.014	0.014	-0.086	0.152	0.000	83.259	0.000	92.948	0.002	0.015	0.002	0.489	2.293	0.003	27.322
31	0.034	0.007	-0.059	0.071	0.000	45.960	0.000	20.365	0.002	0.002	0.015	0.059	13.037	0.002	6.100
32	0.017	0.005	-0.057	0.030	0.000	24.311	0.000	5.174	0.001	0.002	0.009	0.043	6.187	0.007	2.685
34	0.020	0.001	-0.084	0.020	0.000	15.002	0.000	5.837	0.000	0.001	0.004	0.031	5.966	0.004	1.374
36	-0.036	0.002	-0.110	0.184	0.000	87.902	0.000	-11.934	0.000	0.000	0.000	-0.005	1.331	0.002	14.683
37	-0.042	0.002	-0.100	0.446	0.000	89.281	0.000	-6.549	0.000	0.000	0.001	0.011	6.137	0.007	28.032
38	-0.054	0.003	-0.115	0.181	0.000	100.285	0.000	-13.600	0.000	0.000	0.000	-0.006	-0.533	0.005	14.745
39	-0.025	0.003	-0.104	0.211	0.000	33.343	0.000	-6.132	0.000	0.000	0.001	0.000	1.449	0.008	23.715
40	-0.020	0.002	-0.105	0.155	0.000	38.504	0.000	-6.201	0.000	0.000	0.001	0.000	0.192	0.005	21.145
41	-0.048	0.001	-0.108	0.355	0.000	88.945	0.000	-12.453	0.000	0.000	0.000	-0.004	1.319	0.007	29.859
42	-0.029	0.000	-0.113	0.125	0.000	77.701	0.000	-13.135	0.000	0.000	0.001	-0.003	0.001	0.002	19.690
43	-0.039	0.003	-0.114	0.160	0.000	76.794	0.000	-11.773	0.000	0.000	0.000	0.009	-0.261	0.003	22.088
44	-0.045	0.001	-0.099	1.059	0.000	80.778	0.000	-11.648	0.000	0.000	0.000	-0.003	3.846	0.023	21.289
45	-0.022	0.001	-0.115	0.174	0.000	55.992	0.000	-10.007	0.000	0.000	0.000	-0.005	0.535	0.002	11.835
46	-0.027	0.001	-0.106	0.168	0.000	68.234	0.000	-9.310	0.000	0.000	0.000	-0.004	0.615	0.004	18.459
47	-0.004	0.000	-0.095	0.050	0.000	27.379	0.000	-4.495	0.000	0.000	0.000	0.000	0.039	0.007	9.381
48	-0.017	0.001	-0.108	0.072	0.000	43.331	0.000	-8.084	0.000	0.000	0.001	0.001	0.083	0.002	17.562
49	-0.008	0.001	-0.104	0.067	0.000	39.580	0.000	7.253	0.000	0.004	0.001	0.020	0.237	0.002	19.155
50	-0.027	0.001	-0.110	0.069	0.000	82.659	0.000	-7.930	0.000	0.001	0.001	-0.001	0.082	0.002	11.709
51	-0.023	0.000	-0.113	0.112	0.000	114.866	0.000	-14.069	0.000	0.000	0.001	-0.005	0.451	0.002	10.928
52	-0.050	0.008	-0.104	0.312	0.000	121.005	0.000	-15.668	0.000	0.000	0.000	0.061	1.599	0.001	19.997
53	-0.033	0.001	-0.107	0.128	0.000	79.864	0.000	-10.093	0.000	0.000	0.001	0.363	1.983	0.002	16.590
54	-0.032	0.001	-0.106	0.130	0.000	92.161	0.000	-7.797	0.000	0.000	0.000	0.000	2.255	0.003	21.278

Table 11. Cations content of water samples (2). If cation content < detection limit: result is unreliable. If cation content > 2 times the line-range, error is >10%. If cation content < BEC, error is >10%.

sample no.	Mo	Na	Ni	P	Pb	S	Sb	Sc	Si	Sr	Ti	V	Y	Zn	Zr
<i>BEC</i>	0.032	0.862	0.068	0.074	0.167	0.39	0.432	0.004	0.107	0.004	0.076	0.05	0.021	0.011	0.074
<i>Line Range</i>	5.85	58.5	5.85	29.5	5.85	59.5	5.85	0.919	59.1	5.85	5.85	5.85	5.86	5.85	5.87
<i>Det. Lim.</i>	1E-04	0.092	6E-04	0.004	0.011	0.16	0.017	1E-04	0.027	8E-05	0.003	5E-04	2E-04	4E-04	3E-04
<i>Pract. Det. Lim.</i>	3E-04	0.276	0.002	0.012	0.034	0.48	0.051	3E-04	0.082	2E-04	0.01	0.002	6E-04	0.001	9E-04
1	0.000	21.665	0.002	0.003	-0.004	8.399	0.007	0.000	7.530	0.270	0.001	0.000	0.000	0.003	-0.001
2	0.000	7.360	0.007	0.004	-0.004	1.612	0.000	0.000	5.856	0.221	0.000	0.000	0.000	0.005	0.000
3	0.000	10.407	0.011	0.000	0.001	0.204	0.004	0.000	0.739	0.028	0.000	0.000	0.000	0.006	0.000
5	0.000	3.311	0.004	0.003	-0.005	0.252	0.007	0.000	0.594	0.027	0.001	0.000	0.000	0.009	0.000
6	0.004	3.617	0.001	0.005	-0.003	9.611	0.006	0.000	14.459	0.176	0.000	0.000	0.000	0.020	-0.001
7	0.000	8.906	0.007	0.004	0.002	4.695	0.004	0.000	6.136	0.255	0.001	0.000	0.000	0.003	0.000
8	0.001	3.507	0.001	0.004	-0.001	5.467	0.002	0.000	6.862	0.152	0.001	0.000	0.000	0.004	-0.001
9	0.001	5.540	0.007	0.004	0.000	6.323	0.001	0.000	4.294	0.137	0.000	0.001	0.000	0.016	-0.001
10	0.001	15.808	0.002	0.005	-0.004	5.011	0.000	0.000	5.710	0.162	0.001	0.000	0.000	0.004	0.000
11	0.000	8.227	0.000	0.006	-0.003	0.367	-0.002	0.000	14.776	0.146	0.001	0.000	0.000	0.009	-0.001
12	0.002	5.644	0.001	0.000	-0.003	5.861	0.002	0.000	6.564	0.167	0.001	0.000	0.000	0.003	0.000
13	0.000	11.994	0.001	0.005	-0.003	0.263	0.000	0.000	10.334	0.152	0.001	0.000	0.000	0.005	0.000
14	0.000	7.975	0.003	0.007	-0.003	2.772	0.005	0.000	6.772	0.090	0.000	0.000	0.000	0.020	0.000
15	0.000	44.090	0.000	0.012	-0.005	6.999	0.006	0.000	11.573	0.111	0.001	0.000	0.000	0.003	0.000
16	0.000	7.575	0.001	0.002	-0.003	2.152	0.007	0.000	5.993	0.241	0.001	0.000	0.000	0.003	-0.001
17	0.001	2.248	0.001	0.003	-0.004	6.808	0.002	0.000	3.451	0.120	0.001	0.000	0.000	0.002	-0.001
18	0.000	8.492	0.000	0.004	-0.004	1.906	0.002	0.000	7.411	0.216	0.001	0.000	0.000	0.002	0.000
19	0.001	5.034	0.000	0.002	-0.002	2.644	0.010	0.000	4.933	0.104	0.000	0.001	0.000	0.003	-0.001
20	0.001	10.451	0.030	0.013	-0.004	4.411	0.005	0.000	6.237	0.126	0.000	0.000	0.000	0.014	0.000
21	0.000	5.563	0.000	0.005	-0.001	3.254	0.007	0.000	4.861	0.098	0.001	0.000	0.000	0.006	0.000
22	0.000	5.840	0.001	0.005	-0.005	0.167	0.003	0.000	14.038	0.157	0.001	0.000	0.000	0.003	-0.001
23	0.001	3.095	0.002	0.002	-0.001	1.831	0.006	0.000	6.387	0.103	0.001	0.000	0.000	0.006	0.000
24	0.001	2.558	0.000	0.003	-0.001	3.868	0.000	0.000	4.674	0.160	0.001	0.000	0.000	0.013	0.000
25	0.000	8.500	0.001	0.002	-0.006	2.453	0.006	0.000	7.039	0.155	0.000	0.000	0.000	0.002	0.000
26	0.000	7.578	0.002	0.003	-0.001	1.256	0.002	0.000	7.461	0.259	0.001	0.000	0.000	0.002	0.000
27	0.000	6.736	0.000	0.002	-0.003	0.736	0.006	0.000	7.071	0.133	0.001	0.001	0.000	0.002	0.000
28	0.000	4.852	0.000	0.001	-0.002	1.462	0.000	0.000	7.979	0.052	0.001	0.000	0.000	0.002	-0.001
29	0.000	10.544	0.001	0.020	-0.003	6.523	0.006	0.000	6.346	0.138	0.001	0.000	0.000	0.266	-0.001
30	0.005	41.401	0.146	0.055	-0.003	6.582	0.006	0.000	9.856	0.133	0.001	0.000	0.000	0.082	-0.001
31	0.001	11.785	0.006	0.357	0.003	14.468	0.008	0.000	0.512	0.139	0.002	0.004	0.000	0.125	-0.001
32	0.001	2.564	0.003	0.292	0.001	17.543	0.009	0.000	0.494	0.089	0.002	0.006	0.000	0.214	-0.001
34	0.001	1.315	0.004	0.302	0.000	9.936	0.010	0.000	0.325	0.049	0.001	0.003	0.000	0.223	0.000
36	0.000	6.431	0.001	0.002	-0.002	1.537	0.009	0.000	5.607	0.225	0.000	0.000	0.000	0.004	-0.001
37	0.001	4.768	0.001	0.004	-0.001	11.102	0.003	0.000	7.857	0.214	0.001	0.000	0.000	0.004	0.000
38	0.000	14.308	0.000	0.004	-0.001	0.344	0.006	0.000	9.071	0.257	0.001	0.000	0.000	0.002	-0.001
39	0.001	28.272	0.001	0.001	-0.002	3.052	0.003	0.000	5.457	0.287	0.001	0.000	0.000	0.006	-0.001
40	0.000	19.611	0.000	0.002	-0.004	1.987	0.006	0.000	5.363	0.256	0.000	0.000	0.000	0.003	0.000
41	0.000	15.618	0.003	0.004	-0.001	0.596	0.006	0.000	5.405	0.358	0.001	0.000	0.000	0.005	0.000
42	0.001	7.058	0.000	0.002	-0.004	1.680	0.003	0.000	5.413	0.255	0.001	0.000	0.000	0.003	0.000
43	0.000	6.805	0.000	0.003	-0.003	1.076	0.004	0.000	4.624	0.275	0.001	0.000	0.000	0.004	-0.001
44	0.000	58.163	0.000	0.006	-0.001	0.429	0.007	0.000	5.214	0.519	0.001	0.000	0.000	0.006	-0.001
45	0.000	8.181	0.001	0.008	-0.002	0.458	-0.001	0.000	6.316	0.162	0.001	0.000	0.000	0.002	0.000
46	0.001	9.520	0.000	0.001	-0.001	1.407	0.005	0.000	12.368	0.095	0.000	0.000	0.000	0.002	0.000
47	0.001	2.573	0.000	0.001	-0.002	7.353	0.004	0.000	3.191	0.122	0.001	0.000	0.000	0.003	0.000
48	0.001	5.652	0.000	0.001	-0.004	2.689	0.007	0.000	4.939	0.105	0.001	0.000	0.000	0.003	-0.001
49	0.002	9.998	0.032	0.003	-0.003	3.887	-0.001	0.000	4.673	0.093	0.001	0.000	0.000	0.015	-0.001
50	0.000	9.538	0.008	0.000	-0.003	2.382	0.005	0.000	6.761	0.174	0.001	0.000	0.000	0.016	0.000
51	0.000	5.791	0.000	0.002	-0.002	0.819	0.004	0.000	6.679	0.191	0.001	0.000	0.000	0.003	-0.001
52	0.002	4.158	0.000	0.002	-0.003	0.343	0.004	0.000	6.542	0.249	0.002	0.000	0.000	0.004	0.000
53	0.000	5.597	0.004	0.001	-0.004	0.112	0.007	0.000	3.231	0.315	0.002	0.000	0.000	0.006	0.000
54	0.000	6.210	0.001	0.002	-0.006	5.057	0.007	0.000	6.342	0.185	0.001	0.000	0.000	0.006	0.000

Appendix M
Anion content of water samples

Table 12. Content of major anions in water samples.

Sample no.	Anions Results [mg/l]						
	Fluoride	Chloride	Nitrite	Bromide	Nitrate	Phosphate	Sulphate
<i>detection limit</i>	<0.004	<0.1	<0.005	<0.02	<0.04	<0.5	<0.1
1	0.087	27.662	0.003	0.022	21.685	0.113	26.622
2	0.105	2.178	0.016	0.010	2.749	0.102	4.403
3	0.027	3.808	0.006	0.000	0.055	0.089	0.508
5	0.012	13.401	0.036	0.019	0.912	0.082	0.625
6	0.089	11.830	0.007	0.020	46.911	0.085	29.423
7	0.096	17.783	0.004	0.023	0.059	0.073	14.988
8	0.113	1.451	0.012	0.009	0.070	0.076	16.955
9	0.129	1.214	0.011	0.006	0.435	0.072	18.953
10	0.093	9.022	0.045	0.006	10.837	0.064	15.589
11	0.125	0.423	0.006	0.005	0.018	0.067	1.101
12	0.196	4.421	0.021	0.004	1.413	0.059	18.345
13	0.129	0.828	0.007	0.014	0.028	0.064	0.789
14	0.182	3.225	-0.001	0.009	-0.002	0.065	8.481
15	0.241	14.353	0.006	0.071	0.033	0.060	22.059
16	0.122	0.580	0.024	0.004	0.101	0.057	6.453
17	0.124	0.685	0.016	0.006	0.681	0.056	21.304
18	0.153	6.653	0.024	0.014	5.301	0.087	5.675
19	0.131	1.701	0.008	0.007	0.628	0.094	8.249
20	0.198	3.002	0.008	0.010	4.400	0.086	10.409
21	0.273	3.919	0.029	0.011	16.820	0.073	10.029
22	0.084	0.727	0.019	0.005	0.135	0.074	0.509
23	0.134	0.980	0.019	0.007	1.483	0.065	5.267
24	0.117	1.113	0.002	0.004	0.015	0.064	11.904
25	0.193	9.573	0.012	0.012	8.440	0.060	7.569
26	0.087	1.744	0.006	0.006	1.230	0.063	3.411
27	0.090	3.082	0.025	0.008	1.872	0.059	2.106
28	0.104	1.402	-0.001	0.009	4.514	0.061	4.132
29	0.194	15.890	0.007	0.034	0.966	0.079	20.834
30	0.233	6.183	0.035	0.022	0.055	0.057	1.139
31	0.346	11.194	4.328	0.084	22.054	0.190	40.679
32	0.459	9.145	0.128	0.086	51.112	0.375	50.452
34	0.266	6.847	0.067	0.058	26.619	0.489	29.157
36	0.107	0.670	0.010	0.002	1.755	0.091	4.349
37	0.086	6.484	0.035	0.020	0.401	0.090	34.213
38	0.126	0.884	0.003	0.004	0.011	0.080	1.010
39	0.127	0.533	0.001	0.000	0.002	0.078	9.628
40	0.115	0.525	0.019	0.003	0.170	0.078	5.801
41	0.088	0.723	0.017	0.002	0.077	0.067	1.369
42	0.091	0.383	0.009	0.002	0.004	0.057	4.783
43	0.097	0.328	0.017	0.001	0.025	0.059	3.042
44	0.156	1.240	0.007	0.006	0.085	0.060	1.169
45	0.122	0.477	-0.001	0.000	-0.004	0.064	1.308
46	0.125	1.793	-0.001	0.009	-0.004	0.058	4.069
47	0.144	0.937	0.013	0.003	0.725	0.059	23.360
48	0.131	1.733	0.013	0.003	0.473	0.051	8.304
49	0.138	2.060	0.028	0.005	0.696	0.060	9.375
50	0.098	1.391	0.026	0.006	2.595	0.059	6.557
51	0.112	1.048	0.016	0.003	1.243	0.050	2.297
52	0.112	1.047	0.016	0.003	1.243	0.050	2.290
53	0.110	1.035	0.016	0.003	1.226	0.050	2.266
54	0.109	1.028	0.016	0.004	1.221	0.054	2.249

Appendix N

Field measurements of chemical properties of water samples

Table 13. Results of chemical field measurements of water samples.

No.	EC [uS/cm]	temp (EC) [°]	pH	temp (pH) [°]	O2 [mg/L]	temp (O2) [°]	O2 sat. (%)	alkalinity (mol/L)
1	845	26.2	7.29	26	4.72	27.1	71.2	0.0167
2	521	45.1	7.86	33.6	6.1	34.4	104.4	0.01104
3	174.3	37.2	8.07	28.5	3.37	32.7	56	0.00428
5	208.1	45.2	7.47	36.4	3.42	35.6	59	0.00278
6	570	37.6	7.48	28.1	5.05	27.9	76.9	0.01094
7	616	35.9	7.08	27.3	2.72	28.8	42.5	0.01654
8	335	33.7	7.93	26.7	6.94	27.4	105.1	0.00792
9	261	34.1	8.57	26.8	7.44	28.1	114.2	0.00544
10	498	29.3	7.44	27.3	3.54	27.6	55.3	0.01396
11	561	29.4	7.04	27.7	2.45	27.4	37.2	0.01766
12	433	28.5	7.39	26.8	2.68	26.8	40.3	0.0123
13	547	26.5	72.5	7.3	4.83	26.5	72.5	0.018
14	286	26.6	7.08	24.7	2.79	24.7	40.3	0.00842
15	503	27	6.89	25.1	1.79	25.1	26.1	0.0144
16	436	28.2	7.26	26.6	3.3	7.3	50.2	
17	146.1	23.9	8.38	22	7.79	23	109.9	
18	499	26.9	7.02	25.2	2.94	25.1	43	0.01352
19	286	29.4	8.43	29.4	7.46	24.8	107.8	0.00698
20	355	30.3	7.25	26.6	2.85	29.3	44.8	0.00976
21	316	32.6	7.42	27.9	4.29	28.2	65.9	0.00752
22	574	26.8	7.09	23.7	2.12	24	30.1	0.01846
23	347	30.7	7.47	28.3	3.34	28.3	51.2	0.0084
24	396	30.4	7.4	27	2.68	27	40.3	0.0105
25	447	29	7.28	25.2	4.59	25.3	66.3	0.01176
26	489	25.7	7.06	25.6	3.78	25.7	55.4	0.01496
27	353	28	7.4	25.2	3.17	25.5	46.5	0.01054
28	239	30.3	6.85	27.6	4.68	27.4	70.9	0.00646
29	437	28.5	7.13	25.3	1.57	25.6	23.1	0.01208
30	363	28.8	7.46	26	3.33	26.2	49.2	0.01034
31								
32								
34	158.1	21.8	7.31	19.6	7.44	20	98.3	
36	379	30.5	7.2	28.9	2.3	29.6	36.3	0.0135
37	481	25.9	7.32	24.1	1.45	25	21	0.01314
38	562	27.5	7.35	25.6	5.45	26.1	81.7	0.01696
39	306	23.1	7.95	21.9	6.39	23.1	90.5	0.0088
40	331	18.6	8.53	17.9	7.36	18.3	98.8	0.00982
41	458	20.5	7.49	19.2	5.88	19.7	85.1	0.01442
42	445	20.9	7.89	20.1	6.35	19.8	93.2	0.01346
43	363	15	8.32	14.2	6.21	14.5	81.8	0.01122
44	508	16	7.42	14.9	3.32	15	45	0.01586
45	289	26.5	8.38	25.1	7.26	24.8	105.9	0.00858
46	394	25.4	8.1	23.2	7.11	22.2	98.1	0.01274
47	163.1	16.9	8.52	15.9	8.11	16.2	99.5	0.00358
48	407	24.9	8.45	22.7	8.27	23.3	116.8	0.00694
49	320	23.8	8.49	21.3	7.7	21	103.4	0.00668
50	403	26.4	6.89	23.9	3.37	23.5	52.2	0.0098
51	524	27	7.03	25.1	4.47	25	65.4	0.01358
52	542	27.7	7.16	25	2.5	25.9	36.9	0.016
53	409	32	7.29	25.9	0.7	26.4	10.4	0.01336
54								